Syracuse University

SURFACE

Dissertations - ALL

SURFACE

8-2014

THE NON-ERYTHROID MEMBRANE SKELETON AND ITS ROLE IN MECHANOTRANSDUCTION

Eleni Kinfe Degaga
Syracuse University

Follow this and additional works at: https://surface.syr.edu/etd

Part of the Physics Commons

Recommended Citation

Degaga, Eleni Kinfe, "THE NON-ERYTHROID MEMBRANE SKELETON AND ITS ROLE IN MECHANOTRANSDUCTION" (2014). *Dissertations - ALL*. 137.
https://surface.syr.edu/etd/137

Abstract

The thesis is concerned with questions regarding cellular biomechanics and cell surface interactions. A particular focus is thereby on the role of the spectrin membrane skeleton in transducing forces to and from non-erythroid mammalian cells. This spectrin based membrane skeleton has been the focus of much study in the context of red blood cells, as it determines their mechanical properties due to the lack of an extended actin based cytoskeleton. In stark contrast, the corresponding structure in non-erythroids is much less studied and understood, although it seems to play important roles in organization of membrane associated proteins, cellular mechanics, adhesion, traction and possibly mechanotransduction. In this work, I was able to determine the amount -down to the average copy number per cell- of the main protein components of the non-erythroid membrane skeleton, in model cell lines commonly used in cell-mechanics studies. The results of the measurements provided by combining a variety of optical microscopic and biochemical techniques, demonstrate that proteins associated with the membrane skeleton constitute a large ($\sim$10%) fraction of cellular proteins. These results are then compared with the respective quantities after mechanical stimulation of the cells. It is found that external forces result in both an up to 60% changes of the overall amounts of proteins as well as the protein composition of the membrane skeleton itself. In addition, it was established that the fraction of polyubiquitinated spectrin has significantly increased due to stimulation. The work helps to establish the fact that the spectrin based membrane skeleton, while often overlooked in non-erythroids, is indeed a verily generic and important system in mammalian cells that is also quite sensitive to external forces. Thus, the

skeleton should be taken into account when studying cellular mechanics, membrane structure or composition.

Furthermore, I present my successful work on integrating several light based methods to simultaneously measure traction forces of adherent cells as well as internal strains in their membrane skeleton. For the proof of principle experiments and optimization procedures, I used $NIH - 3T3$ fibroblast and $H9c2(2-1)$ cardiomyocyte cell lines, both of which are known to be mechanically active. Using my method, I demonstrate that the internal strains in the membrane skeleton of fibroblasts are correlated with the polyacrylamide substrate stiffness. The later has also a measureable impact on the generated cellular traction forces. These findings open up a first glimpse on the questions that can now be addressed with this method and it promises to help to refine our still rudimentary understanding of the interrelated mechanisms of cellular mechanotransduction and force generation machinery.

Cells are exposed not only to mechanical forces but also to electrical, chemical and magnetic forces found in their environment. In a separate series of experiments, I observed that cellular behavior of 3T3 fibroblasts on glass supported lipid bilayers depend on the detail of lipid charge mixtures in the bilayer as well as the head group compositions. Live cell-supported lipid membrane hybrids are frequently used in dissecting membrane based inter-cellular communication. This work indicates that in the interpretation of the observed cell behavior on this hybrid system, the lipid bilayer itself and not only the protein augmentation can play an important role.

Abstract in Amharic

ጭብጥ

ሴሎች ወይንም ህያው የሆነ ነገር ሁሉ የተገነባባቸው ህዋሳት የተሰሩባቸውን ፕሮቲኖች እና ንጥረ ነገሮችን የአወቃቀራቸውን እና የጥቅማቸውን ግንኙነት ለማጥናት ሴሎቿ በአካባቢያቸው የሚሰነዘርባቸውን የተለያዩ ኃይሎች በምን ሁኔታ አወቃቀራቸውን በጊዜ እና በቦታ በመለዋወጥ ተረድተው ኃይሉን እንደሚያስተላልፉት ማጥናት ያስፈልጋል። ምክኒያቱም ህዋሶቿ (ሴሎቿ) በውጪያዊ ኃይል ምክኒያት አወቃቀራቸውን በጊዜ እና በቦታ ይቀያይራሉ፤ ይህ መቀያየርም ሴሎቿ ከሚሰጡት ዘሪፈ ብዙ ጠቀሜታ ጋር በጥብቁ ይገናኛል። የውጪያዊው ኃይል ህዋሶቿ ላይ በሚያደርገው ተጽህኖ ውስጥ የሚሳተፉ ብዙ የህዋሱ ንጥረ ነገሮች እና አካላት አሉ። ስለዚም ይሄንን ግንኙነት በቀላል ለማጥናት የህዋሱን የተወሰነ ክፍል ወስዶ በጥልቀት መመራመር ያሻል። እኔም ለዚህ ጥናት የመረጥኩት የህዋሱ አካል የውጭኛው ሽፋን እና ከሽፋኑ ጋር የተያያዙ ፕሮቲኖችን ነው ምክኒያቱም እነዚህ የሴል ክፍሎች ለውጪያዊ ኃይል የተጋለጡ ናቸው። እናም በዚ የውጪያ ኃይል የማስተላለፍ ፣ የህዋስ አወቃቀር እና ጠቀሜታ ግንኙነት ላይ ከፍተኛ ሚና ይጫወታሉ ብዬ በማስብ ነው። በዚህ ጥናታዊ የተግባር ምርምር ጽሁፍ ውስጥ በመጀመሪያው ክፍል ስለ ጥናቱ ጠቃላ አውቀት እንደ መንደርደሪያ ከሰጠሁ በኋላ፤ በሁለተኛው ክፍል ስፔክትሪን እና አንክሪን የሚባሉ ከህዋሱ ሽፋን ጋር የተያያዙ እና ለሽፋኑ ድጋፍ የሚሰጡ ፕሮቲኖች በዚ ኃይል የማስተላለፍ ሂደት ውስጥ ያላቸውን ሚና በተመለከት በላቦራቶሪ (የምርምር ጣቢያ) የሰበሰብኳቸውን የምርምር መረጃዎች በማቅረብ መረጃዎቼን አብራራለሁ። በሶስተኛው ክፍል ደግሞ ፣ ሴሎች በአካባቢያቸው ኃይል ተከበው ሲንቀሳቀሱ (ሲጓዙ) እነሱም ወደአካባቢው የሚሰነዝሩት ኃይል አለ። በዚ ኃይል እና በስፔክትሪን እና አንክሪን ድጋፍ በሚንቀሳቀሰው የህዋሱ ሽፋን ላይ በሚፈጠረው ኃይል መካከል የሚኖረውን ጥብቅ ግንኙነት በመጠን ለክቼ አቀርባለሁ። የሁለተኛው እና የሶስተኛው ክፍል ጥናቴም ስፔክትሪን የሚባለውን ፕሮቲን የውጫዊውን ኃይል ወደህዋሱ የውስጠኛው አካል በማስተላለፍ ሂደት ከፍተኛ ሚና እንዴት ሊኖረው እንደሚችል ያሳየናል። ያም ማለት ስፔክትሪንን ቀይ የደም ህዋስ ላልሆኑ ህዋሶችም ጭምር እንደ ኃይል አስተላላፊ (ፎርስ ሴንሰር እንዲሁም ፎርስ ትራንስዲሰር) እንደሚያገለግል ያረጋግጥልናል። በአራተኛው የጥናታዊ ጽሁፌ ክፍልም፤ ይህንን ምርምር ለማድረግ በምርምር ጣቢያ የተጠምኩባቸውን መሳሪያዎች እና ቴክኒኮችን ዘርዝሬ አቀርባለሁ። በአምስተኛ እና በመጨረሻው ክፍልም የዚህን ጥናት የወደፊት ሂደት ፣ ጥናቱ በልብ፤ በነርቭ ህዋሶች እንዲም በካንሰር ህክምና ምርምር ላይ ያለውን ግብአትነት እና ጠቀሜታ እንዲሁም ለሳይንሳዊ ምርምር እና ሪፖርት ሊበቁ የሚችሉ ነገር ግን ከጊዜ እና ከሁኔታ አንጻር ያላተኮርኩባቸውን ተጨማሪ ግኝቶችን አቀርባለሁ።

THE NON-ERYTHROID MEMBRANE SKELETON AND ITS ROLE IN MECHANOTRANSDUCTION

By

Eleni Degaga

B.Ed. in Physics. Bahir Dar University, 2006

PGD. African Institute for Mathematical Sciences, 2008

M.Sc. in Physics. Syracuse University, 2010

———————————

Dissertation

Submitted in partial fulfillment of the requirements for the degree of

Doctor of Philosophy in Physics

Syracuse University

August 2014

Acknowledgements

First and foremost, I would like to thank my supervisor Martin Bernard Forstner. He has taught me, both formally and informally, how to be a very good experimentalist. I have learned a lot over the years from his unique point of views on research, his interesting insights on every issue and his personal expectations of excellence. I greatly appreciate all his vast contributions of times, ideas, and resources to make my Ph.D. experience enjoyable and stimulating. The joy and enthusiasm he has for his research was contagious, motivational and inspirational for me during tough times in the research journey. Every member of our lab have contributed immensely to my personal and professional growth at Syracuse University. The group has been a source of friendships as well as good advice. Thank you very much Adolphe, Kathleen and Ian for sharing all the excitements of research and unforgetable moments, I will miss you all.

I strongly feel that, I am prepared for academic and professional career thanks to the holistic experiance that included research and teaching. I would like to mention the most valueable teaching experiance I acquired as a graduate assistant and research advisor for many undergraduate students. I am grateful to find colleagues and friends to encourage me to take on the challenges in research. I am especially greatful to have met Cristina Marchetti who was the reason why I decided to go to pursue a career in research. She was and remains as one of my best role models for a great scientist and mentor.

Contents

List of Figures

Thesis outline

The thesis is organized in several chapters. A general introduction is given in chapter 1. Chapter 2 deals with the spectrin-ankyrin membrane skeleton and findings on how this system could play roles in cellular mechanotransduction. As a continuation of the second chapter, in Chapter 3, experimental method developments and primary results will be presented on how in live cells, the traction forces cells exert on their environment and the internal strains developed in the non-erythroid spectrin membrane skeleton correlations can be measured. In chapter 4, the work on characterizing the behaviors of fibroblasts cell lines cultured on supported lipid bilayers of different charge and head group compositions will be compared. In chapter 5, the materials and methods used in all the experiments will be described in detail. In the final chapter 6, general accomplishments, their relevance, limitations, future directions and perspectives will be stated.

Chapter 1

General Introduction

1.1   Motivation and scientific scope

The study of the mechanisms of cellular life is complicated in part due to the strong interrelationship of the structures, functions and dynamical rearrangements of the different molecules and proteins in a living cell. Given the currently available tools, it is not yet possible to visualize all of these molecules simultaneously and with high enough precision or temporal resolution for a thorough investigation. To demonstrate the interdependent nature of cellular components and structures, a closer look at the actin cytoskeleton of a typical eukaryotic cell may serve as an example. In Fig.1.1B, it can be observed that the actin cytoskeleton re-arranged itself to support the func-tion of cell division and thus the organization of the cytoskeleton looks di erent from the actin structures of resting cells depicted in Fig.1.1A. One way to make inroads in our understanding of this inseparable interdependence of cellular structures and
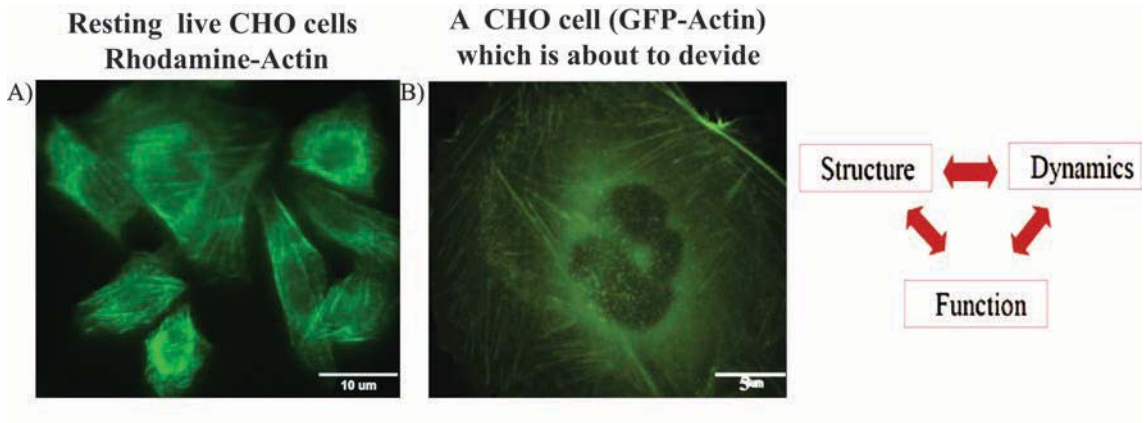
Figure 1.1: Epi-fluorescent images of actin in (Chinese hamster ovary) CHO cells, A) green is rhodamine phalloidin stained actin in resting CHO cells B) GFP-actin transfected CHO cells showing the organization of the actin stress fibers during cell division (the dark central spots are the two nuclei of the daughter cells).

biological functions is by probing the dynamic response of the different cellular structures and proteins to extrinsic perturbations. These can be of mechanical, chemical or electrical in nature [1-3]. One of these, namely mechanical perturbations, are of particular interest within the context of this work.

Cells are exposed to a variety of mechanical forces such as shear stress [5], mechanical stretch [6], hydrostatic pressure [7, 8], and gravity [9]. Cells can sense and translate a broad range of mechanical forces into sets of bio-chemical signals that ultimately regulate cellular processes [10, 11] such as cells adhesion [12-14], proliferation [15], apoptosis [16], or ubiquitination [17]. However, the specific mechanisms by which mechanical forces lead to particular molecular and cellular responses are much less understood [18]. Thus, many open questions remain as to how cells exploit mechanical forces -whether applied from the environment or intrinsically generated-

to regulate their bio-chemical functions [19]. Studying such questions at the molecular level requires measurements of mechanical properties of molecules (in particular proteins) [19], protein folding pathways [20] and characterizing how functional states of proteins are changing under mechanical loads [18, 22-24]. It is this last aspect that, the first part of the research described in this thesis is mostly focused on.

At this point only a few cellular molecules have been identified to act as mechanical signal converters [25, 26]. However, there are many identified signaling pathways, such as extracellular signal-regulated kinases (ERK) [27], mitogen-activated protein (MAP) kinases [28], glycogen synthase kinase-3 (GSK) [29] and G-protein receptor (G alpha q) pathway [30], it is very difficult to study cellular mechanotransduction without choosing a specific system [31]. Since the cell membrane and its associated cytoskeletal proteins are directly exposed to the different environmental perturbations, they are a logical starting point for my investigations. Thus, the particular focus on the work described here will be on the spectrin-ankyrin membrane skeleton of non-erythroid cells. This membrane skeleton is a key mechanical structure because of its location and arrangement in linking the membrane and the cytoskeleton [32]. It is responsible for coordinating many proteins such as ion channels [33], exchangers [34], adhesion molecules [35] and cytoskeletal elements [36]. This structure has so far seen very little attention in the context of non-erythroids. Thus, also force generation and transduction from cells and to the cells is usually thought associated only with the actin cytoskeleton [37], myosin motors [38] microtubules [39] and proteins at the focal adhesion complexes [40]. However, the membrane skeleton is a part of

the cytoskeletal acting as a shell [41] and also the cytosolic internal part of the membrane [42]. Thus it is a wide open question to what extent the much under-studied non-erythroid membrane skeleton is being used for mechanical sensation, generation and force transduction. Thus, I set out to investigate its possible involvement in mechanotransduction and will discuss in detail its response to external forces. In addition and as first step to extend these studies to live cells, this thesis will present a methodology that enables the correlation of the traction forces of non- erythroid cell colonies and the corresponding internal strains in the spectrin membrane skeleton. It is my hope that this work will contribute to revealing the theoretical and experimental mysteries that still surround cellular mechanotransduction [43, 44].

1.2 Mechanotransduction in cells

Mechanotransduction describes the process by which external physical stimuli are translated into biochemical activity and plays an important role in many biological functions on both the cell and tissue level [45]. The ability of cells to respond to changes in their physical environments is vital in the maintenance of physiological processes that affect the entire body [46]. In response to the physical stimuli, cells adjust their shape and function affecting their behaviors such as protein content [20, 47, 48] migration [49], and ubiquitination [47, 50, 51]. Most of the time, defects in mechanotransduction through acquired environmental mutations results in various diseases [52]. Mechanoreceptors such as integrins [53], cadherin [54], focal adhesions [55] and stretch-activated Ca^{2+} channels [56] were identified. However, there are other various signal transduction players that still await identification [57] and

that are involved in the mechanotransduction processes that ultimately regulate the mechanism of cellular life. Therefore, there is a need for further identification of major mechanical signal transducers in order to both understand the overall mechanism better and to comprehend the bio-mechanical and biochemical properties of cells. The identification of mechanosensors not only can elucidate the mechanisms of mechanotransduction and fate commitments but also bring new prospects to mechanical cell control as well as to drug development for clinical applications [58].

In the general process of mechanotransduction, there are three stages involved. **1) Mechanoreception:** a physical force is detected by the cell and the message is translated from the point of force application to the inside of the cell and for that purpose, cells use mechanical signal receivers (mechanoreceptors) [59]

2) Signal transmission: once the external force is received by mechanoreceptors, the signal then needs to be translated within the cell to different locations throughout the cell. For this signal transmission, cells seem to involve the cytoskeleton structures, the membrane skeleton as well as individual proteins [60].

3) Cellular response: when the mechanical signal reaches a destination, it affects biochemical activities that ultimately cause alterations in cell behavior (see Fig.1.2. right hand side) through a variety of molecular mechanisms [61].
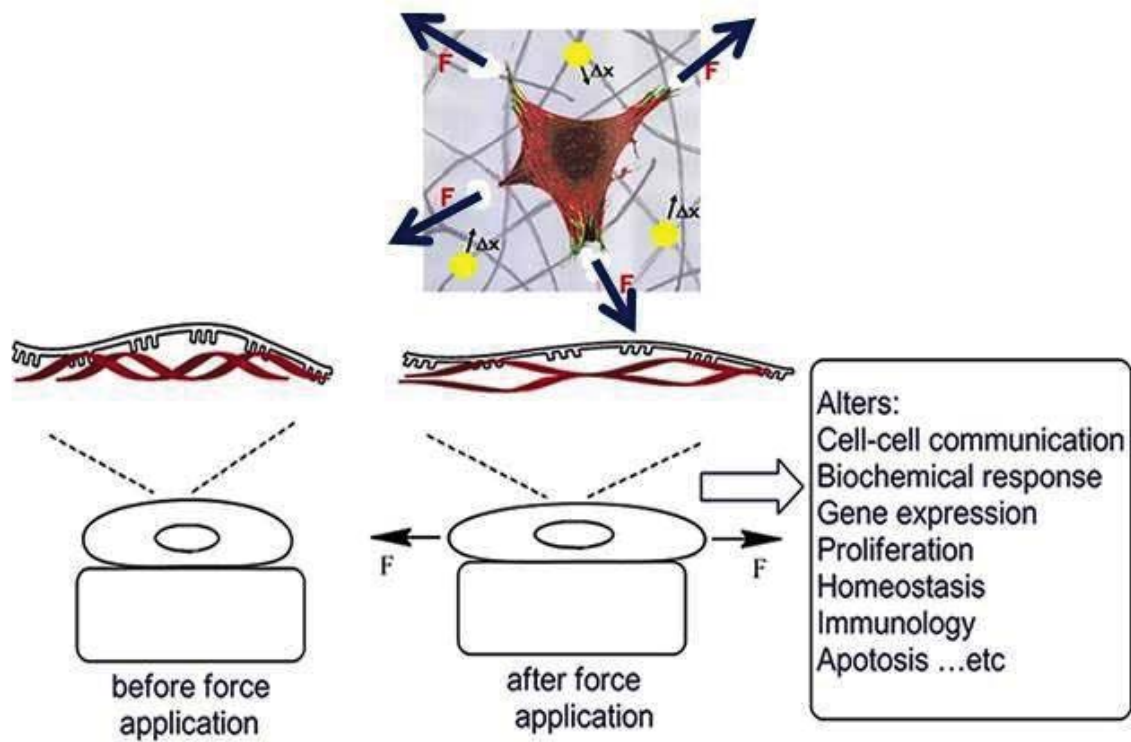
Figure 1.2: A simple schematic of mechanotransduction illustrating the deformation of the cell membrane, the underlying membrane skeleton and the resulting possible functional outcomes.

1.2.1 External force applications to cells

The general area of mechanobiology tries to answer the effect of mechanical forces on living cells, whole tissues and systems [62]. These responses can currently not be fully predicted with either theoretical models or experiments alone because of the complexity of the underlying biological mechanisms [63]. There should be a powerful combination of theoretical model developments and extensive experimental approaches to fill this gap in the field. There are different methodologies developed and used experimentally to mechanically stimulate a single or a group of cells in the

7
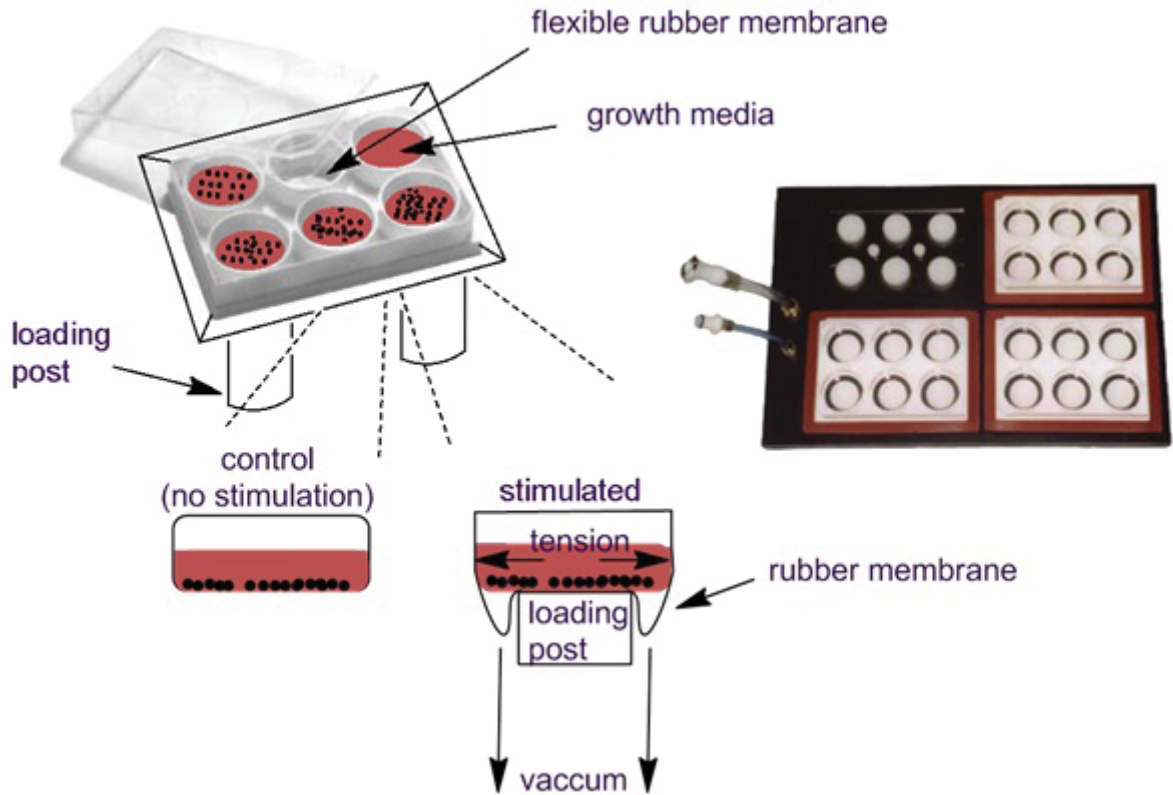
Figure 1.3: Mechanical stimulation of adherent cells (represented by the black dots) using a commercially available Flex-cell system. Shown are the basic operational principle and the actual 6 well plates used to exert strains.

study of mechanotransduction [64]. Examples of such methods are atomic force microscopy [65], hydrostatic compression [66], platen compression [67], optical tweezers [68], magnetic tweezers [69], viscometers [70] and flow chambers [71]. In this work, an equi-biaxial strain application system [72] has been utilized (see Fig.1.3). In this system, cells are plated on a circular flexible m e mbrane w h ich c a n b e s t rained in both the radial and circumferential directions. Both the radial and circumferential components of the strains are constant. This is achieved by confining the membrane at its boundary and keeping it in-plane during the stretching. In this system, cells

8

are plated on a circular flexible membrane which can be strained in both the radial and circumferential directions. Both the radial and circumferential components of the strains are constant by making the membrane to be confined on its periphery and is stretched by keeping it to stay in plane. Although it can not be fully achieved experimentally, I briefly show below (with a few assumptions) the theoretical proof that this stress is indeed equi-biaxial.

For a membrane in state of plane stress, the equilibrium equations are given in cylinderical coordinates as [73]:

$$\frac{\partial \sigma_r}{\partial r} + \frac{1}{r}\frac{\partial \tau_{r\theta}}{\partial \theta} + \frac{\sigma_r - \sigma_\theta}{r} = 0 \tag{1.1}$$

$$\frac{1}{r}\frac{\partial \sigma_\theta}{\partial \theta} + \frac{\partial \tau_{r\theta}}{\partial r} + \frac{2\tau_{r\theta}}{r} = 0 \tag{1.2}$$

Where σ_r and σ_θ are the riadial and circumferential stresses and $\tau_{r\theta}$ is a shear stress component that acts on the radial surface in the circumferential direction.

In order to show that the membrane stress field is equibiaxial. A stress function ($\Phi(r,\theta)$) can be introduced which satisfy the equlibrium equations above when the normal force to the plane of the membrane is zero by setting its components (the stress components in radial and circumferential directions) as [74]:

$$\sigma_r = \frac{1}{r}\frac{\partial \Phi}{\partial r} + \frac{1}{r^2}\frac{\partial^2 \Phi}{\partial \theta^2} \tag{1.3}$$

$$\sigma_\theta = \frac{\partial^2 \Phi}{\partial r^2} \tag{1.4}$$

$$\tau_{r\theta} = \frac{1}{r^2}\frac{\partial \Phi}{\partial \theta} - \frac{1}{r}\frac{\partial^2 \Phi}{\partial r \partial \theta} \tag{1.5}$$

9

Using this function Φ, a single partial differential equation can be written which can be used to solve the two dimentional stress field. Assuming that the membrane elasticity is not altered after strain application (the displacement field is continuous), which satisfies the compatibility condition. We can write the compatibility equation in cylindrical coordinates as:

$$\nabla^4\Phi = \left(\frac{\partial^2}{\partial r^2} + \frac{1}{r}\frac{\partial}{\partial r} + \frac{1}{r^2}\frac{\partial^2}{\partial\theta^2}\right)\left(\frac{\partial^2\Phi}{\partial r^2} + \frac{1}{r}\frac{\partial\Phi}{\partial r} + \frac{1}{r^2}\frac{\partial^2\Phi}{\partial\theta^2}\right) = 0 \qquad (1.6)$$

Since the strain applicaion keeps the rotational symmetry of the wells during stretching, the stress depends only on r ($\frac{\partial^2\Phi}{\partial\theta^2} = 0$). Which simplifies eqn.1.6 to have one independent varaible:

$$\nabla^4\Phi = \left(\frac{\partial^2}{\partial r^2} + \frac{1}{r}\frac{\partial}{\partial r}\right)\left(\frac{\partial^2\Phi}{\partial r^2} + \frac{1}{r}\frac{\partial\Phi}{\partial r}\right) = 0 \qquad (1.7)$$

$$= \frac{\partial^4\Phi}{\partial r^4} + \frac{2}{r}\frac{\partial^3\Phi}{\partial^3} - \frac{1}{r2}\frac{\partial^2\Phi}{\partial r^2} + \frac{1}{r3}\frac{\partial\Phi}{\partial r} = 0 \qquad (1.8)$$

The general solution of the differential equation becomes of the form $\Phi = A\ log(r) + B\ r^2\ log(r) + Cr^2 + D$ where A, B and C are the constants of the general solution which can be used to find a particular solution using boundary conditions. The stress components can be obtained by differentiating the general solution of the function:

$$\frac{\partial\Phi}{\partial r} = \frac{A}{r} + Br(1 + 2log(r)) + 2rC = r\sigma_r \qquad (1.9)$$

$$\frac{\partial^2\Phi}{\partial r^2} = -\frac{A}{r^2} + B(3 + 2log(r)) + 2C = \sigma_\theta \qquad (1.10)$$

But when $r = 0$, σ_r and σ_θ approach to infinity, which is infinite stress at the center of the membrane in the well and is physically impossible to have. Therefore

$$A = B = 0 \implies \sigma_r = \sigma_\theta = 2C \tag{1.11}$$

The stress is constant and equibiaxial in the radial and circumferential directions.

1.2.2 Forces cells exert on their environment

Not only does mechanosensing involve responses to external forces, but cells also use internally generated stresses to probe the mechanical properties of their environment and show a wide range of responses to extracellular stiffness [75]. As a continuation of the first part of my research, the relationships between the internal strains developed inside the cells with the traction forces cells exert on their environment has been studied and the method development on how this is done will be presented.

1.2.3 The membrane skeleton as a signal transducer

Traditionally the major parts of the cytoskeleton are considered to be the actin filaments, intermediate filaments, and microtubules including their regulatory and motor proteins [76]. Often neglected, however, is the part at the very edge of the cell, just beneath the plasma membrane as shown in Fig.1.4. This membrane skeleton and its components seem to have mechanical as well as biological functions. The spectrin based membrane skeleton provides scafolding for membrane proteins and anchors f-actin and associated proteins. It is directly connected to membrane proteins as well as lipids attached to the plasma membrane which in turn is exposed to environmental mechanical stimulations.

11

1.2.3.1 The erythroid membrane skeleton

Spectrin was named after the preparations of hemoglobin-free erythrocyte mem branes, also referred to as ghosts (specters). It was identified for its role in providing mechanical stability to erythrocytes in the absence of an extended actin cytoskeleton [34]. Instead, the supra-molecular spectrin tetramer determines the mechanical deformability of the red blood cells and its elasticity enables them to flow through narrow blood vessels. This protein complex is a heterotetramer composed of two head to head dimeric subunits arranged in anti-parallel fashion [77]. The heterotetramer is 200-260 nm in length and 3-6 nm in width forming intriguing geometric structures (**Fig.**1.5). Red blood cells consist of roughly $33,000$ protein hexagons and pentagons that looks like a microscopic geodesic dome [78].
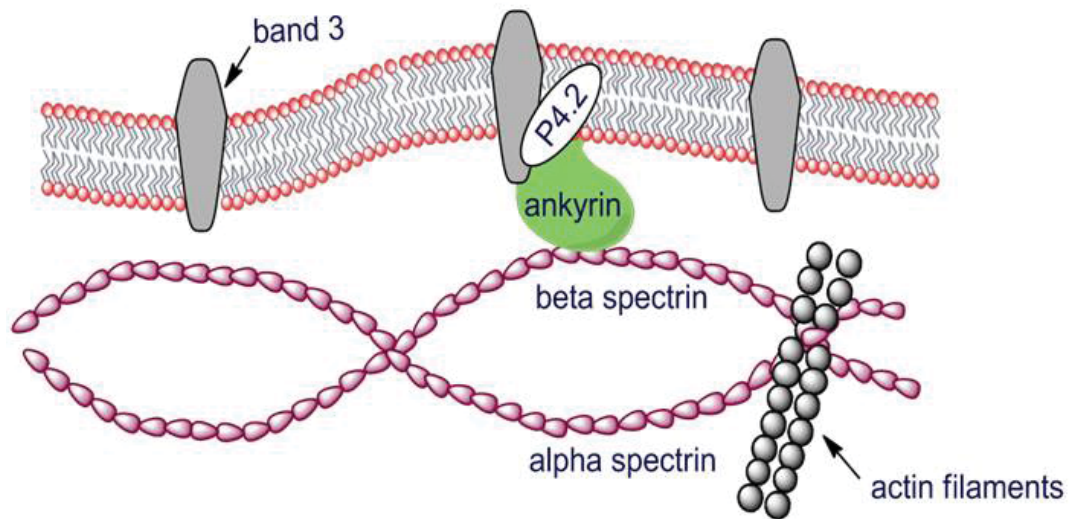
Figure 1.4: Major components of the erythroid membrane skeleton
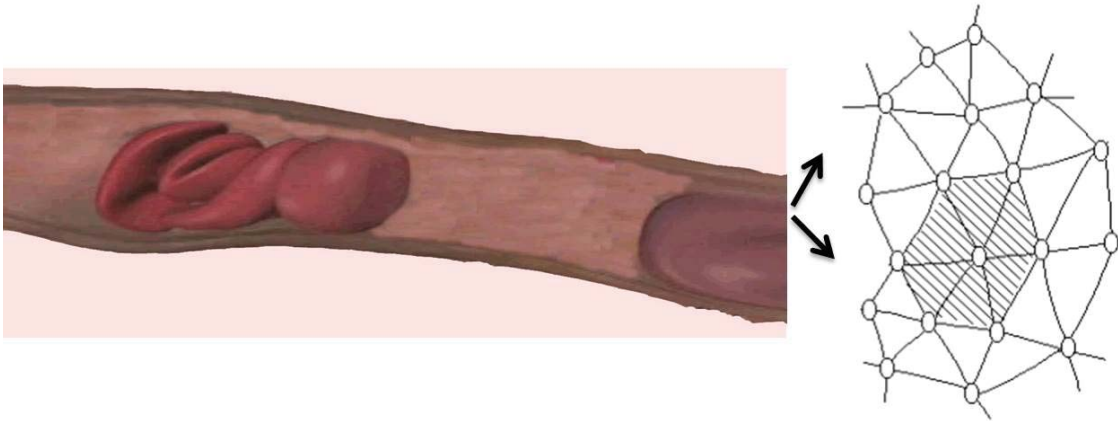
Figure 1.5: Importance of spectrin in deformability of erythroid cells important for blood flow through capillaries (left side). The cells' elasticity is a direct consequence of the intriguing hexagonal structures formed by the membrane skeleton as shown in the zoom in (right) [4].

1.2.3.2   The non-erythroid membrane skeleton

Initially, spectrin was considered to be exclusive to erythrocytes [79]. However, soon, non-erythrocyte isoforms also known as spectrin $\alpha - II$, brain spectrin [80], calspectin [81] or fodrin [82] were identified. Spectrin binds directly or indirectly to a large variety of proteins as shown in Fig.1.6, such as ankyrin -which anchors spectrins to the plasma membrane and a variety of its components [83] as well as actin [84], lipids [85], leading lamellae [86], tyrosine kinases [87], voltage-dependent sodium-channels [88], Tes and EVL [89], calmoduline [90], calpactin [91], and the membrane [92]. In non-erythrocytes no larger-scale organization beyond the spectrin tetramers has been identified so far.
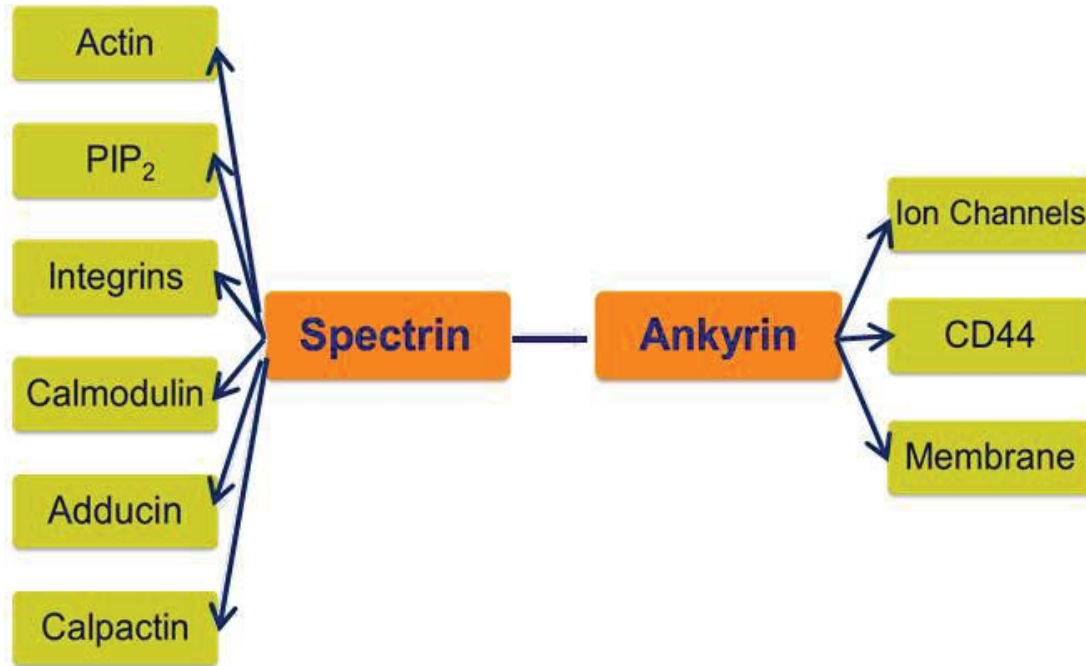
Figure 1.6: Spectrin acting as extensive scaffold for protein organization in nonery-throid cells

1.2.3.3 The spectrin repeat

On a molecular level Spectrins are composed of $17 - 23$ domains most of which are based on the spectrin motive (see fig.1.7) made up of 106 amino acid repeating se-quence of three antiparallel helixes that are connected with unstructured loops [93]. It has been shown that these spectrin repeats can act as a reversible springs, as the helixes align in a more linear fashion when forces pull on the repeat. The re-sulting spring constant is about 1700 pN/nm [94]. They can serve structural purposes, by coordination of cytoskeletal interactions with high spatial precision, as well as a switchboard for interactions with multiple proteins with a more regulatory role

14

[95]. They are also important interaction sites for multiple structural and signaling proteins [96]. The binding properties of the repeats perform important roles in the biology of the proteins where they are found, and lead to the assembly of complex, multi-protein structures involved both in cytoskeletal architecture as well as in forming large signal transduction complexes [97].
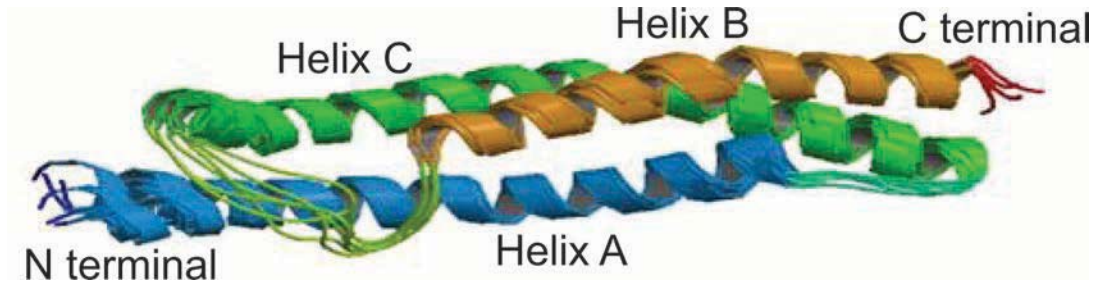
Figure 1.7: Spectrin repeat's tri-helical structure [PDB]

1.2.4 Ubiquitination as a cellular response

There are different biochemical responses to the received and transmitted mechanical signals. In the first part of experiments described in this work, there was a focus on ubiquitination for reasons that will be discussed in detail in chapter two. Ubiquitination is a posttranslational modification like phosphorylation which is very important for homeostasis [98]. The ubiquitously presented small protein ubiquitin can be attached to substrate proteins as a single moiety or in the form of polymeric chains in which successive ubiquitin molecules are connected through specific iso-peptide bonds. The majority of intracellular proteins are degraded by the ubiquitin (Ub)-proteasome pathway (UPP) [99]. Degradation of a protein via the ubiquitin-proteasome pathway involves two discrete and successive steps. First, the substrate

is tagged by the attachment of multiple ubiquitin molecules, a process that is facilitated by E1 ubiquitin activating, E2 ubiquitin conjugating and E3 ubiquitin ligating enzymes. In the second step, the tagged protein is then degraded by the 26S proteasome complex which results in free and reusable ubiquitin [100].
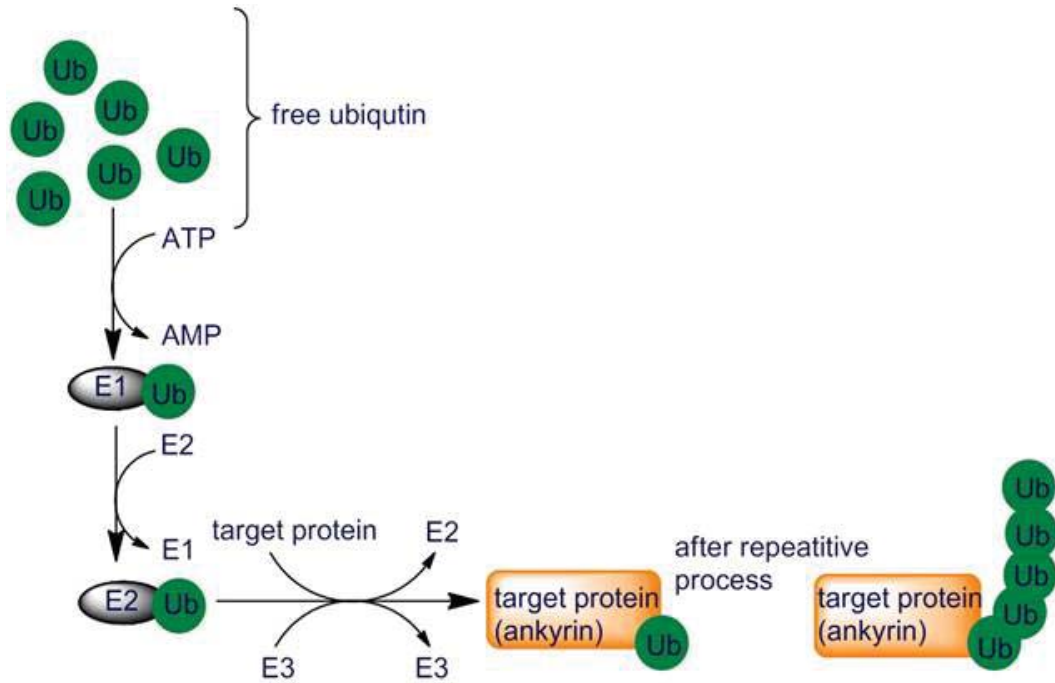
Figure 1.8: Schematic of polyubiquitination of a target protein (here ankyrin). Free ubiquitin is first bound by the E1 ubiquitin activating enzyme and then transferred to the target via the E2 ubiquitin conjugating and then E3 ubiquitin ligating enzymes.

1.3 References

1) Brighton, C.T., et al., Activation of the Phosphoinositide Cascade in the Proliferation Response of Rat Calvarial Bone-Cells Exposed to a Capacitively Coupled Electrical-Field. Electromagnetics in Medicine and Biology, 1991: p. 105-110.

2) Brooks, A.R., P.I. Lelkes, and G.M. Rubanyi, Gene expression profiling of vascular endothelial cells exposed to fluid mechanical forces: Relevance for focal susceptibility to atherosclerosis. Endothelium-Journal of Endothelial Cell Research, 2004. 11(1): p. 45-57.

3) Tanioka, N., S. Sawada, and T. Hosokawa, Proliferative and metastatic activities of mouse tumor cells exposed to a strong static magnetic field. Bioelectrochemistry and Bioenergetics, 1996. 40(1): p. 29-34.

4) Engineering, J.S.o., Scientists discover secret behind human red blood cell's amazing flexibility http://www.jacobsschool.ucsd.edu/uploads/news_release/2005/Squeezing.jpg, October 21, 2005

5) Bongrazio, M., et al., Evidence for modulation of genes involved in vascular adaptation by prolonged exposure of endothelial cells to shear stress. Cardiovascular Research, 2000. 47(2): p. 384-393.

6) Hirsch, J., et al., Increased Susceptibility to Mechanical Stretch Injury after Tobacco Smoke Exposure in Rat Alveolar Type II Cells. American Journal of Respiratory and Critical Care Medicine, 2009. 179.

7) Landau, J.V. and J.H. Mcalear, Micromorphology of F1 and Primary Human Amnion Cells Following Exposure to High Hydrostatic Pressure. Cancer Research, 1961. 21(6): p. 812-&.

8) Haberstroh, K.M., et al., A novel in-vitro system for the simultaneous exposure of bladder smooth muscle cells to mechanical strain and sustained hydrostatic pressure. Journal of Biomechanical Engineering-Transactions of the Asme, 2002. 124(2): p. 208-213.

9) Takahashi, S., et al., Increased levels of UV-induced protease activity in human UVAP-1 cells exposed to gravity-changing stress: involvement of E-64-sensitive proteases in suppression of UV mutagenicity. Cell Biology International, 2003. 27(1): p. 53-60.

10) Ravasio, A., et al., Alveolar cells sense the air-liquid interface and protect the lung from surface forces. A microscopic study. Biophysical Journal, 2007: p. 598a-598a.

11) Lehoux, S., Y. Castier, and A. Tedgui, Molecular mechanisms of the vascular responses to haemodynamic forces. Journal of Internal Medicine, 2006. 259(4): p. 381-392.

12) Sackmann, E. and S. Goennenwein, Cell adhesion as dynamic interplay of lock-and-key, generic and elastic forces. Progress of Theoretical Physics Supplement, 2006(165): p. 78-99.

13) Basson, M.D., An intracellular signal pathway that regulates cancer cell adhesion in response to extracellular forces. Cancer Research, 2008. 68(1): p. 2-4.

14) Davies, P.F., A. Robotewskyj, and M.L. Griem, Quantitative Studies of Endothelial-Cell Adhesion - Directional Remodeling of Focal Adhesion Sites in Response to Flow Forces. Journal of Clinical Investigation, 1994. 93(5): p. 2031-2038.

15) Pietramaggiori, G., et al., Tensile forces stimulate vascular remodeling and epidermal cell proliferation in living skin. Annals of Surgery, 2007. 246(5): p. 896-902.

16) Kaiser, D., et al., Apoptosis induced by lack of hemodynamic forces is a general endothelial feature even occuring in immortalized cell lines. Endothelium-New York, 1999. 6(4): p. 325-334.

17) Cattin, M.E., et al., Degradation of delK32-lamin by the ubiquitin-proteasome system partially protects against force impairment in engineered heart tissue. Cardiovascular Research, 2012. 93: p. S67-S67.

18) Eastwood, M., D.A. McGrouther, and R.A. Brown, Fibroblast responses to mechanical forces. Proceedings of the Institution of Mechanical Engineers Part H-Journal of Engineering in Medicine, 1998. 212(H2): p. 85-92.

19) Ingber, D.E., Tensegrity: The architectural basis of cellular mechanotransduction. Annual Review of Physiology, 1997. 59: p. 575-599.

20) Ingber, D.E., Cellular mechanotransduction: putting all the pieces together again. Faseb Journal, 2006. 20(7): p. 811-827.

21) Javadi, Y., J.M. Fernandez, and R. Perez-Jimenez, Protein Folding Under Mechanical Forces: A Physiological View. Physiology, 2013. 28(1): p. 9-17.

22) Liu, C.J., et al., Single-chain mechanical property of poly(N-vinyl-2-pyrrolidone) and interaction with small molecules. Journal of Physical Chemistry B, 2005. 109(31): p. 14807-14812.

23) Coste, B., Feeling the pressure? Identification of two proteins activated by mechanical forces. M S-Medecine Sciences, 2011. 27(1): p. 17-19.

24) Sudhir, K., et al., Mechanical strain stimulates a mitogenic response in coronary vascular smooth muscle cells via release of basic fibroblast growth factor. Am J Hypertens, 2001. 14(11 Pt 1): p. 1128-34.

25) Burridge, K. and E.S. Wittchen, The tension mounts: Stress fibers as force-generating mechanotransducers. Journal of Cell Biology, 2013. 200(1): p. 9-19.

26) Morris, C.E., Are Stretch-Sensitive Channels in Molluscan Cells and Elsewhere Physiological Mechanotransducers. Experientia, 1992. 48(9): p. 852-858.

27) Gortazar, A.R., et al., Crosstalk between Caveolin-1/Extracellular Signal-regulated Kinase (ERK) and beta-Catenin Survival Pathways in Osteocyte Mechanotransduction. Journal of Biological Chemistry, 2013. 288(12): p. 8168-8175.

28) Katz, S., R. Boland, and G. Santillan, Modulation of ERK 1/2 and p38 MAPK signaling pathways by ATP in osteoblasts: Involvement of mechanical stress-activated calcium influx, PKC and Src activation. International Journal of Biochemistry & Cell Biology, 2006. 38(12): p. 2082-2091.

29) Liu, D. and R.L. Duncan, MAPK and GSK signaling pathways are involved in the mechanical responses of cementoblasts to fluid shear stress. Journal of Bone and Mineral Research, 2005. 20(9): p. S240-S240.

30) Kim, M., et al., Mechanical stimulation activates G alpha q signaling pathways and 5-hydroxytryptamine release from human carcinoid BON cells. Journal of Clinical Investigation, 2001. 108(7): p. 1051-1059.

31) Mofrad, M.R.K., Exploring Cellular Mechanotransduction at the Focal Adhesions, One Molecule at a Time. Biophysical Journal, 2011. 100(3): p. 447-447.

32) Mills, J.W. and L.J. Mandel, Cytoskeletal Regulation of Membrane-Transport Events. Faseb Journal, 1994. 8(14): p. 1161-1165.

33) Krebs, J., et al., The regulation of the calcium signal by membrane pumps. Helvetica Chimica Acta, 2003. 86(11): p. 3875-3888.

34) Bennett, V., Spectrin-Based Membrane Skeleton - a Multipotential Adapter between Plasma-Membrane and Cytoplasm. Physiological Reviews, 1990. 70(4): p. 1029-1065.

35) Lelievre, S.A. and M.J. Bissell, Communication between the cell membrane and the nucleus: Role of protein compartmentalization. Journal of Cellular Biochemistry, 1998: p. 250-.

36) Luna, E.J. and A.L. Hitt, Cytoskeleton Plasma-Membrane Interactions. Science, 1992. 258(5084): p. 955-963.

37) Shao, Y., et al., Global architecture of the F-actin cytoskeleton regulates cell shape-dependent endothelial mechanotransduction. Integrative Biology, 2014. 6(3): p. 300-311.

38) Howard, J., Mechanical-to-chemical transduction by motor proteins. Biophysics of the Cochlea: From Molecules to Models, 2003: p. 37-46.

39) VanEngelenhoven, J., D.M. Shasby, and A.B. Moy, Microtubules shift load-bearing mechanical forces in cultured endothelial cells. Molecular Biology of the Cell, 1996. 7: p. 3345-3345.

40) Seong, J., N. Wang, and Y.X. Wang, Mechanotransduction at focal adhesions: from physiology to cancer development. Journal of Cellular and Molecular Medicine, 2013. 17(5): p. 597-604.

41) Sako, Y. and A. Kusumi, Compartmentalized Structure of the Plasma-Membrane for Receptor Movements as Revealed by a Nanometer-Level Motion Analysis. Journal of Cell Biology, 1994. 125(6): p. 1251-1264.

42) Morone, N., et al., Three-dimensional reconstruction of the membrane skeleton by electron tomography reveals its association with the plasma membrane restricting the diffusion of membrane molecules. Biophysical Journal, 2007: p. 92a-93a.

43) Ronan, D. and P. Gillespie, Metazoan mechanotransduction mystery finally solved. Nature Neuroscience, 2005. 8(1): p. 7-8.

44) Huang, H.D., R.D. Kamm, and R.T. Lee, Cell mechanics and mechanotransduction: pathways, probes, and physiology. American Journal of Physiology-Cell Physiology, 2004. 287(1): p. C1-C11.

45) Ko, K.S. and C.A.G. McCulloch, Intercellular mechanotransduction: Cellular circuits that coordinate tissue responses to mechanical loading. Biochemical and Biophysical Research Communications, 2001. 285(5): p. 1077-1083.

46) DuFort, C.C., M.J. Paszek, and V.M. Weaver, Balancing forces: architectural control of mechanotransduction. Nature Reviews Molecular Cell Biology, 2011. 12(5): p. 308-319.

47) Bruscolini, P., A. Pelizzola, and M. Zamparo, Downhill versus two-state protein folding in a statistical mechanical model. Journal of Chemical Physics, 2007. 126(21).

48) Abe, H. and H. Wako, Analyses of simulations of three-dimensional lattice proteins in comparison with a simplified statistical mechanical model of protein folding. Physical Review E, 2006. 74(1).

49) Abe, H. and H. Wako, Application of a statistical mechanical model for protein folding to a three-dimensional lattice protein. Journal of the Physical Society of Japan, 2004. 73(5): p. 1143-1146.

50) Jaitovich, A., et al., Ubiquitin-proteasome-mediated degradation of keratin intermediate filaments in mechanically stimulated A549 cells. Journal of Biological Chemistry, 2008. 283(37): p. 25348-25355.

51) Cieplak, M., T.X. Hoang, and M.O. Robbins, Thermal folding and mechanical unfolding pathways of protein secondary structures. Proteins-Structure Function and Genetics, 2002. 49(1): p. 104-113.

52) Iguchi, K., Statistical mechanical foundation for the two-state transition in protein folding of small globular proteins. International Journal of Modern Physics B, 2002. 16(13): p. 1807-1839.

53) Natoli, R.M., C.C. Scott, and K.A. Athanasiou, Temporal effects of impact on articular cartilage cell death, gene expression, matrix biochemistry, and biomechanics. Annals of Biomedical Engineering, 2008. 36(5): p. 780-792.

54) Bastolla, U., M. Vendruscolo, and E.W. Knapp, A statistical mechanical method to optimize energy functions for protein folding. Proceedings of the National Academy of Sciences of the United States of America, 2000. 97(8): p. 3977-3981.

55) Barakat, A.I., Responsiveness of vascular endothelium to shear stress: Potential role of ion channels and cellular cytoskeleton (review). International Journal of Molecular Medicine, 1999. 4(4): p. 323-332.

56) Pietsch, J., et al., Interaction of Proteins Identified in Human Thyroid Cells. International Journal of Molecular Sciences, 2013. 14(1): p. 1164-1178.

57) Lewalle, A. and K.H. Parker, Axisymmetric Optical-Trap Measurement of Red Blood Cell Membrane Elasticity. Journal of Biomechanical Engineering-Transactions of the Asme, 2011. 133(1).

58) Liu, Y.S.A. and O.K. Lee, In Search of the Pivot Point of Mechanotransduction: Mechanosensing of Stem Cells. Cell Transplantation, 2014. 23(1): p. 1-11.

59) Azuma, N., et al., Endothelial cell response to different mechanical forces. Journal of Vascular Surgery, 2000. 32(4): p. 789-794.

60) Gillespie, P.G. and R.G. Walker, Molecular basis of mechanosensory transduction. Nature, 2001. 413(6852): p. 194-202.

61) Nakayama, K., [Mechanotransduction and cellular response--a challenge toward development of mechano-pharmacology]. Yakugaku Zasshi-Journal of the Pharmaceutical Society of Japan, 2006. 126(8): p. 565-77.

62) Nelson, C.M., Bioengineering and mechanobiology: pushing (and pulling) the limits of cellular mechanics. Molecular Biology of the Cell, 2012. 23(6): p. 969-969.

63) Franz, T. and B.D. Reddy, Numerical studies of problems in biophysics, biomechanics and mechanobiology. International Journal for Numerical Methods in Biomedical Engineering, 2012. 28(1): p. 1-2.

64) Van Vliet, K.J., G. Bao, and S. Suresh, The biomechanics toolbox: experimental approaches for living cells and biomolecules. Acta Materialia, 2003. 51(19): p. 5881-5905.

65) Charras, G. and M.A. Horton, Cellular mechanotransduction and its modulation: An Atomic Force Microscopy study. Biophysical Journal, 2001. 80(1): p. 305a-306a.

66) Tasevski, V., et al., Influence of mechanical and biological signals on gene expression in human MG-63 cells: evidence for a complex interplay between hydrostatic compression and vitamin D3 or TGF-beta 1 on MMP-1 and MMP-3 mRNA levels. Biochemistry and Cell Biology-Biochimie Et Biologie Cellulaire, 2005. 83(1): p. 96-107.

67) Kisiday, J.D., et al., Dynamic Compression Stimulates Proteoglycan Synthesis by Mesenchymal Stem Cells in the Absence of Chondrogenic Cytokines. Tissue Engineering Part A, 2009. 15(10): p. 2817-2824.

68) Singer, W., S. Bernet, and M. Ritsch-Marte, 3D-force calibration of optical tweezers for mechanical stimulation of surfactant-releasing lung cells. Laser Physics, 2001. 11(11): p. 1217-1223.

69) Sniadecki, N.J., Minireview: A Tiny Touch: Activation of Cell Signaling Pathways with Magnetic Nanoparticles. Endocrinology, 2010. 151(2): p. 451-457.

70) Purvis, N.B., Jr. and T.D. Giorgio, The effects of elongational stress exposure on the activation and aggregation of blood platelets. Biorheology, 1991. 28(5): p. 355-67.

71) Huesa, C., M.H. Helfrich, and R.M. Aspden, Parallel-plate fluid flow systems for bone cell stimulation. Journal of Biomechanics, 2010. 43(6): p. 1182-1189.

72) Chung, E., et al., Peyronie's Disease and Mechanotransduction: An In Vitro Analysis of the Cellular Changes to Peyronie's Disease in a Cell-Culture Strain System. Journal of Sexual Medicine, 2013. 10(5): p. 1259-1267.

73) C., E.R. and C.A. Simmons, Introductory biomechanics: From cells to organisms 1ed. Cambridge Texts in Biomedical Engineering 2007. p. 76-86.

74) Timoshenko, S. and J.N. Goodier, Theory of Elasticity 1970, New York McGraw-Hill.

75) Gershlak, J.R., et al., Mesenchymal stem cells ability to generate traction stress in response to substrate stiffness is modulated by the changing extracellular matrix composition of the heart during development. Biochemical and Biophysical Research Communications, 2013. 439(2): p. 161-166.

76) Wen, Q. and P.A. Janmey, Polymer physics of the cytoskeleton. Current Opinion in Solid State & Materials Science, 2011. 15(5): p. 177-182.

77) An, X.L., et al., Inter-subunit interactions in erythroid and non-erythroid spectrins. Biochimica Et Biophysica Acta-Proteins and Proteomics, 2011. 1814(3): p. 420-427.

78) Bennett, V. and J. Healy, Organizing the fluid membrane bilayer: diseases linked to spectrin and ankyrin. Trends Mol Med, 2008. 14(1): p. 28-36.

79) Hiller, G. and K. Weber, Spectrin Is Absent in Various Tissue-Culture Cells. Nature, 1977. 266(5598): p. 181-183.

80) Oh, Y. and L.W.M. Fung, Brain proteins interacting with the tetramerization region of non-erythroid alpha spectrin. Cellular & Molecular Biology Letters, 2007. 12(4): p. 604-620.

81) Morimoto, K., et al., Binding-Sites of Calmodulin and Actin on the Brain Spectrin, Calspectin. Neurochemical Research, 1984. 9(8): p. 1124-1125.

82) Kanda, K., T. Tanaka, and K. Sobue, Calspectin (Fodrin or Nonerythroid Spectrin)-Actin Interaction - a Possible Involvement of 4.1-Related Protein. Biochemical and Biophysical Research Communications, 1986. 140(3): p. 1051-1058.

83) Lubman, O.Y., S.V. Korolev, and R. Kopan, Anchoring Notch genetics and biochemistry: Structural analysis of the ankyrin domain sheds light on existing data. Molecular Cell, 2004. 13(5): p. 619-626.

84) Lux, S.E., K.M. John, and B. Pease, Functional Heterogeneity of Spectrin - Effect on Interactions with Actin. Federation Proceedings, 1978. 37(6): p. 1507-1507.

85) O'Toole, P.J., I.E.G. Morrison, and R.J. Cherry, Investigations of spectrin-lipid interactions using fluoresceinphosphatidylethanolamine as a membrane probe. Biochimica Et Biophysica Acta-Biomembranes, 2000. 1466(1-2): p. 39-46.

86) Merilainen, J., et al., Binding of the Alpha-Fodrin Sh3 Domain to the Leading Lamellae of Locomoting Chicken Fibroblasts. Journal of Cell Science, 1993. 105: p. 647-654.

87) Ziemnicka-Kotula, D., et al., Identification of a candidate human spectrin Src homology 3 domain-binding protein suggests a general mechanism of association of tyrosine kinases with the spectrin-based membrane skeleton. Journal of Biological Chemistry, 1998. 273(22): p. 13681-13692.

88) Srinivasan, Y., et al., Ankyrin and Spectrin Associate with Voltage-Dependent Sodium-Channels in Brain. Nature, 1988. 333(6169): p. 177-180.

89) Rotter, B., et al., alpha II-Spectrin interacts with Tes and EVL, two actin-binding proteins located at cell contacts. Biochemical Journal, 2005. 388: p. 631-638.

90) Burns, N.R. and W.B. Gratzer, Interaction of calmodulin with the red cell and its membrane skeleton and with spectrin. Biochemistry, 1985. 24(12): p. 3070-4.

91) Cheney, R.E. and M.B. Willard, Characterization of the interaction between calpactin I and fodrin (non-erythroid spectrin). Journal of Biological Chemistry, 1989. 264(30): p. 18068-75.

92) Bennett, V., J. Davis, and W.E. Fowler, Brain spectrin, a membrane-associated protein related in structure and function to erythrocyte spectrin. Nature, 1982. 299(5879): p. 126-31.

93) Djinovic-Carugo, K., et al., The spectrin repeat: a structural platform for cytoskeletal protein assemblies. Febs Letters, 2002. 513(1): p. 119-123.

94) Paramore, S., et al., Extending a spectrin repeat unit. I: Linear force-extension response. Biophysical Journal, 2006. 90(1): p. 92-100.

95) Djinovic-Carugo, K., et al., The spectrin repeat: a structural platform for cytoskeletal protein assemblies. Febs Letters, 2002. 513(1): p. 119-23.

96) An, X., et al., Phospholipid binding by proteins of the spectrin family: a comparative study. Biochem Biophys Res Commun, 2005. 327(3): p. 794-800.

97) Sonnenberg, A., A.M. Rojas, and J.M. de Pereda, The structure of a tandem pair of spectrin repeats of plectin reveals a modular organization of the plakin domain. J Mol Biol, 2007. 368(5): p. 1379-91.

98) Shibata, S., et al., Kelch-like 3 and Cullin 3 regulate electrolyte homeostasis via ubiquitination and degradation of WNK4. Proc Natl Acad Sci U S A, 2013. 110(19): p. 7838-43.

99) Lecker, S.H., A.L. Goldberg, and W.E. Mitch, Protein degradation by the ubiquitin-proteasome pathway in normal and disease states. Journal of the American Society of Nephrology, 2006. 17(7): p. 1807-1819.

100)   Glickman, M.H. and A. Ciechanover, The ubiquitin-proteasome proteolytic pathway: Destruction for the sake of construction. Physiological Reviews, 2002. 82(2): p. 373-428.

Chapter 2

Quantitation of force induced changes in the non-erythroid membrane skeleton

2.1 Abstract

Unlike the spectrin based membrane skeleton of red blood cells, its non-erythroid counterpart has overall seen very little attention. It is however assumed that the non-erythrocytes, membrane skeleton is mostly composed of heterotetramers of $\alpha - II$ and $\beta - II$ spectrins. Because of a suspected role of $\alpha - I$ and $\alpha - II$ spectrins as mechanotransducers via a stretch dependent exposure of a E2/E3 ubiquitinating site for self ubiquitination, there was an interest to investigate the effect of mechanical stimulation, on the spectrin-ankyrin-B membrane skeleton of $NIH3T3$ mouse embryonic fibroblasts and $C3H10T\frac{1}{2}$ pluripotent stem cells. Using a combination of

quantitative fluorescence microscopy and biochemical techniques, I have measured and determined that before stimulation the spectrins and ankyrin-B are highly abundant, making up more than 10% of cytosolic and membrane protein thus constituting a significant part of the membrane skeleton. Both cell types contain actually all four major isoforms of spectrin. However, while $\alpha - II$ spectrin is indeed the dominant α-spectrin isoform in $3T3$ cells, it is found that in $10T\frac{1}{2}$ cells, it is $\alpha - I$ spectrin. Also, at least half of the $\alpha-$spectrins do not have $\beta-$spectrin counterparts and thus can not possibly organize in heterotetramers. Mechanical stimulation decreases the overall spectrin amount by up to 60%, while ankyrin-B abundance increases by up to 30%. The compositions of the spectrin pools change with a significant decrease of the dominant $\alpha-$spectrin isoforms. The fraction of polyubiquitinated spectrin actually increases, which at least in part can account for the reduction in spectrins and is in line with the proposed mechanically enhanced ubiquitination activity of $\alpha-$spectrins.

2.2   Significance

The proteinous structure underneath the plasma membrane, called the membrane skeleton, has only been studied to a limited extent in non-red blood cells, compared to its counterpart in erythrocytes, despite its undisputed biological importance. This study reveals that in widely used cell lines the non-erythroid membrane skeleton and its main components are vastly abundant and constitute a major portion of the cells protein. Evidence is also presented that indicates that the assumed organization of the skeleton is not sufficient to explain the observed composition of the different

spectrins. The application of mechanical stimulation to the cells leads to drastic changes in the membrane skeleton that seem to point towards an active role of spectrins in force sensing.
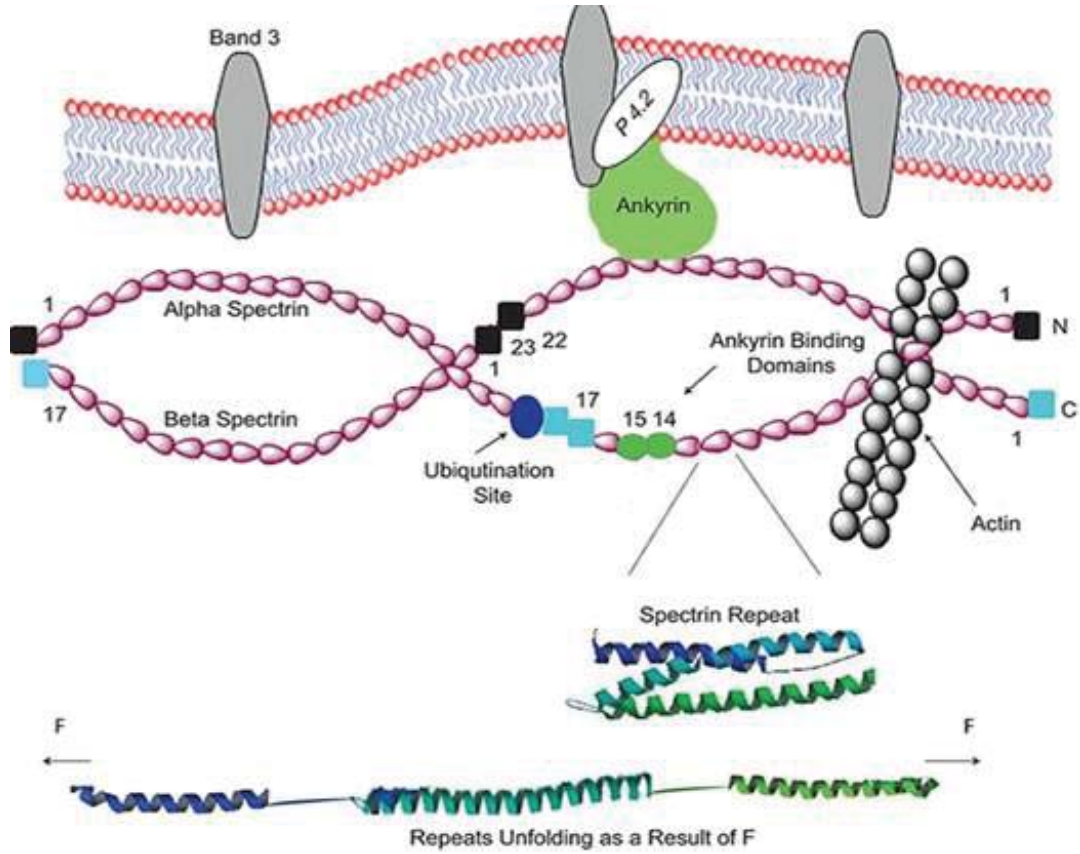
Figure 2.1: Functional domains of the spectrin tetramer showing that each dimer is formed by one $\alpha - II$ and one $\beta - II$ spectrin units built with the tri-helical spectrin repeats that unfolds as a result of mechanical force.

2.3 Introduction

The spectrin membrane skeleton in non-erythrocytes has been much less studied compared to the erythroid and specialized cells. However, in general it is assumed

26

that spectrins underneath the cellular plasma membrane of non-erythrocytes, also organize in tetramers where each dimer is formed by one $\alpha - II$ and one $\beta - II$ spectrins [1, 2]. This non-erythroid membrane skeleton protects the plasma membrane [3], as well as helps accumulate proteins and organizes the membrane [4], for example coordinating ion exchangers [5, 6] adhesion molecules [7] and cytoskeletal elements [8]. Moreover, it is known that spectrin expression and regulation are important for fundamental cellular functions [9-12] and consequently, spectrin mutations lead to a variety of human diseases, such as certain forms of cardiac arrhythmia and spino-cerebellar ataxia [13] while knockdown of the non-erythroid $\alpha - II$ spectrin is in fact lethal [11]. Interestingly, one spectrin repeat in $\alpha - I$ spectrin has two active sites, each of which has a demonstrated combined ubiquitin-conjugating enzyme (E2) and ubiquitin ligase (E3) functionality, that act among other targets also on $\alpha - I$ spectrin itself [14]. As the sequence alignment of the non-erythroid $\alpha - II$ spectrin and the $\alpha - I$ spectrin of these sites shows (fig.2.2), the E2/E3 sites in $\alpha - I$ and $\alpha - II$
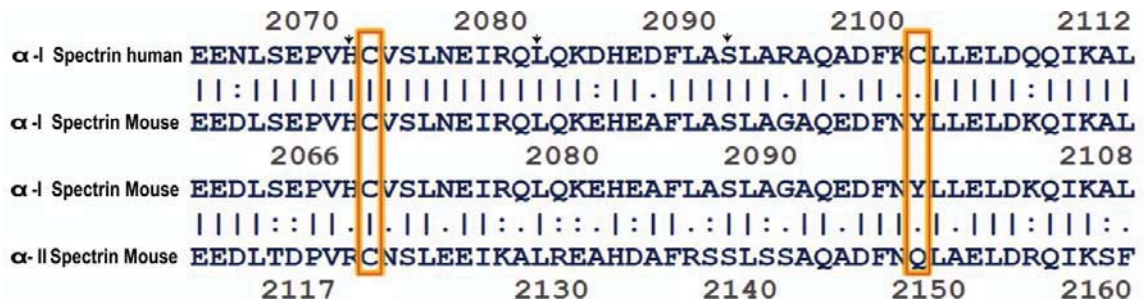
Figure 2.2: Sequence homology of the $E2/E3$ ubiquitination/ligation sites in human $\alpha - I$ spectrin and the murine $\alpha - I$ and $\alpha - II$ spectrins

spectrin are similar but not identical. Nevertheless, At least one of the sites is conserved in both the $\alpha - I$ and $\alpha - II$ spectrin of mice and each of the two Cysteine containing sites (Cys2071 and Cys2100) of human $\alpha - I$ spectrin is capable to act

as E2/E3 enzyme. Combining these facts, a picture emerges in which force induced restructuring and accessibility of the E2/E3 sites in $\alpha-$spectrins might render their mechano-sensitive activity. Because the affected polyubiquitination via the lysine 48 linkage marks proteins for proteasomal degradation [15, 16], there was an interest to investigate the effect of mechanical stimulation on the non-erythroid spectrin based membrane skeleton. Since they are widely used in mechanotransduction, the focus was on on NIH $3T3$ fibroblasts and the $10T\frac{1}{2}$ mesenchymal stem cell line and used a variety of biochemical and optical microscopy techniques, to investigate their membrane skeleton components before and after mechanical stimulation. Surprisingly, it has been found out that before stimulation the spectrins and ankyrin-B are highly abundant in these cell lines, making up more than 10% of membrane associated and cytosolic proteins and thus need to be considered a significant part of the non- erythrocyte cytoskeleton. Furthermore, both cell types carry in general all four major isoforms of spectrin but while in $3T3$, $\alpha-II$ spectrin dominates as expected, in $10T\frac{1}{2}$ cells the $\alpha-I$ isoform is the dominant $\alpha-$spectrin. For both cell lines, it is determined that at least half of the $\alpha-$spectrins do not have $\beta-$spectrin counterparts and can thus not be organized in the 'typical' heterotetramere. Furthermore, mechanical stimulation leads to a drastic reduction of spectrins in both cell types, while at the same time the amount of ankyrin-B increases. A more detailed analysis reveals that the composition of the respective spectrin pools changes with a significant decrease of the dominant $\alpha-$ spectrin isoform. Interestingly, the fraction of polyubiquitinated spectrin actually increases, which, at least in part, could account for the reduction in spectrin and at the same time is in line with a possible enhanced ubiquitination

activity of $\alpha-$spectrin due to mechanical stresses.

2.4 Results

To give a visual impression of the changes in spectrin and ankyrin-B abundance, 20% periodic strain is applied at a frequency of 1Hz for 24 hours, then fixed and immune-fluorescently stained. The representative fluorescence images in fig.2.3 provide an immediate visualization of some of the basic findings. In $3T3$ cells, exposure to mechanical stimulation results in a drastically reduced amount of spectrin (fig.2.3B) when compared to the non-stimulated control (fig.2.3A). Similarly, $10T\frac{1}{2}$ cells exhibit an equally significant reduction in spectrin content. In stark contrast is the amount of ankyrin-B that is detected in the two cell types after mechanical stimulation. In both cases much more ankyrin-B is present after they have been mechanically stimulated (fig.2.3 F and H) compared to the controls (fig.2.3 E and G, respectively). Through careful image acquisition and analysis, the ratio by which the overall content of spectrin and ankyrin-B is changed can be extracted in the two cell types. In $3T3$ cells, spectrin is reduced by $(55\pm7)\%$ while ankyrin-B is increased by $(31\pm2)\%$. Whereas in $10T\frac{1}{2}$ cells spectrin is reduced by $(62\pm8)\%$ while ankyrin-B is increased by $(26\pm3)\%$ (see fig.2.4). The molecular weights for the 4 dominant spectrin types, $\alpha-I$, $\alpha-II-$, $\beta-I$ and $\beta-II-$ spectrins are 268kDa, 285kDa, 252kDa and 259kDa respectively. Thus, on SDS-PAGE gels the different main spectrin isoforms can easily be identified once they have been purified from cell lysates using immunoprecipitation (IP). The resulting gels allow for a more detailed look at the changes in composition of the overall cellular spectrin pool. In addition, they can also been exploited to validate the
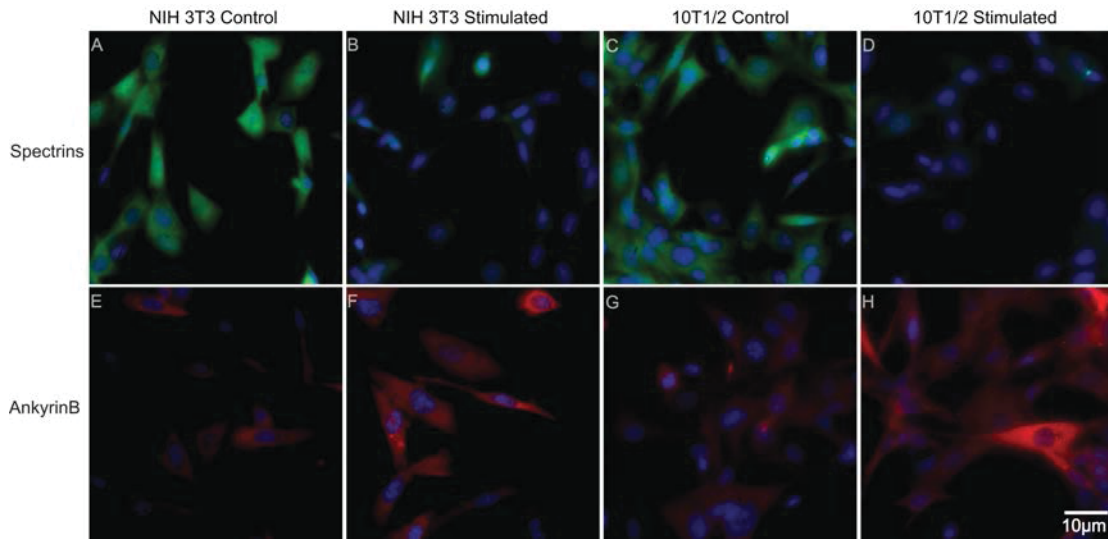
Figure 2.3: Quantitative fluorescence images of fixed and immune-stained cells, comparing mechanically stimulated and non-stimulated controls. Blue indicates the cells' nucleus visualized by DAPI staining of DNA. In the upper row the green fluorescent signal indicates the composition of spectrin. Clearly visible is the lower fluorescence signal from the mechanically stimulated $3T3$ and $10T\frac{1}{2}$ (B and D) when compared to their non-stimulated counterparts (A and C). In contrast, the red fluorescence signal indicating the presence of ankyrin-B has increased after mechanical stimulation (F and H) when compared to the $3T3$ (E) and $10T\frac{1}{2}$ (G) non-stimulated controls.
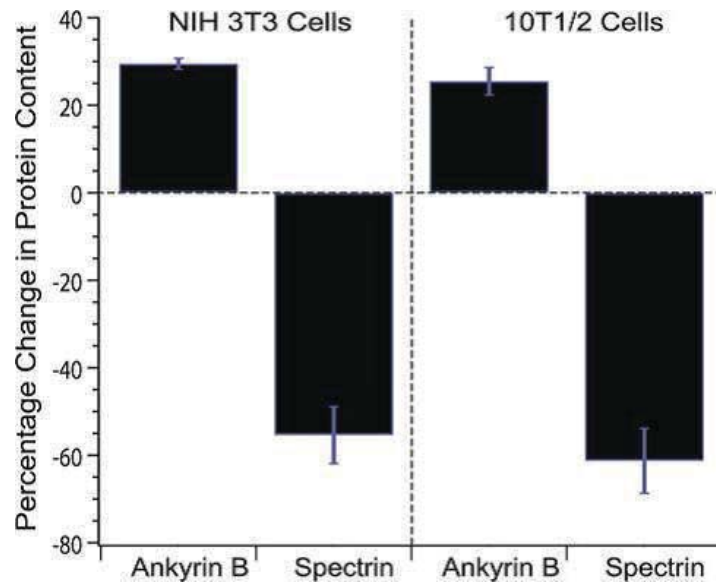
Figure 2.4: Percentage change in the composition of spectrins and ankyrin-B due to mechanical stimulation as assessed by quantitative fluorescence imaging. Left of the dashed line are the $3T3$ results, right of it the corresponding result from $C3H10T\frac{1}{2}$cells. The results are based on the signal from at least 300 cells per condition. The error bars are based on one standard deviation.
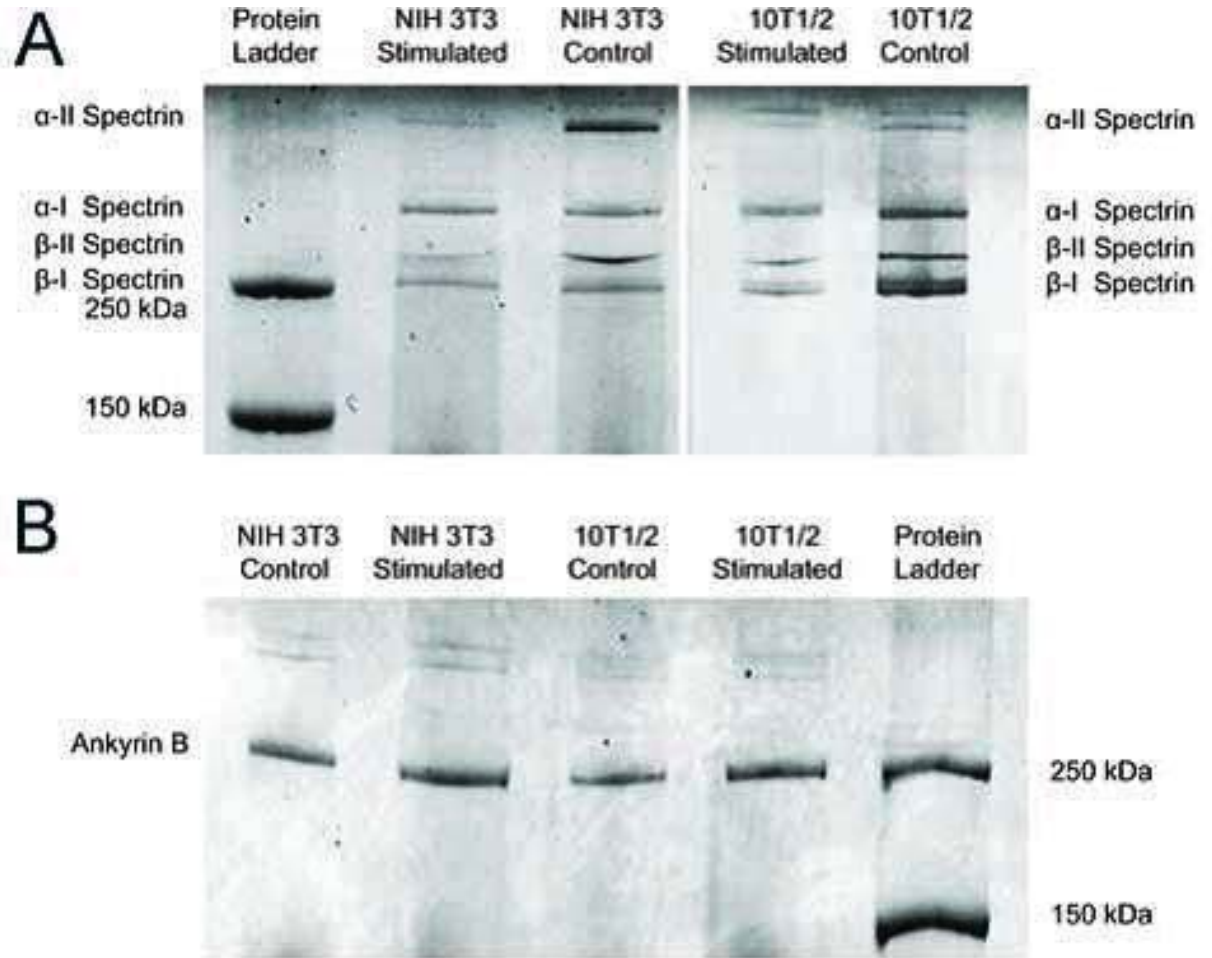
Figure 2.5: Spectrin and ankyrin B composition differences due to mechanical stimulation in $3T3$ and $10T\frac{1}{2}$ cells. A) Coomassie blue stained SDS-PAGE gel after immunoprecipitation with anti-spectrin antibody. B) Similar gel, but after immunoprecipitation with anti-ankyrin-B antibody.
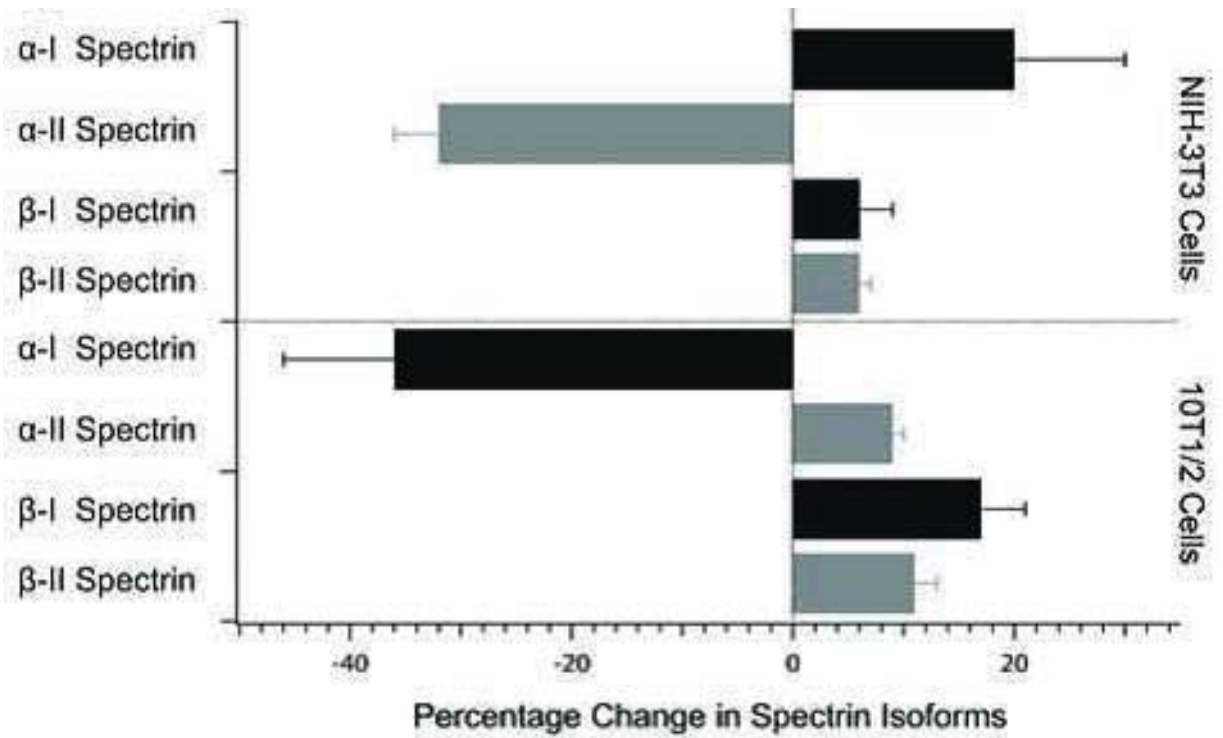
Figure 2.6: The signal from the bands in the gels was used to assess the percentage change in the different spectrin isoforms due to mechanical stimulation.

quantitative immunofluorescence based microscopy described above. Typical results for SDS-Page gels after the anti-spectrin IP are shown in fig.2.5A. A first thing to note is that the spectrin composition for the two cell types is already significantly different from each other even in the non-stimulated case, i.e. the controls in fig.2.5A. Careful analysis of the intensity of the bands in those $3T3$ and $10T\frac{1}{2}$ controls gives an overall spectrin composition for $3T3$ cells of $(32\pm6)\%\alpha-I$, $(42\pm4)\%\alpha-II$, $(10\pm2)\%\beta-I$ and $(16\pm7)\%\beta-II$ spectrins while for $10T\frac{1}{2}$s the corresponding percentages are $(79\pm9)\%$, $(0.4\pm0.1)\%$, $(8\pm3)\%$ and $(16\pm6)\%$. After mechanical stimulation, the composition of the spectrin pool changes to $(52\pm8)\%\alpha-I$, $(10\pm1)\%\alpha-II$, $(15\pm3)\%\beta-I$ and $(23\pm9)\%\beta-II$ spectrin for the 3T3 cells and $(38\pm4)\%$, $(9\pm1)\%$, $(25\pm3)\%$ and $(27\pm8)\%$ for $10T\frac{1}{2}$ cells. Within the spectrin pool of a particular cell type the relative changes are depicted in fig.2.6. Notably, a significant reduction of $\alpha-II$ spectrin for $3T3$ cells and $\alpha-I$ spectrin in the case of the $10T\frac{1}{2}$ cells is balanced by a relative increase in the other major spectrin isoforms. In order to turn the observed relative changes into absolute changes of particular spectrins and ankyrin-B in the studied cells it is necessary to measure absolute protein weights which is done in the next part of the experiment.

Table 2.1: Detailed changes in spectrin and ankyrin-B percentage compared to total protein contents and compositions due to mechanical stimulation in NIH 3T3 and $10T\frac{1}{2}$ cells as determined by Immunoprecipitation, SDS-PAGE gels and Bradford assays.

Cell type	Protein	Control			Stimulated		
		Measured protein content per cell $(10^{-12}g)$	Number of protein molecules per cell	Average percentage of total protein content	Measured protein content per cell $(10^{-12}g)$	Number of protein molecules per cell	Average percentage of total protein content
	All Spectrins	53 ± 5		7 ± 3	19 ± 6		3 ± 1
	$\alpha - II$ **Spectrin**	22 ± 2	$(48 \pm 5)x10^6$	3 ± 1	10 ± 3	$(21 \pm 6)x10^6$	1.2 ± 0.5
NIH $3T3$	$\alpha - I$ **Spectrin**	17 ± 2	$(37 \pm 4)x10^6$	2.1 ± 0.5	2.2 ± 0.5	$(4 \pm 1)x10^6$	0.3 ± 0.1
	$\beta - II$ **Spectrin**	9 ± 1	$(19 \pm 2)x10^6$	1.3 ± 0.3	5 ± 2	$(10 \pm 3)x10^6$	0.6 ± 0.1
	$\beta - II$ **Spectrin**	5 ± 0.5	$(13 \pm 2)x10^6$	0.6 ± 0.1	3 ± 1	$(7 \pm 2)x10^6$	0.4 ± 0.1
	Ankyrin-B	38 ± 2	$(104 \pm 4)x10^6$	5 ± 2	47 ± 2	$(130 \pm 4)x10^6$	6.2 ± 0.5
	All Spectrins	43 ± 5		6 ± 1	15 ± 5		2.3 ± 0.5
	$\alpha - II$ **Spectrin**	10 ± 2	$(22 \pm 4)x10^6$	2.3 ± 0.5	1.2 ± 0.3	$(3 \pm 1)x10^6$	0.24 ± 0.05
$10T\frac{1}{2}$	$\alpha - I$ **Spectrin**	22 ± 4	$(47 \pm 7)x10^6$	3 ± 1	6 ± 2	$(12 \pm 4)x10^6$	0.8 ± 0.2
	$\beta - II$ **Spectrin**	7 ± 1	$(16 \pm 2)x10^6$	1.1 ± 0.2	4 ± 1	$(10 \pm 2)x10^6$	0.6 ± 0.1
	$\beta - I$ **Spectrin**	4.3 ± 0.3	$(10 \pm 1)x10^6$	0.5 ± 0.1	4 ± 2	$(9 \pm 3)x10^6$	0.5 ± 0.1
	Ankyrin-B	41 ± 2	$(112 \pm 5)x10^6$	6 ± 2	51 ± 2	$(140 \pm 4)x10^6$	7 ± 1

In order to turn the observed relative changes into absolute changes of particular spectrins and ankyrin-B in the studied cells, it is necessary to measure absolute protein weights. Bradford assays are a well-established method to measure the absolute concentration of proteins in a sample [17]. Thus, if the molecular weights of the molecules are known and the composition in terms of different isoforms (like from the SDS-PAGE gel analysis in fig.2.5) one can calculate the copy number of these proteins in the sample and ultimately the average number of a particular molecule per cell. For the later one has to of course make sure the samples are obtained from known quantity of cells (as is in this study). In order to connect the relative changes established above with the absolute weight and cellular molecular content, a series of Bradford assays were performed. To compare the amounts of spectrins and ankyrin-B to the overall protein content, both whole cell lysates and specific proteins as purified by IP were analyzed. Table summarizes the results of these measurement and subsequent calculations. The later take explicitly into account that during the IP process only a certain percentage of the protein in question is captured. Since both $\alpha - I$ and $\alpha - II$ spectrins in mouse cells are carrying at least one site (Fig 2.2) which is sufficient for acting as an $E2/E3$ ubiquitinating enzyme activity [18] as well as with the conservation of the a ubiquitination site, there was a curiosity to see if the change in spectrin could be correlated to a change in spectrins poly-ubiquitination state. To that end a western blot on whole cell lysate with a poly-ubiquitin specific for the lysine 48 bush-like chain were performed. Since this modification marks the protein for proteaosomal degradation. As seen in fig.2.7 the α spectrins are heavily poly-ubiquitinated via the lysine 48 connection. In addition, also ankyrin-B, the

36

other known ubiquitination target of the α spectrins [19] can be seen clearly in the Western blot. Of course, since the labeling scheme is against all polyubiquitnated proteins in the lysate other bands are also visible. The quantitation of polyubiquitination state of the α spectrins if further validated by the results of running two consecutive IPs first against the spectrins and then against lysine 48 poly ubiquitnation which acts as a signal for proteasomal degredation [20]. The corresponding SDS-PAGE gel is depicted in fig.2.7B and exhibits some strong signal at the α spectrins' location. Interestingly, this method also shows additional signals at the $\beta-$ spectrin locations in the case of the $10T\frac{1}{2}$ cells. In order to assess the change in the degree of poly-ubiquitination of the spectrins it needs to be taken into account that overall the amount of spectrins has decreased as demonstrated above. Thus, seemingly similar intensities in the bands of either gel indicates actually a much higher degree of poly-ubiquitination of the spectrins in the mechanically stimulated case. The polyubiquitination signal when normalized to the available spectrin content is also visualized in the graph of fig.2.8, that indicates a $(225\pm75)\%$ change in the case of $3T3$ cells and $(125\pm40)\%$ for the $10T\frac{1}{2}$ cells, respectively.

2.5   Discussion and conclusions

Already in the non-stimulated cells several key findings should be highlighted. The first thing to note is that spectrins and the associated ankyrin-B making up more than 10 weight percent of all proteins in the cells under investigation.
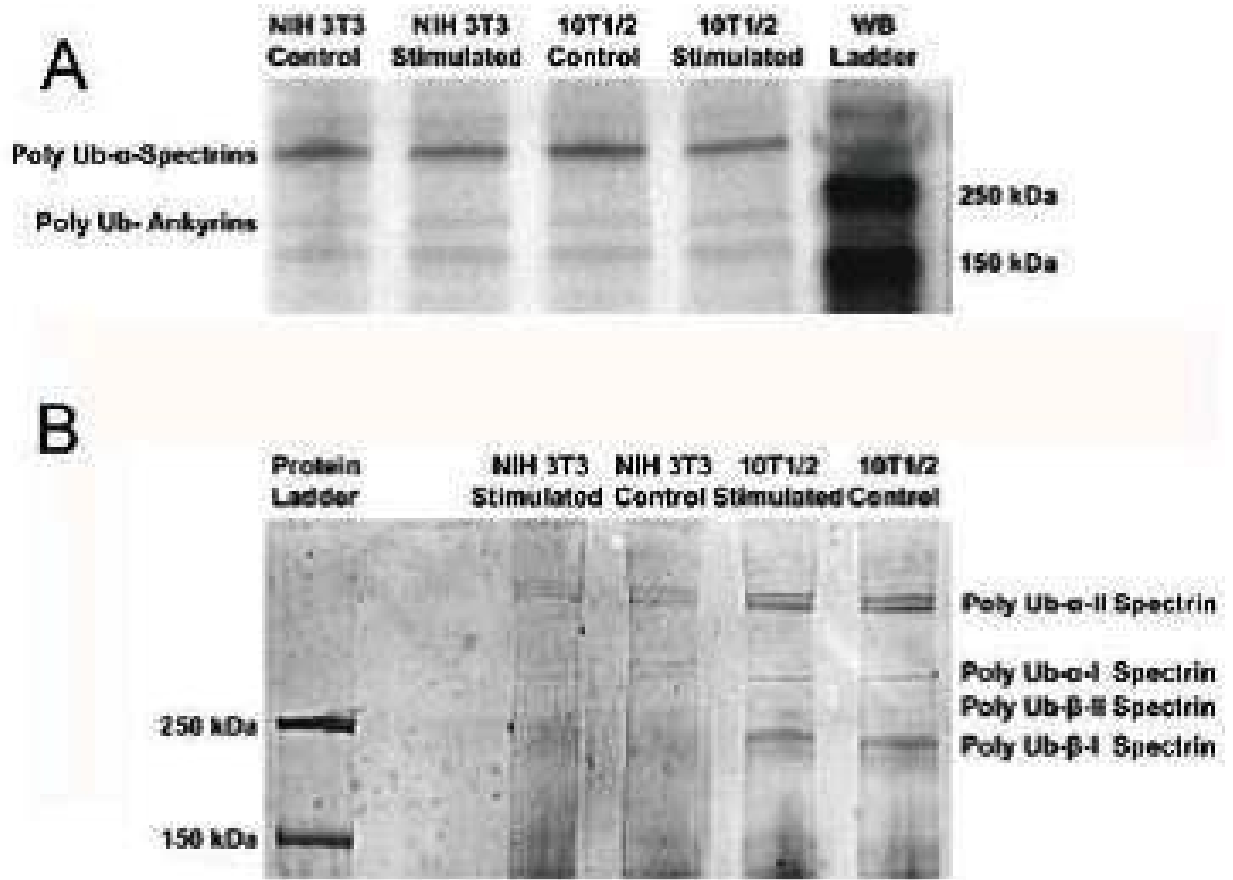
Figure 2.7: Detection of poly-ubiquitination levels of spectrins. A) Western blot of the whole cell lysate with anti-poly-ubiquitin antibody. B) SDS-PAGE gel after consecutive IPs with anti-spectrin and then anti- poly-ubiquitin antibody.
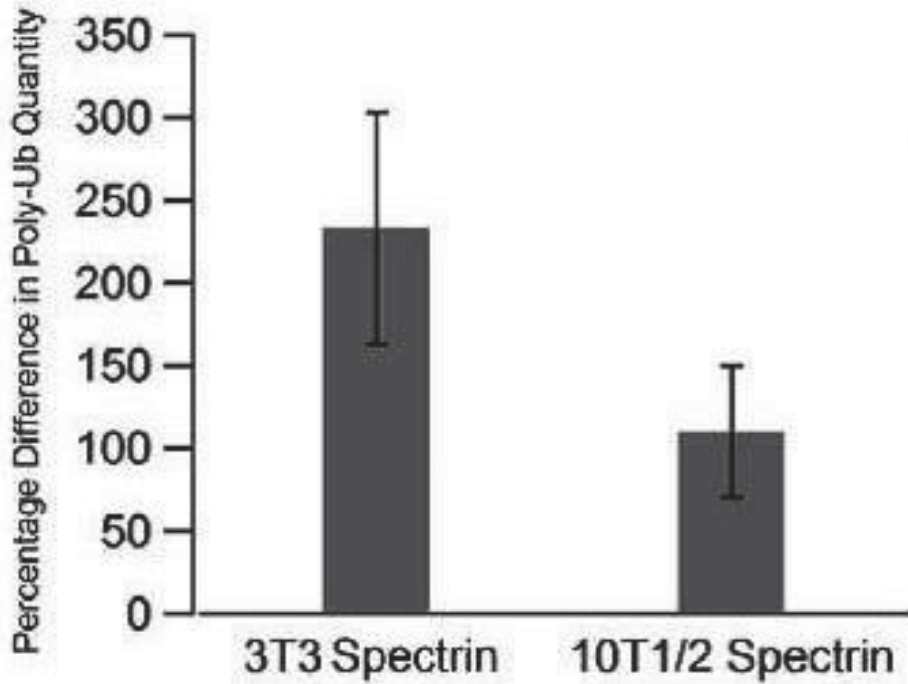
Figure 2.8: Taking the changes in protein content due to mechanical stimulation into account, the change in polyubiquitinated spectrin changes dramatically in both 3T3 and 10T1/2 cells.

If one considers that the actin content of eukaryotic non-muscle cells tops out at roughly 20% by weight [21], the spectrin-ankyrin-B system has to be considered one of the major protein components in these cells. Although, spectrin is abundant in both cell types, there are significant differences in the composition of the spectrin pool. While in the $3T3$ cells $\alpha - II$ spectrin dominates, it is the $\alpha - I$ isoform that provides the majority of the α spectrins in the $10T\frac{1}{2}$ cells. Yet, the overall amount of α spectrins seems similar with roughly 85 x 10^6 ($3T3$) and 70 x $10^6 10T\frac{1}{2}$ average molecules per cell. Also interesting is that the ratio of α spectrins to β spectrins is about 2.5 for $3T3$ and 2.6 for $10T\frac{1}{2}$. If most of the spectrin would indeed be in

the form of the well-known tetramer composed of two α and two β spectrins one would expected this ratio to be much closer to 1. Thus, it appears that there is an extensive excess of α-spectrins in both cell types. For example, the nucleus residing alpha II spectrin with a molecular weight 230kDa [22]) does not appear in any of the gels. This is probably because the cell lysate and protein extraction method used which delivers predominantly plasma membrane proteins and cytosolic proteins, while organelles and the nucleus with their content get mostly discarded. Thus, it appears that at least half of all α-spectrins can not be part of classical tetramers. At this point it remains an open question if that much alpha spectrin might be in the cytosol fulfilling unknown functions or if there are other organizational multi-protein complexes as part of the non-erythroid membrane skeleton that are much richer in α-spectrins. After the cells have been mechanically stimulated, the α to β spectrin ratio drops to approximately 1.5 for $3T3$ and 0.8 for $(10T1/2)$. This change is mostly due to a significant decrease in the relative (see fig.2.5) and absolute (Table 2.1) amount of α-spectrins. At the same time the levels of ankyrin-B are significantly elevated in both cell types. The overall decrease in spectrins and increase of ankyrin-B is summarized in fig.2.9 where the relative change of the total spectrin and ankyrin-B amounts per cell is plotted for all three methods utilized in this study. Within their error, they show very good agreement, thus underscoring that carefully executed; quantitative fluorescence imaging of immunofluorescently labeled cells can provide about as much information about protein levels as the traditional SDS PAGE gels. However, the former supports the potential benefit of providing also spatial information about protein distribution with in the cell. Regarding the

underlying cause of these large changes in spectrins and ankyrin-B there are, as always, a variety of possible reasons. However, it is striking that the fraction of poly-ubiquitinated spectrin has significantly increased. Thus, if one considers the flow equilibrium between protein synthesis and degradation, an increase in the fraction of polyubiquitinated protein will lead to a shift of the equilibrium point towards overall less protein. Thus, it seems reasonable that the changes of spectrin can at least in part be contributed to the change in the protein fraction labeled for degradation. It is of course tempting to conclude that the increased polyubiquitination is really due to an increased self-ubiquitination of the α spectrins, as the $E2/E3$ ubiquitinating domain might have easier access during stretching of spectrin tetramer. Alas further studies are required to show conclusively if spectrin is just passively modulated by external forces or plays indeed an active role as mechano-transducer. Nevertheless, our study does demonstrate that the spectrin-ankcyrin systems can be a significant part of the non-erythrocyte cytoskeleton. The particular composition of the spectrin pool depends on the cell type and given the measured abundance of both major α and β spectrin isoforms, the classification of spectrins into erythroid and non-erythroid spectrins seems not particularly adequate anymore for mouse fibroblasts and $10T\frac{1}{2}$ cells. External periodic mechanical forces can lead to significant changes in the spectrin-ankyrin-B membrane skeletons. The observed overall decrease of spectrin should be in part be caused by increased protein degradation due to a higher fraction of poly-ubiquitinated spectrin. Having established the compositional importance of spectrins and ankyrins in non-red blood cell and given the multitude of mechanical and biochemical functions carried by the involved proteins, exploring

the consequences of the large changes in the membrane skeleton due to external
mechanical forces should be a particularly fruitful and a very important endeavor.
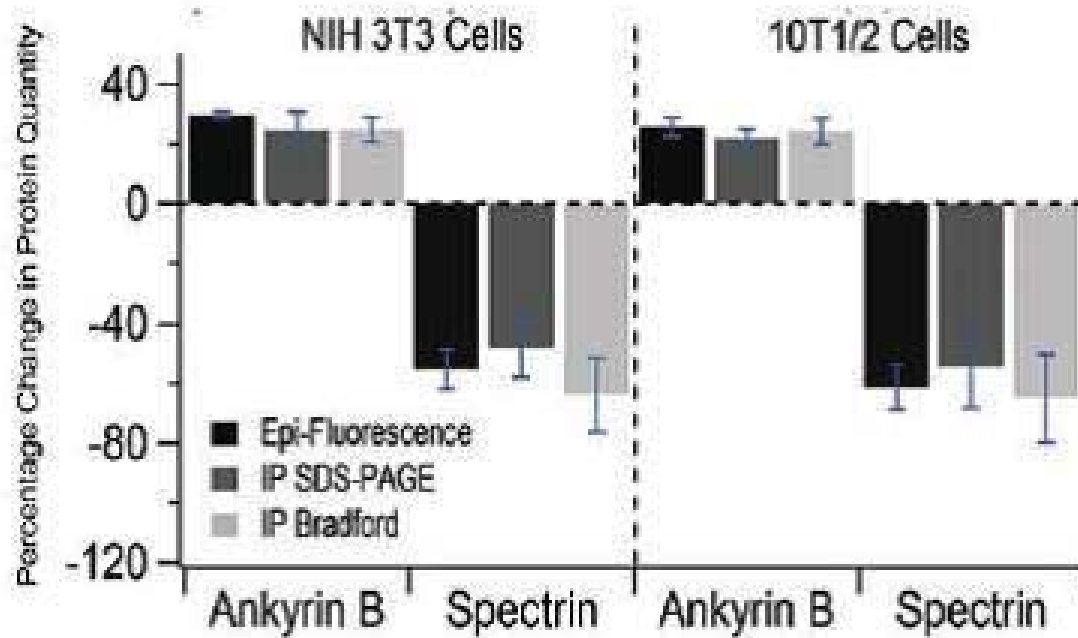
Figure 2.9: Comparison of the detected changes in spectrin and ankyrin-B composition using quantitative immunofluorescence imaging, SDS-PGE gels and Bradford assays. Plotted are the percentage change for both $3T3$ and $10T\frac{1}{2}$ cells.

2.6   References

1.   Desilva, T.M., et al., Analysis of Human Red-Cell Spectrin Tetramer (Head-to-Head) Assembly Using Complementary Univalent Peptides. Biochemistry, 1992. 31(44): p. 10872-10878.

2.   Bignone, P.A., et al., Phosphorylation of a threonine unique to the short C-terminal isoform of betaII-spectrin links regulation of alpha-beta spectrin interaction to neuritogenesis. Journal of Biological Chemistry, 2007. 282(2): p. 888-96.

3.   Morris, C.E., Mechanoprotection of the plasma membrane in neurons and other non-erythroid cells by the spectrin-based membrane skeleton. Cellular & Molecular Biology Letters, 2001. 6(3): p. 703-720.

4.   Pinder, J.C. and A.J. Baines, A protein accumulator. Nature, 2000. 406(6793): p. 253-4.

5.   Dubreuil, R.R., Functional links between membrane transport and the spectrin cytoskeleton. Journal of Membrane Biology, 2006. 211(3): p. 151-161.

6.   Melkerson-Watson, L.J., et al., Development of Na+/K+-ATPase polarity in the rat kidney proximal tubule: Regulation of the cytoskeletal elements, ankyrin and spectrin, during the redistribution Na+/K+-ATPase in the proximal tubule prior to birth. Pediatric Research, 2000. 47(4): p. 449a-449a.

7.   Collec, E., et al., Novel role for the Lu/BCAM-spectrin interaction in actin cytoskeleton reorganization. Biochemical Journal, 2011. 436: p. 699-708.

8.   Mills, J.W. and L.J. Mandel, Cytoskeletal Regulation of Membrane-Transport Events. Faseb Journal, 1994. 8(14): p. 1161-1165.

9.   Norman, K.R. and D.G. Moerman, alpha spectrin is essential for morphogenesis and body wall muscle formation in Caenorhabditis elegans. Journal of Cell Biology, 2002. 157(4): p. 665-677.

10.   Lee, J.K., et al., Cell-Shape and Interaction Defects in Alpha-Spectrin Mutants of Drosophila-Melanogaster. Journal of Cell Biology, 1993. 123(6): p. 1797-1809.

11.   McMahon, L.W., et al., Knockdown of alpha II spectrin in normal human cells by siRNA leads to chromosomal instability and decreased DNA interstrand cross-link repair. Biochemical and Biophysical Research Communications, 2009. 381(2): p. 288-293.

12.   Voas, M.G., et al., alpha II-spectrin is essential for assembly of the nodes of Ranvier in myelinated axons. Current Biology, 2007. 17(6): p. 562-568.

13.   Bennett, V. and J. Healy, Organizing the fluid membrane bilayer: diseases linked to spectrin and ankyrin. Trends Mol Med, 2008. 14(1): p. 28-36.

14.   Hsu, Y.J., W.E. Zimmer, and S.R. Goodman, Erythrocyte spectrin's chimeric E2/E3 ubiquitin conjugating/ligating activity. Cell Mol Biol (Noisy-le-grand), 2005. 51(2): p. 187-93.

15.   Sun, F., et al., Mitochondrial accumulation of polyubiquitinated proteins and differential regulation of apoptosis by polyubiquitination sites Lys-48 and-63. Journal of Cellular and Molecular Medicine, 2009. 13(8B): p. 1632-1643.

16.   Pickart, C.M. and M.J. Eddins, Ubiquitin: structures, functions, mechanisms. Biochimica Et Biophysica Acta-Molecular Cell Research, 2004. 1695(1-3): p. 55-72.

17.   Ku, H.K., et al., Interpretation of protein quantitation using the Bradford assay: Comparison with two calculation models. Analytical Biochemistry, 2013. 434(1): p. 178-180.

18.   Hsu, Y.J. and S.R. Goodman, Spectrin and ubiquitination: A review. Cellular and Molecular Biology, 2005. 51: p. Ol801-Ol807.

19.   Chang, T.L., et al., Ankyrin is a target of spectrin's E2/E3 ubiquitin-conjugating/ligating activity. Cellular and Molecular Biology, 2004. 50(1): p. 59-66.

20.   Oustwani, C.S., et al., Nitric Oxide Increases Lysine 48-Linked Ubiquitination Following Arterial Injury. Journal of Surgical Research, 2011. 170(1): p. E169-E177.

21.   Korn, E.D., Actin polymerization and its regulation by proteins from nonmuscle cells. Physiol Rev, 1982. 62(2): p. 672-737.

22.   McMahon, L.W., C.E. Walsh, and M.W. Lambert, Human alpha spectrin II and the Fanconi anemia proteins FANCA and FANCC interact to form a nuclear complex. Journal of Biological Chemistry, 1999. 274(46): p. 32904-8.

Chapter 3

Correlating cellular traction forces and strains in the non-erythroid membrane skeleton

3.1 Abstract

Living cells are not limited to only sense external forces and turn them into cellular signals, but they can also generate forces and exert them on their environment. These generated forces in turn could be modulated by the particular mechanical properties of the cell's surroundings. It is notable that depending on the biological function, different patterns of force generation mechanisms are utilized by eukaryotic cells. For example, cells that migrate will engage in different force generation patterns than

cells undergoing mitosis (cell division). Nevertheless, either of the cellular mechanisms necessitates complex mechanical interactions between the cell and its substrate. While certainly much of the actual force generation can be attributed to the actin-myosin system, it has not been investigated to what extent the non-erythroid, spectrin-based membrane skeleton is involved in these mechanical process. Given the interesting spring like properties of the underlying spectrin repeats, it seems the membrane skeleton is well suited to either propagate mechanical forces or temporarily store mechanical energy via elastic deformations or both. Thus, I set out to shine light on this question using $3T3$ fibroblast and $H9c2(2-1)$ cardiomyocyte cell lines, which are both known to be mechanically active. In order to gain some understanding of the connection between force application to the substrate and deformation of the membrane skeleton, it was necessary to first develop the appropriate measurement methodology. The goal was thereby to be able to measure the traction forces that cells exert on polyacrylamide hydrogels of varying elastic modulus and correlate that information with the corresponding strain response of the spectrin membrane skeleton. In order to accomplish this, I was able to successfully merge traction force microscopy and FRET based strain sensor read-out, so both could be accomplished on the same sample almost simultaneously (on cell's relevant timescales). The preliminary data produced with this new methodology demonstrate convincingly that the internal strains in the membrane skeleton for cell fibroblast colonies are associated with the varying polyacrylamide substrate stiffness. Although with the current experimental set up (without cell sorting), a conclusive statement can not be made about a direct correlation between the internal strains and the traction forces. It is

46

established that cellular traction forces are correlated with alterations in substrate stiffness, which was observed in the data. The method is ready to be easily applied after cell sorting, to provide detailed quantitative information about the correlation even at the single cell level.

3.2   Significance

In non-erythroid cells, there is a significant knowledge gap regarding the properties and functions of the spectrin based membrane skeleton. This is especially true in the area of cellular biomechanics, where the question of membrane skeleton's contribution to mechanical processes has never been addressed. This is even more surprising since spectrins have not only intriguing mechanical properties (see chapter 1 section 2.3.1) but the skeleton is also tightly integrated with the rest of the cytoskeleton, via connections to adhesion points, actin as well as the plasma membrane. Thus, it should be responsive to cellular force generation, the resulting deformation of the cell and the environment. Nevertheless, its possible role in force transduction in non-erythroids has been ignored to a great extent so far. Thus, contributing to filling this gap will provide important information, regarding the role of the membrane skeleton in the dynamic re-arrangement of the cytoskeleton and the overall mechanical machinery of non-erythroid mammalian cells. The hope is that this work will spur more questions regarding our understanding of the intricate mechanisms of cellular biomechanics.

3.3   Introduction

The mechanical properties of both natural and synthetic extracellular matrices and cellular substrates regulate several aspects of cell structure and function [1]. Adherent cells like fibroblasts and cardiomyocytes rely on the transmission of the traction forces generated by the actin-myosin complex [2] and Arp2/3 activated actin polymerization controlled by WASP family proteins [3] to adhere, spread, contract and migrate on the extracellular matrix. Cellular traction forces are essentially bidirectional and dynamic across the interface between the cell and the extracellular matrix (ECM). Most cells can modulate traction forces dynamically according to extracellular signals to maintain cell homeostasis and to initiate many cellular activities such as endogenous tension [4], growth [5], cell-cell recognition [6] and downstream signaling at focal adhesions [7]. These cells adhere on a substrate by attaching their focal adhesions via integrins as depicted in Fig.3.1. There are quite a few mediators of cellular mechanotransduction that have been identified so far. Among them are: ECM, cell-ECM interactions, and cell-cell adhesions, particular membrane compo-nents, specialized surface processes, cytoskeletal filaments, and nuclear structures [8]. Although all these cell adhesion and signal transduction mediators are known at this point, the precise mechanisms that regulate the strength of adhesion and magnitude of generated forces applied to the extracellular matrix remain poorly understood [9]. However, what becomes very quickly clear is that the spectrin based membrane skeleton is known to associate and bind to many of the mediators shown in Fig 3.1.
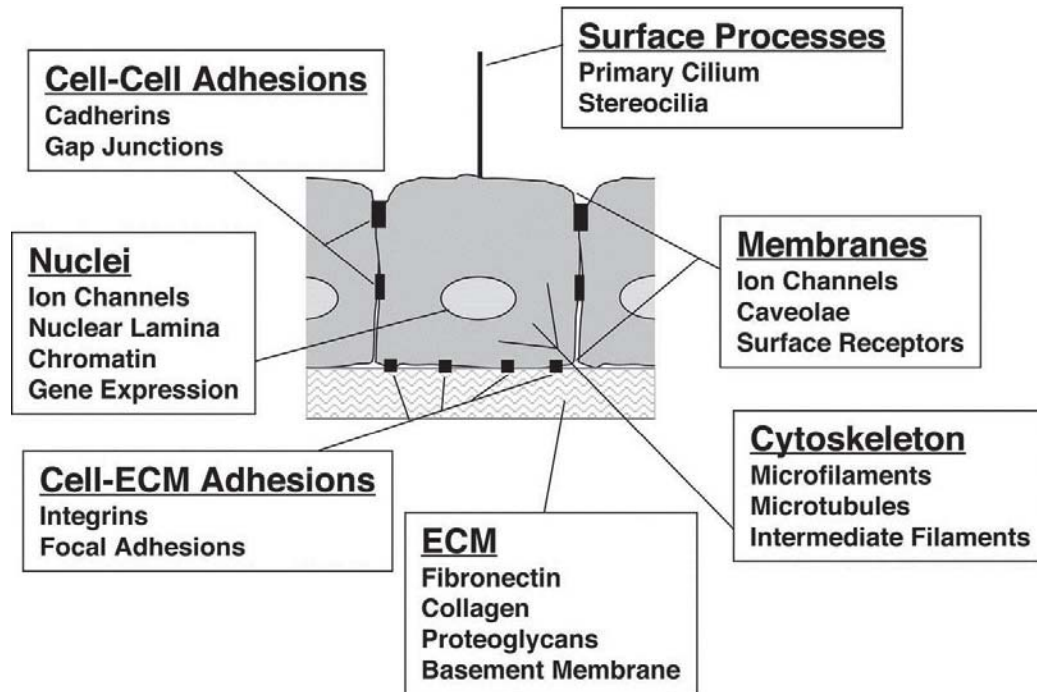
Figure 3.1: Mediators of cellular mechanotransduction. ECM, cell-ECM, and cell-cell adhesions, membrane components, specialized surface processes, cytoskeletal filaments, and nuclear structures [8].

In addition to this fact of the structure and location of the membrane skeleton's spectrin, there is also accumulating evidence that spectrin is involved in a direct and indirect complex formation with integrins [10, 11]. Furthermore, the SH3 domain of spectrins is involved in initiating Rac activation in integrin clusters, which in turn initiate cell adhesion and spreading [12]. Also, spectrin and ankyrin are needed for accumulation of E-cadherin at the lateral membrane of epithelial cells [13]. Spectrin interacts with Tes and EVL, two actin-binding proteins located at cell contacts [14]. Finally, spectrin associates with vinculin at focal adhesions [15] as well as with ion channels [16, 17]. Therefore, it is hypothesized that, forces generated by the actin-myosin complex will couple into the spectrin skeleton and affects spectrin's numerous

connections, organizations and function of the mentioned molecules. To understand these possible complex connections in detail, the exact relationship between the strain distribution in the membrane skeleton and the forces generated and exerted by the cells on their substrate needs to be studied.

3.3.1 Traction force microscopy

Cell traction forces are tangential tension forces exerted by cells on their environment or on a substrate they adhere to. Non-erythroid cells exert traction forces for example when they move in order to support cellular functions. Cell movement is usually divided into several steps: protrusion of the leading edge of the cell, adhesion of the leading edge and de-adhesion at the cell body with the rear, and cytoskeletal contraction to pull the cell forward [18]. Traction forces that cells exert on their substrate when they move can be measured experimentally with traction force microscopy by using either nano-pillars with known size and elasticity [19] or micro-beads (tracer beads) [20]. The last approach, which is widely applicable, is utilized in this work. It involves observing and measuring the displacements of beads embedded on a deformable substrate the cells are surrounded with and computing the traction field from the measured displacement. I implemented this method in our lab which was originally pioneered by the seminal work of Harris and co-workers [21] and has since seen improvements by others such as Wang [22] and Butler [22]. The force exerted on the substrate by adherent cells results in deformations in the substrate which can be tracked by measuring the displacement field of embedded fluorescent micro-beads (see Fig.3.2). The displacement field is usually extracted from a pair of images, one
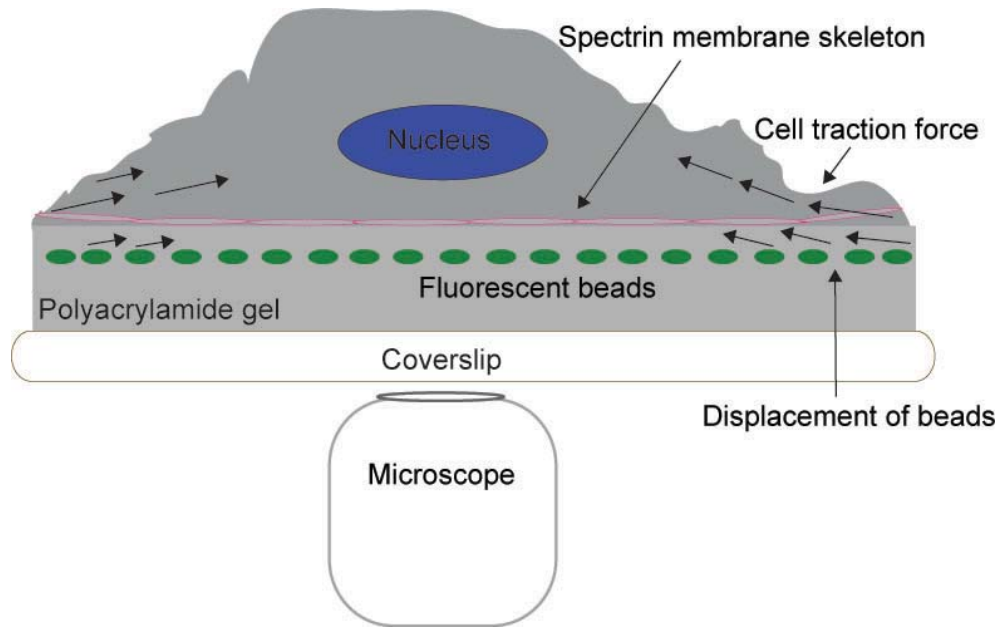
Figure 3.2: Schematic of Traction force microscopy experiments: The traction force exerted by the cell peripheries deforms the polyacrylamide gels which displaces the embedded beads. The positions of the beads before and after deformation can be obtained from the fluorescent images of the micro-beads. The displacement of the beads can then be used to reconstruct the traction forces exerted using the known stiffness of the PA gels. The pink structure represents the spectrin membrane skeleton in non-erythroid cells.
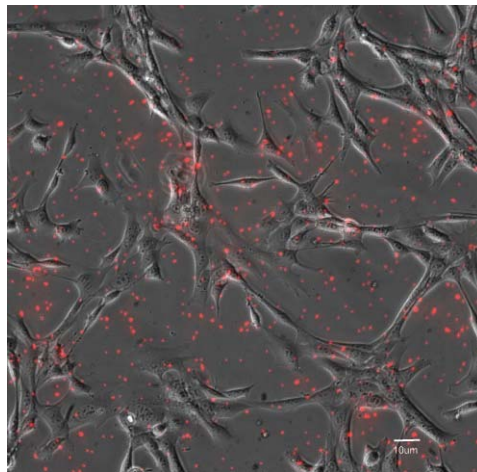
Figure 3.3: Composite of a brightfield and fluorescent images: visible are 3T3 fibroblasts attached to the underlying polyacrylamide gel. In the red fluorescent channel, the embedded beads are clearly visible but they are not in the same focal plane with the cells as it appears. They are localized in a different focal plane inside the PA gels.

image showing the bead position of the substrate as it has deformed under cell traction and the other showing the position of the beads in the un-deformed substrate. Assuming both the displacement field $u(x)$ and the traction stress field $T(x)$ are two-dimensional in the plane of the substrate and neglecting the very small normal displacement and force. The relationships between the traction displacement field and the traction stresses can be written as:

$$\vec{u}_i(x) = \int \sum_j G_{ij}(x - x')\vec{T}_j(x')dx' \tag{3.1}$$

Where

$$G_{ij}(x) = \frac{1+\nu}{\pi E}\left((1-\nu)\frac{\delta_{ij}}{r} + \nu(\frac{x_i x_j}{r^3})\right) \tag{3.2}$$

$$= \frac{1+\nu}{\pi E r^3}\begin{bmatrix} (1-\nu)r^2 + \nu x^2 & \nu xy \\ \nu xy & (1-\nu)r^2 + \nu y^2 \end{bmatrix}$$

Where E is the young's modulus and ν is the Poisson's ratio [23]. This is a forward problem which helps to calculate the displacement field from the applied traction force fields. But since what is measured is the displacement, the interest is to get the solution of the inverse problem using the relevant Green's function Gij by approximating the polyacylamide gel as a semiinfinite solid. But Gij is not diagonal in real space because tractions at one point are coupled to displacements of beads at different points distributed in a different focal plane. So, each displacement can not be mapped easily to the corresponding traction in real space. This makes the inversion in real space complex by requiring the construction and inversion of very large matrices [24]. That can be avoided by using the Fourier transform traction cytometery (FTTC) method [25]. Doing the inversion in Fourier space simplifies the

52

problem due to the fact that the matrix remains diagonal in k space because of no coupling between different wave vectors [26]. It uses the property of the convolution theorem which states that the Fourier transform of a convolution is the product of the Fourier transforms of the functions being convolved [27]. Then solution to the inverse problem in calculating traction forces from the displacements can be calculated as:

$$\vec{T}(x) = FT_2^{-1}(G(\vec{\kappa})^{-1}\vec{u}(\vec{\kappa})) \tag{3.3}$$

Where FT_2^{-1} is the two dimentional inverse fourier transform and $G(\vec{\kappa})^{-1}$ is the inverse of the Fourier transform of G.

$$\vec{G}(\vec{\kappa}) = 2\pi \frac{1+\nu}{\pi E \kappa^3} \begin{bmatrix} (1-\nu)\kappa^2 + \nu k_y^2 & \nu k_x k_y \\ \nu k_x k_y & (1-\nu)\kappa^2 + \nu k_x^2 \end{bmatrix}$$

And the appropriate strain energy exerted on the substrate can be calculated as:

$$E_s = \frac{1}{2} \int T(x).u(x)dA \tag{3.4}$$

Phase contrast and fluorescent microscopy of the microbeads were utilized for the data collection of traction forces as shown in Fig.3.3 and Fourier Transform Traction Cytometery (FTTC) and particle image velocimetery (PIV) [28] were used for the analysis of the measuremets to quantitatively detrmine the deformation of the sub-strate.

3.3.2 Assessing strains in the membrane skeleton

Since proper study of force generation and its modulation necessitates the utilization of living cells, it was paramount that the strain measurement is compatible with living cells. This leaves very few potential candidates for strain measurement. A well suited approach was to use a technique that utilizes FRET (Forster Resonance Energy Transfer). Luckily, a FRET based strain sensor that integrates into the spectrin skeleton was recently developed by Prof. Sachs group at SUNY Buffalo which they generously shared with us. I was able by proper choice of optical components and fluorescent dyes to combine this method with TFM to simultaneously evaluate the traction force exerted by the cells. In general, FRET can potentially be used as a molecular ruler to monitor the nano-metric displacements between donor and acceptor fluorescent molecules as shown in Fig.3.4 and potentially the corresponding force exerted on the linkages between them [29]. FRET occurs between the electronic ex-cited states of two fluorophores. It is the radiation-less transmission of energy from a donor molecule to an acceptor molecule. According to Forster, the efficiency of FRET is dependent on the inverse sixth power of the intermolecular separation [30], making it particular useful over distances comparable to the dimensions of biological macromolecules.

Conditions for FRET to occur

1) The excitation spectrum of the acceptor must overlap with the emission spectrum of the donor. The degree of overlap is expressed as a normalized overlap integral (J).

2) Donor and acceptor molecules must be with in $(1 - 10)$nm.

3) Donor and acceptor transition dipole orientations must be nearly parallel.

4) The fluorescence lifetime of the donor molecule must be long enough to allow the FRET to occur. When such conditions are met, the rate of every transfer via FRET can be expressed by [31].

$$k_T = \left(\frac{1}{\tau_D}\right)\left(\frac{R_0}{r}\right)^6 \tag{3.5}$$

Where k_T is the rate of energy transfer and τ_D is the lifetime of the donor in the absence of acceptors or any other quenching effects, r is the distance separating the donor and acceptor fluorophores. And R_0 is the Forster radius, the distance at which
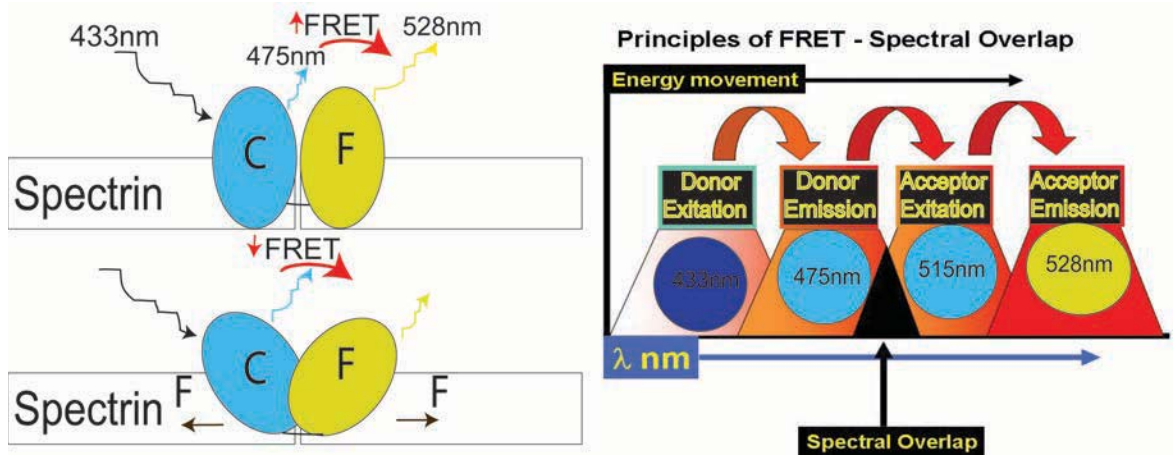
Figure 3.4: Circularly modified donor and acceptor FRET pairs whose FRET efficiency is modulated by the angle between them. When the strain in the membrane skeleton increases, the dyes orientation changes from a resting parallel state which results in the highest energy transfer to an orthogonal state, which results the least energy transfer. On the right [41] is shown spectral conditions for FRET to happen: The donor emission spectra have to overlap with the acceptor excitation (absorption) spectra for FRET to happen. For ideal FRET pairs, the donor excitation spectra and acceptor excitation spectra have to be well isolated.

energy transfer is 50%. It is dependent on the spectral properties of the donor and acceptor dyes given by [32].

$$R_0 = 2.11 \times 10^{-2} \left[o^2 J(\lambda)\eta^{-4}Q_D\right]^{\frac{1}{6}} nm$$

Where o^2 is the relative dipole orientation factor (0-4), for randomly oriented donors and acceptors, $o^2 = \frac{2}{3}$, $J(\lambda)$ is the normalized overlap integral in the region of the donor emission and acceptor excitation spectra, η represents the refractive index of the medium, and $Q(D)$ is the quantum yield of the donor.

There are many ways of calculating FRET efficiency [33, 34]. The one used for this work is using the relationship between the FRET fluorescent intensity to the Acceptor signal [35]. To estimate the FRET signal correctly we need to take in to account of bleed through of the donor in the acceptor channel. And the cross talk of a direct excitation of the acceptor by the donor excitation light. For that, the coefficients c_D and c_A which are a measure of the fraction of contamination from the total signal have to be calculated to obtain the correct signal.

$$FRET_{corr} = FRET_{uncorrected}(I_{DA}) - c_D I_{DD} - c_A I_{AA} \qquad (3.6)$$

$$E_f = FRET_{corr}/I_{AA} \qquad (3.7)$$

Where $c_D I_{DD}$ is fluorescence signal due to bleed through of the donor and $c_A I_{AA}$ is the cross talk intensity of a direct excitation of the acceptor by the donor excitation. And E_f is the FRET efficiency. The coefficients can be estimated using either donor only and acceptor only samples or donor bleached and acceptor bleached samples in cases that donor/acceptor images are not allowed. When we have an acceptor bleached or donor only sample, the signal we get in the FRET channel can be used to estimate c_D. In the ideal situation of no bleed through, there shouldn't be a signal in the FRET channel because, we don't have an acceptor and FRET does not happen. So, everything we get in this channel is a contamination and needed to

be corrected $c_D = I_{FRET}/IDD$. Similarly with a donor bleached or acceptor only sample, the signal we get in the FRET channel can be used to estimate c_A and the crosstalk needs to be corrected. The other commonly used method of calculating FRET efficiency is by measuring the donor fluorescence lifetime in the presence and absence of an acceptor. In this method the efficiency is calculated as

$$E_f = 1 - \left(\frac{\tau_{DA}}{\tau_D}\right) \tag{3.8}$$

[36, 37] where τ_{DA} is the donor lifetime in the presence of the acceptor and τ_D is the donor lifetime in the absence of the acceptor.

For the experiments performed, a new FRET-based sensor construct inserted in to non-erythroid spectrin, called cpstFRET by a kind donation from (Dr. Sachs's, SUNY Buffalo, NY) have been obtained [38].
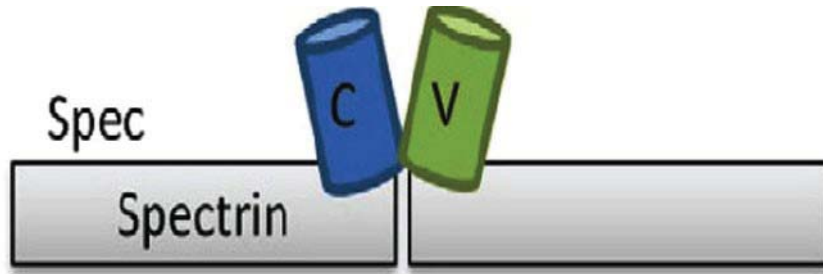
Figure 3.5: Circularly permutated cerulean (donor) and venus (acceptor) inserted at amino acid 1200 of the spectrin repeat in the non-erythroid membrane skeleton used for the measurement of strain in the membrane skeleton.

3.4 Results and discussion

Traction force measurements have to be performed very carefully in terms of external mechanical perturbations, otherwise measurements become very unreliable. In order to avoid collecting and misinterpreting such incorrect data, care must be taken in the preparation of the gel as well as the execution of the experiment. For example the first focus of implementing the traction force microscopy was to investigate if the polyacrylamide substrate preparation procedure described in chapter 5 section 9.2, produced a smooth substrate surface or not. In chapter 5 section 9.4, it is described in detail how the smoothness and uniformity of the PA gel was checked. In fact, the effect of coating that is not executed carefully and the concentrations of cross linkers and EMC proteins are not optimized can be seen in in fig.3.6. What was found that equally important is that all procedures are performed on a flat bench or table surface including all coverslip preparation and activation as well as seeding the cells. If these procedural conditions are not met, uniform and smooth substrate can not be created, and gels similar to the one depicted in fig.3.5 in the top left panel are the result. Unfortunately, suboptimal formation of the bio-functionalized gel affects the cell morphology which in turns impacts the deformation the cell applies to the substrate and thus the embedded beads. Ultimately this would lead to a misinterpretation of the experiments, thus much care was taken in working out the proper methods and experimental steps to create the proper gels in a reliable and repeatable manner.

The next step was to characterize the mechanical properties of the gels. The particular focus was thereby on the validation of the Young's Modulus of the PA
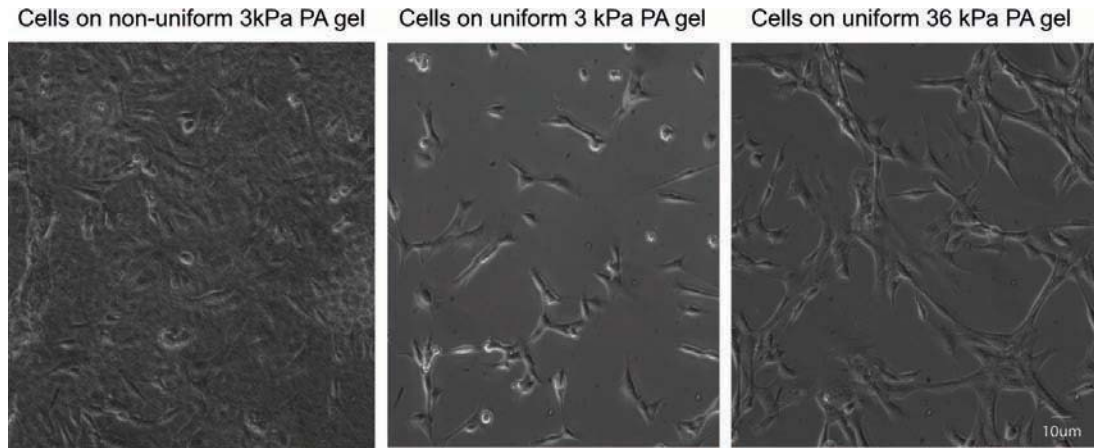
Figure 3.6: Impact of uniformity of collagen coating on cell growth, imaging and measurement: upper left panel shows cells plated on non-uniform 3kPa PA gel. The non-uniformity of the protein coating affected cell morphology, it can also be observed that cells did not grow in the same focal plane, but intruded deep into the hydrogel. This of course leads to deformations of the substrate which are not due to cellular traction forces.

gels produced for the experiments. Although we started with particular bulk gel stiffness in mind in order to determine the ratio of acrylamide/bis- acrylamide before preparation of the PA substrates as described in chapter 5 section 9.2, the properties of the resulting gel had to be still validated as many factors contribute to the stiffness of PA gels. Local stiffnesses of PA gels can be measured by two common techniques: Atomic Force Microscopy (AFM) [42] or using a way to impose well defined forces to the gel, for example by the weight of a steel ball [39]. Since it is easily available and does not require special instrumentation, I used the steel ball method to check the local stiffness of the gels used in this study. To that end, a steel ball with radius 0.5mm was placed on a gel with embedded fluorescent beads as described a bove. The ball was easily identified in the microscope since it blocks the light path and thus throws a shadow as depicted in **Fig.**3.6. The microscope was then focused on the

top layer of the beads to image the fluorescent beads directly beyond the center of the steel ball which gives a position of the surface of the compressed gel along the z axes optical path, z_2. Using a magnet, the ball was removed and the gel was left untouched for 30 minutes so it could elastically relax and return to the unstrained configuration. The scope was then re-focused on the top layer of beads again to take an image of the fluorescent beads in the relaxed gel (the resulting z axis position is denoted with z_1). Using Hertz theory [22] the elastic modulus E was then calculated as:

$$E = \frac{3(1 - \nu^2)f}{4\sqrt{r\sigma^3}} \tag{3.9}$$

Where σ is indentation depth of the steel ball on to the PA gels which is the difference between the positions before and after the gel recovery ($z_2 - z1$). The force f the ball exerts on the gel with Poisson's ratio $\nu = 0.48$ [40] is corrected by the buoyance force $f_b = \rho\ V\ g$. So, $f = mg - \rho\ V\ g$ where ρ is the density of the ball, V is the volume of the submerged part of the ball with depth σ and g is the acceleration due to gravity.
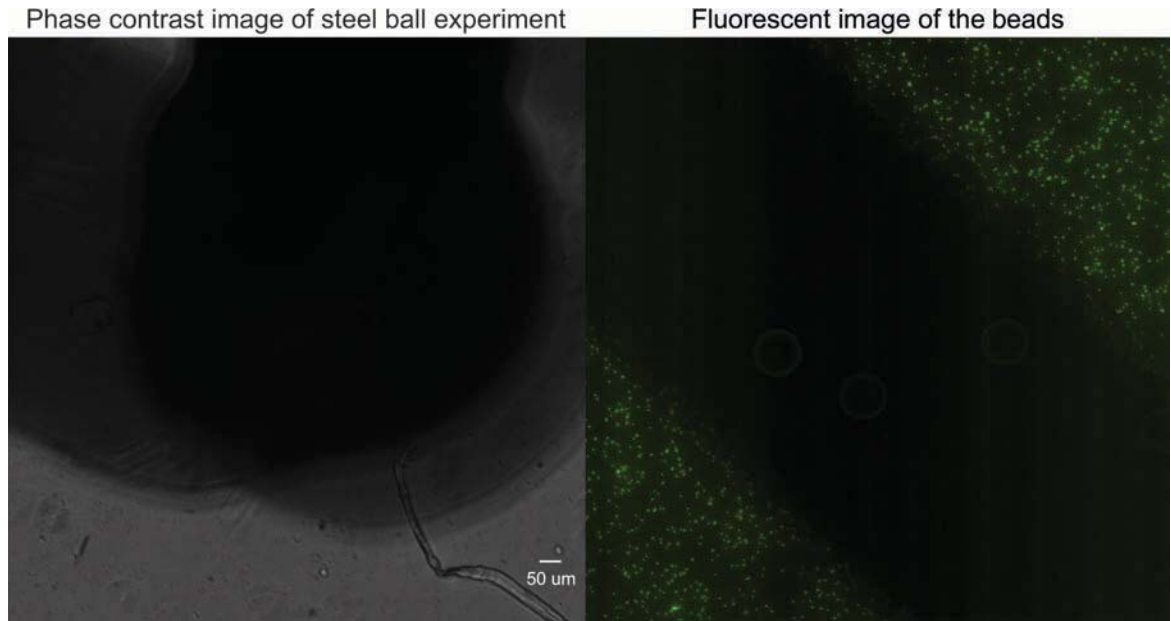
Figure 3.7: Validation of elastic modulus: Validation of elastic modulus of the PA hydrogels visualization of the steel when it blocks the light path shown with phase contrast image (left image) and the fluorescence images taken on the blocked side to extract the the displacement of beads after a complete recovery of the gel

In addition to protein coating and validation of the elastic modulus, the other very sensitive issue, that is important to control properly in order to optimize data quality, is the distribution of fluorescence beads in the gel. Since traction stresses in 2D are measured, the beads would be ideally uniformly distributed in exactly one, well-defined, plane. In experimental situations it is very challenging to achieve true uniformity of the bead's distribution without very specialized instrumentation. Instead it was found that inverting the gel sandwich before PA gel polymerization with adequate sonication and degasing of the PA-bead solution described in chapter 5 section 9.2 results in a relatively uniform bead distribution with a limited spread into along the z axis (into the gel). The effect of the remaining non-planar deviations

of beads can be minimized in the imaging step by taking fluorescent images of the beads in the same focal plane.
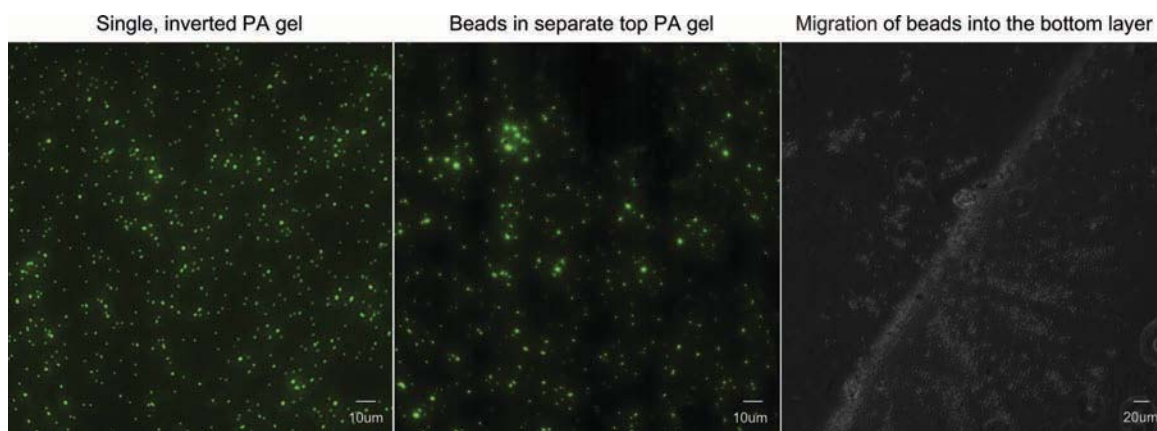
Figure 3.8: Experimental tests to optimize bead location within one focal plane. The left image shows bead distributions when bead mixed PA gels are allowed to polymerize by inverting the coverslip-PA sandwich to concentrate the beads in the top of the gel. The middle image shows the result if two layers of PA gels are formed one on top the other but the beads are embedded only in the top thin PA gel to keep the beads in the top plane. The phase contrast image shows smearing of beads from the top bead mixed PA gel to the bottom which demonstrates that it is experimentally difficult to create the two layers without the beads penetrating also the bottom gel.

While the outcome of the transfection experiments of GFP-actin (about 5kbp) as shown in **Fig.**1.1 seemed originally very promising, it was very quickly realized that high transfection efficiency was directly linked to the small size of the DNA construct. When the full cspFRET sensor construct was used, this was very di erent. The cor-responding plasmid DNA is > 10kbp and thus much more difficult to introduce to the cells. The probability of successful transfection (leaving everything else equal) does not scale linearly with the size of the construct. It is observed that the transfection efficiency was indeed very low for this construct using the same conditions as for the

smaller DNAs. Optimization of the procedure by changing the DNA transfection agent ratio resulted in a better transfection efficiency ($> 10\%$) as observed in **Fig**.3.9. Fluorescent bead images embedded on 3kPa (soft), 16kPa (intermediate) and 60kPa
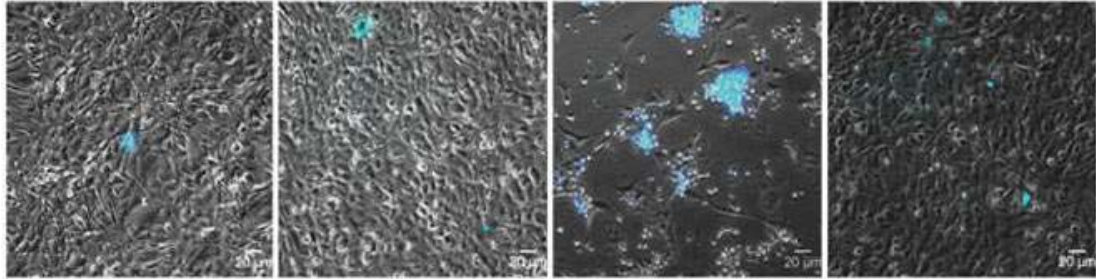
Figure 3.9: Transfection optimization of spectrin-FRET construct by varying transfection agent:DNA of different trials. The improved transfection is shown for ratios of 3:1,7:1, 4:2 and 7:2 from left to right respectively.
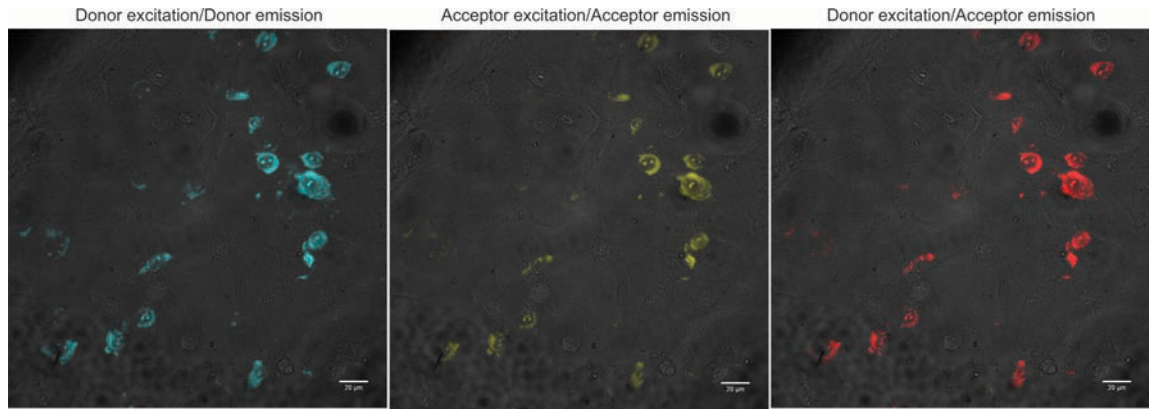
Figure 3.10: Donor channel, acceptor channel and FRET channel images of the transfected spectrin construct on firbroblasts using fugene HD transfection agent (transfection efficiency $> 10\%$).

(hard) polyacrylamide gels were taken before and after the fibroblasts or cardiomyocytes were undergoing trypsin treatment of to dislodge them from the gel and thus allow the deformed gel to return to its native configuration. The bead images before

trypsin treatment gives the force loaded image and the bead image taken 30 minutes after trypsinization at the same focal plane gives a zero force image which were used to calculate the traction forces, using particle image velocimetry and Fourier transform traction microscopy analyses as explained in section 3.1 of this chapter. Briefly, the background subtracted before and after images of the fluorescent beads images were combined as an ImageJ image stack. The displacement fields were then calculated utilizing a PIV plugin [28, 43, 44] for ImageJ which utilizes a normalized correlation coefficient algorithm to match and correlate the bead positions before interpolation and calculation of the displacements. Once the displacements are calculated the data is stored and used by the FTTC plugin to reconstruct the force field as described in section 3.2 of this chapter. The reconstructed force fields were then used to produce the color coded vector plots shown in the left hand images below. The magnitude of the resultant traction forces is calculated from these components and used to plot a force magnitude stress map shown in the middle column of Fig3.12 which gives the stress distribution of a transfected fibroblast cell monolayer. These maps were generated using a 16-color lookup table to translate force magnitude into distinct colors. Image stack. The displacement fields were then calculated utilizing a PIV plugin [28, 43, 44] for ImageJ which utilizes a normalized correlation coefficient algorithm to match and correlate the bead positions before interpolation and calculation of the displacements. Once the displacements are calculated the data is stored and used by the FTTC plugin to reconstruct the force field as described in section 3.2 of this chapter. The reconstructed force fields were then used to produce the color coded vector plots shown in the left hand images below. The magnitude

64

of the resultant traction forces is calculated from these components and used to plot a force magnitude stress map shown in the middle column of fig. 3.11 which gives the stress distribution of a transfected fibroblast cell monolayer. These maps were generated using a 16-color lookup table to translate force magnitude into distinct colors. The results show that there is non-uniform traction force distribution over the cell monolayers of both cell types. On average traction magnitudes increase with substrate stiffnesses and they are very high (in kPa) for the cardiomyocytes cell lines compared to the fibroblasts (Pa).
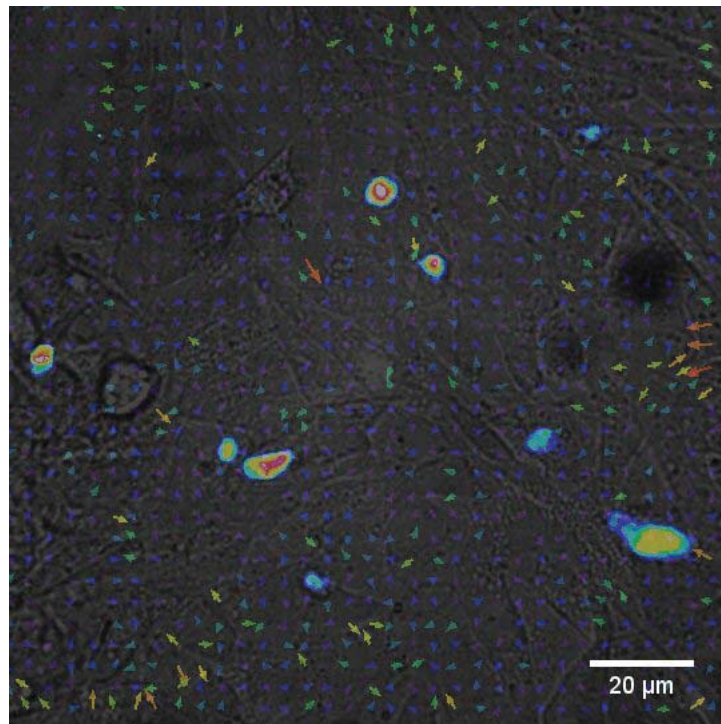
Figure 3.11: Method is ready for correlation measurements: overlay of color coded vector plot from the x and y components of the reconstructed traction forces of fibroblasts with the FRET signal from the csp-FRET to show the strain distrubution.
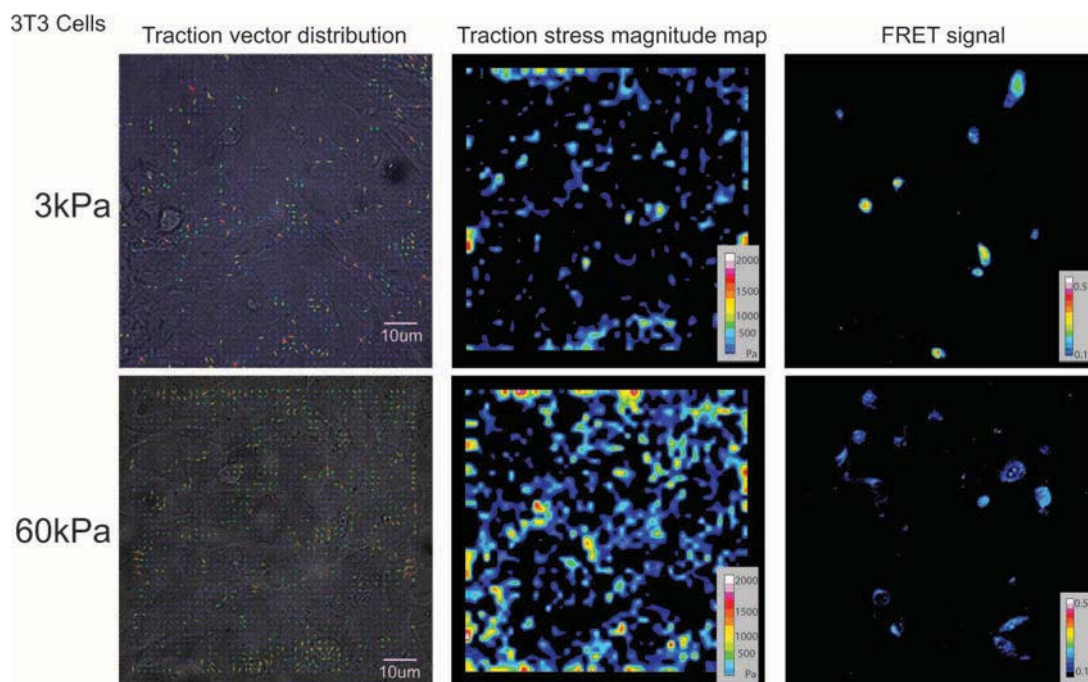
Figure 3.12: Fibroblast cells seeded on soft (3kPa) and hard (60kPa) polyacrylamide hydrogels containing fluorescent beads: color coded vector plot from the x and y components of the reconstructed traction forces are shown in the first column. The force magnitude stress map is shown as a measure of the traction force distribution in the cell monolayer in the middle column. The FRET efficiency signal is shown as a measure of the strain distribution in the membrane. For the angularly modulated FRET pairs described in the introduction high FRET efficiency corresponds to less strain and low FRET corresponds to high strain.

In order to analyze the FRET images, the RiFRET ImageJ plugin [45] was utilized. to calculate FRET correction coefficients and analysis as introduced in section 3.2 of this chapter. Briefly, first the background intensity was subtracted from the donor/donor, acceptor/acceptor and donor/acceptor as well as the donor bleached and acceptor bleached samples. Since donor (acceptor) only images are not available, donor bleached and acceptor bleached samples were used to calculate the correction coefficients. The signals in the FRET channel of donor bleached/acceptor bleached

were used to estimate the correction coefficients due to bleed through and crosstalk described in chapter 3.3. The coefficients were utilized to calculate the percentage of the signals not due to FRET and were thus subtracted from the uncorrected (contaminated FRET) before calculating the FRET efficiency. The FRET efficiency signal shown in the third column of **Fig**.3.l2 and 3.13 are typically in the range of 10-50% and represents the is the ratio of corrected FRET to acceptor emission. As described in section 3.3 of this chapter the FRET efficiency is due to the nature of the sensor a direct read out of the strain distribution in the membrane skeleton. For better visualizations of the FRET efficiency, the image is color coded using a 16-color lookup table. The FRET signal varies from cell to cell as the traction magnitude does. But since the transfection efficiency is low as expected from the length of the construct and cells were not sorted (number of transfected cells could have increased if they were sorted). The signal obtained from the small number of cells can not be good representatives for the average strain distribution over the cell monolayer. In general, for the fibroblast monolayers there average FRET signal from cells on the 60kPa are lower than the 3kPa signal. Low FRET corresponds to high strain so the
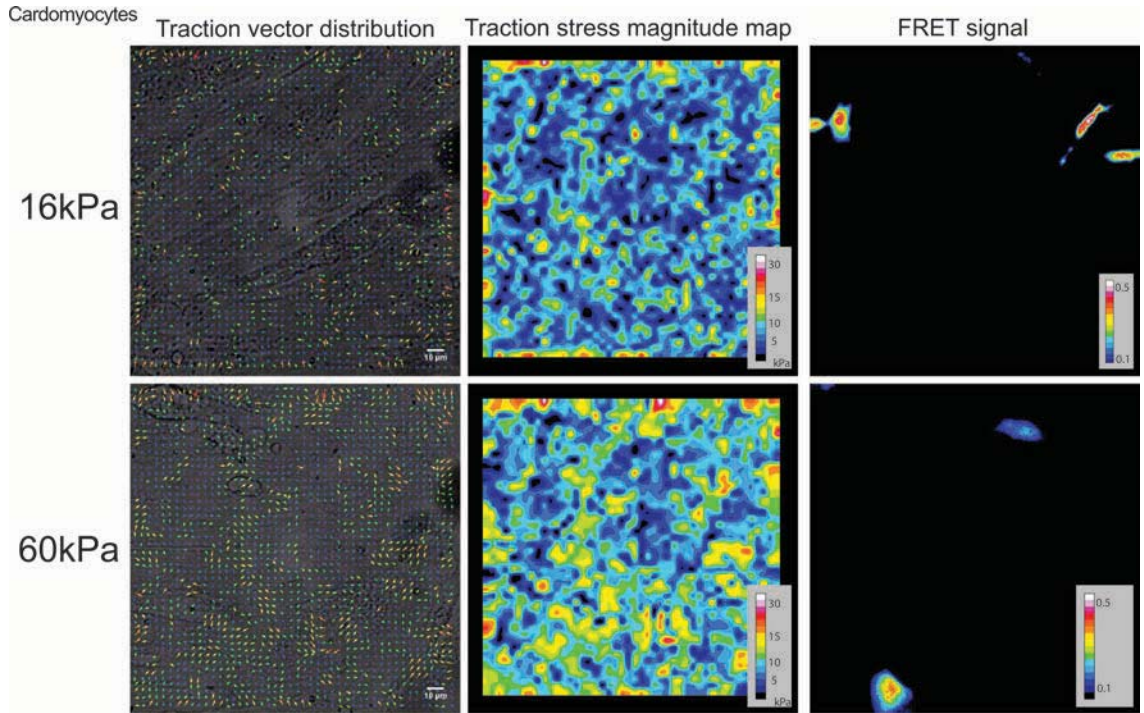
Figure 3.13: Cardiomyocytes seeded on intermediate (16kPa) and hard (60kPa) poly-acrylamide hydrogels containing fluorescent beads: color coded vector plot from the x and y components of the reconstructed traction forces are shown in the first column. The force magnitude stress map is shown as a measure of the traction force distribution in the cell monolayer in the middle column. The FRET efficiency signal is shown as a measure of the strain distribution in the membrane. For the angularly modulated FRET pairs described in the introduction high FRET efficiency corresponds to less strain and low FRET corresponds to high strain.

stress magnitude maps are directly correlated with the FRET. The number of the transfected cells are better than the cardiomyocytes and give a good representation of the strain distribution. But when it comes to the cardiomyocytes the 60kPa FRET signal is different for the two transfected cells and a comparison of the FRET signal can not be done using such small cell numbers. Further experiments needed to be performed to test the relationships in detail between the FRET signal and the traction magnitudes. But already in the preliminary experiments it is observed that

68

the traction magnitudes are in general higher when the PA gels are stiffer and that overall the traction stresses of the cardiomyocytes are about 15 times higher then the ones generated by the fibroblast cell monolayers.

In order to move forward and use this new combinational method for in depth experiments a few more optimizations, in particular with respect to cell number of transfected cells, needed to be performed. With the newly available fluorescence activated cell sorter at SU, however, this should be a straight forward operation. In conclusion, I have demonstrated that I have successfully integrated a fluorescently read-out of cellular strains with traction force microscopy measurements. This approach promises to be a powerful tool to investigate the intricate interrelation ship between force generation, sensing and mechanical properties of the cellular environment and the cell itself.

3.5 References

1. Joy, A., et al., Control of surface chemistry, substrate stiffness, and cell function in a novel terpolymer methacrylate library. Langmuir, 2011. 27(5): p. 1891-9.

2. Bershitsky, S.Y. and A.K. Tsaturyan, Force generation and work production by covalently cross-linked actin-myosin cross-bridges in rabbit muscle fibers. Biophysical Journal, 1995. 69(3): p. 1011-21.

3. Veltman, D.M. and R.H. Insall, WASP Family Proteins: Their Evolution and Its Physiological Implications. Molecular Biology of the Cell, 2010. 21(16): p. 2880-2893.

4. Maruthamuthu, V., et al., Cell-ECM traction force modulates endogenous tension at cell-cell contacts. Proc Natl Acad Sci U S A, 2011. 108(12): p. 4708-13.

5. Underwood, C.J., et al., Cell-generated Traction Forces and the Resulting Matrix Deformation Modulate Microvascular Alignment and Growth during Angiogenesis. Am J Physiol Heart Circ Physiol, 2014.

6. Gomez, G.A., R.W. McLachlan, and A.S. Yap, Productive tension: force-sensing and homeostasis of cell-cell junctions. Trends Cell Biol, 2011. 21(9): p. 499-505.

7. Chicurel, M.E., C.S. Chen, and D.E. Ingber, Cellular control lies in the balance of forces. Curr Opin Cell Biol, 1998. 10(2): p. 232-9.

8. Ingber, D.E., Cellular mechanotransduction: putting all the pieces together again. Faseb Journal, 2006. 20(7): p. 811-827.

9. Jasaitis, A., et al., E-cadherin-dependent stimulation of traction force at focal adhesions via the Src and PI3K signaling pathways. Biophysical Journal, 2012. 103(2): p. 175-84.

10. Bialkowska, K., S. Kulkarni, and J.E.B. Fox, Signaling across beta 3 integrin involves the calpain-induced formation of spectrin-integrin complexes; Evidence that the SH3 domain of spectrin participates in the activation of RAC within these clusters. Blood, 2000. 96(11): p. 241a-241a.

11. Reuzeau, C., et al., Covisualization in living onion cells of putative integrin, putative spectrin, actin, putative intermediate filaments, and other proteins at the cell membrane and in an endomembrane sheath. Protoplasma, 1997. 199(3-4): p. 173-197.

12. Bialkowska, K., T.C. Saido, and J.E.B. Fox, SH3 domain of spectrin participates in the. activation of Rac in specialized calpain-induced integrin signaling complexes. Journal of Cell Science, 2005. 118(2): p. 381-395.

13. Kizhatil, K., et al., Ankyrin-G is a molecular partner of E-cadherin in epithelial cells and early embryos. Journal of Biological Chemistry, 2007. 282(36).

14. Rotter, B., et al., alpha II-Spectrin interacts with Tes and EVL, two actin-binding proteins located at cell contacts. Biochemical Journal, 2005. 388: p. 631-638.

15. Opas, M., K. Turksen, and V.I. Kalnins, Adhesiveness and distribution of vinculin and spectrin in retinal pigmented epithelial cells during growth and differentiation in vitro. Developmental Biology, 1985. 107(2): p. 269-80.

16. Bennett, V. and D.M. Gilligan, The Spectrin-Based Membrane Skeleton and Micron-Scale Organization

of the Plasma-Membrane. Annual Review of Cell Biology, 1993. 9: p. 27-66.

17.   Jenkins, S.M. and V. Bennett, Ankyrin-G coordinates assembly of the spectrin-based membrane skeleton, voltage-gated sodium channels, and L1 CAMs at Purkinje neuron initial segments. Journal of Cell Biology, 2001. 155(5): p. 739-46.

18.   Ananthakrishnan, R. and A. Ehrlicher, The forces behind cell movement. Int J Biol Sci, 2007. 3(5): p. 303-17.

19.   Kuo, C.W., et al., Polymeric nanopillar arrays for cell traction force measurements. Electrophoresis, 2010. 31(18): p. 3152-3158.

20.   Style, R.W., et al., Traction force microscopy in physics and biology. Soft Matter, 2014. 10(23): p. 4047-55.

21.   Harris, A.K., D. Stopak, and P. Wild, Fibroblast Traction as a Mechanism for Collagen Morphogenesis. Nature, 1981. 290(5803): p. 249-251.

22.   Lo, C.M., et al., Cell movement is guided by the rigidity of the substrate. Biophysical Journal, 2000. 79(1): p. 144-152.

23.   Timoshenko, S. and J.N. Goodier, Theory of Elasticity 1970, New York McGraw-Hill.

24.   Huang, J.Y., et al., Determination of Cellular Tractions on Elastic Substrate Based on an Integral Boussinesq Solution. Journal of Biomechanical Engineering-Transactions of the Asme, 2009. 131(6).

25.   Sabass, B., et al., High resolution traction force microscopy based on experimental and computational advances. Biophysical Journal, 2008. 94(1): p. 207-20.

26.   Michel, R., et al., Inverse problems for the determination of traction forces by cells on a substrate: a comparison of two methods. Comput Methods Biomech Biomed Engin, 2012. 15 Suppl 1: p. 27-9.

27.   Zayed, A.I., A convolution and product theorem for the fractional Fourier transform. Ieee Signal Processing Letters, 1998. 5(4): p. 101-103.

28.   Wernet, M.P., Two-dimensional particle displacement tracking in particle imaging velocimetry. Appl Opt, 1991. 30(14): p. 1839-46.

29.   Kong, H.J., et al., FRET measurements of cell-traction forces and nano-scale clustering of adhesion ligands varied by substrate stiffness. Proceedings of the National Academy of Sciences of the United States of America, 2005. 102(12): p. 4300-4305.

30.   T., F., Intermolecular energy migration and fluorescence. Ann. Phys., 1948. 2: p. 55-75.

31.   Chen, Y. and A. Periasamy, Quantitative FRET data analysis: Protein localization in living specimens - art. no. 60891W. Multiphoton Microscopy in the Biomedical Sciences VI, 2006. 6089: p. W891-W891.

32.   Chen, Y. and A. Periasamy, Intensity range based quantitative FRET data analysis to localize protein molecules in live cell nuclei. Journal of Fluorescence, 2006. 16(1): p. 95-104.

33.   Gopich, I.V. and A. Szabo, FRET efficiency distributions of multistate single molecules. J Phys Chem B, 2010. 114(46): p. 15221-6.

34.   Xu, X., J.A. Brzostowski, and T. Jin, Using quantitative fluorescence microscopy and FRET imaging to measure spatiotemporal signaling events in single living cells. Methods Mol Biol, 2006. 346: p. 281-96.

35.   Wang, S., Q. Wu, and Z.C. Hua, Optimization of FRET algorithms for sensitized-emission FRET

detection. Chinese Optics Letters, 2012. 10(7).

36.   Yaghini, E., et al., Fluorescence lifetime imaging and FRET-induced intracellular redistribution of Tat-conjugated quantum dot nanoparticles through interaction with a phthalocyanine photosensitiser. Small, 2014. 10(4): p. 782-92.

37.   McGinty, J., et al., In vivo fluorescence lifetime tomography of a FRET probe expressed in mouse. Biomed Opt Express, 2011. 2(7): p. 1907-17.

38.   Meng, F.J. and F. Sachs, Orientation-based FRET sensor for real-time imaging of cellular forces. Journal of Cell Science, 2012. 125(3): p. 743-750.

39.   Kraning-Rush, C.M., et al., Quantifying traction stresses in adherent cells. Methods Cell Biol, 2012. 110: p. 139-78.

40.   Boudou, T., et al., An extended relationship for the characterization of Young's modulus and Poisson's ratio of tunable polyacrylamide gels. Biorheology, 2006. 43(6): p. 721-728.

41.   Institute of Cell and Molecular Science, T.B.B, The Blizard Building, Barts, UK http://www.icms.qmul.ac.uk/flowcytometry/uses/fret/ FRET. 1 November 2013.

42.   Salerno, M., et al., AFM Measurement of the Stiffness of Layers of Agarose Gel Patterned With Polylysine. Microsc Res Tech, 2010. 73(10): p. 982-990.

43.   Tseng, Q., et al., Spatial organization of the extracellular matrix regulates cell-cell junction positioning. Proc Natl Acad Sci U S A, 2012. 109(5): p. 1506-11.

44.   Tseng, Q., Study of multicellular architecture with controlled microenvironment". Ph.D. dissertation. Université de Grenoble. , 2011.

45.   Roszik, J., et al., Evaluation of Intensity-Based Ratiometric FRET in Image Cytometry-Approaches and a Software Solution. Cytometry Part A, 2009. 75A(9): p. 761-767.

Chapter 4

Additional experimental findings

4.1 Behavior of fibroblasts on lipid bilayers

What have been used in chapter three as cellular substrates were polyacrylamide gels with relatively uniform stiffness over their area. The PA gels are great in the measurement of the stress-strain correlation. When it comes to the biophysics and biochemistry of cell-cell communication, solid supported lipid bilayers (SLBs) are perfect platforms. They are a good substitute for the environment where cells communicate. SLB not only give us a better substrate which is close to the real cellular environment, it also helps to study the interaction between the membrane skeleton and lipid molecules as well as the skeleton's role in cell-cell communication. The system reduces non-specific bindings when we would like to specifically focus on a single protein of interest in cell-cell communication. In this system, only the protein of interest can be inserted into the cell-membrane-SLB junction. Use of a planar membrane fixes the orientation of the membrane-membrane interface and makes it

73
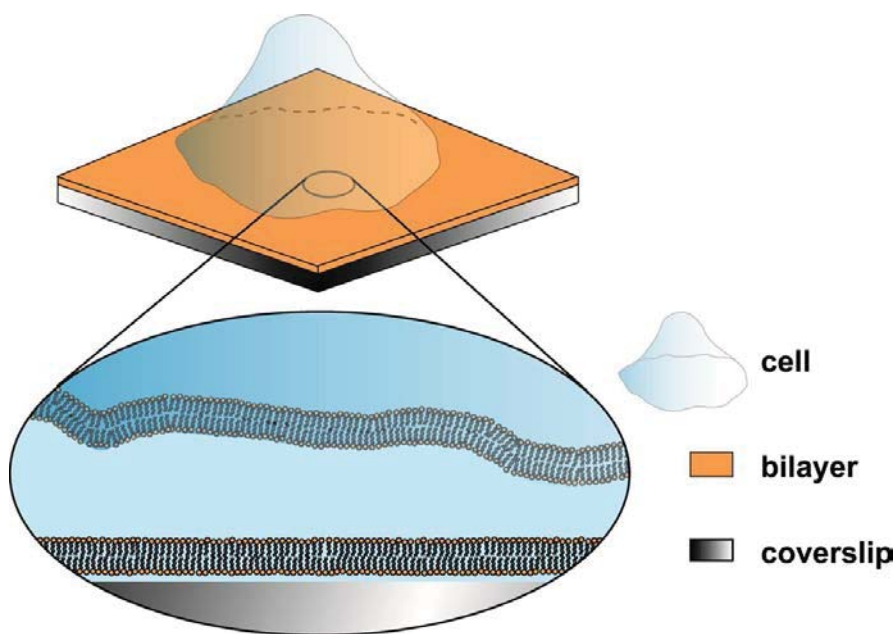
Figure 4.1: Cells on SLB consist of a lipid bilayer placed on a coverslip covered with aqueous solution and separated from the substrate by very thin hydration layer

easily accessible to imaging with optical instruments. Such systems have been used and were very successful in studying the neuronal and immunological synapse [1]. So there was an interest to implement the method to study the role of the membrane skeleton in cell-cell communication. To that end, similar to what is done in chapter 3, for the work on stress-strain correlations; Step by step characterizations were needed. Interestingly the effect of electrostatic interaction at the cell-cell interface on cell adhesion and density has not been well characterized experimentally. Therefore studying this in detail and characterizing this cellular behavior as a function of SLB charge and sugar compositions became the first p riority. In this work, the impact of surface charge and head group compositions on the morphology and proliferation of *NIH* 3T3 fibroblasts have been investigated. The primary results of the experiments are shown in Fig.4.5 and Fig.4.6.

74

4.1.1 Supported lipid bilayer preparation
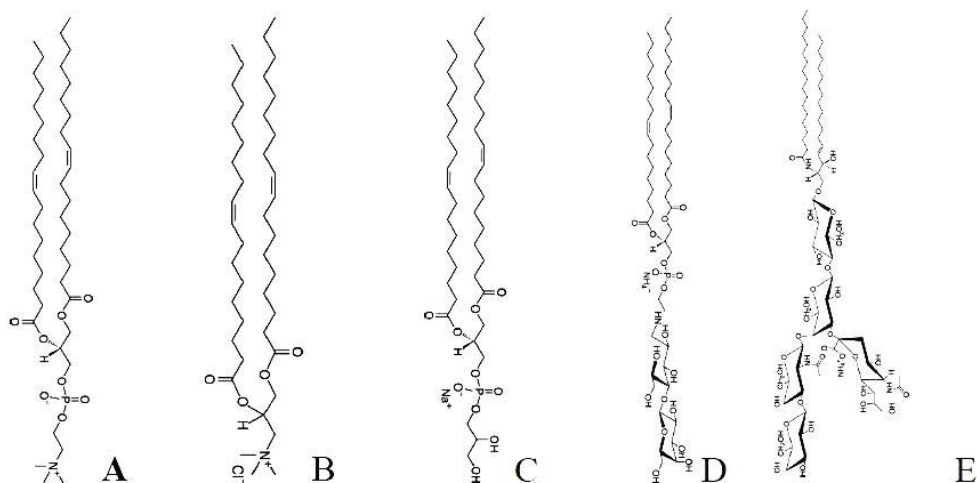
Figure 4.2: Lipids used : A) 1,2-dioleoyl-sn-glycero-3-phosphocholine (DOPC, charge 0; B) 1,2-dioleoyl-3- trimethylammonium-propane (DOTAP, charge +1); C) 1,2-dioleoyl-sn-glycero-3-phospho-(1'-rac-glycerol) (DOPG; charge -1); D) 1,2-dioleoyl-sn-glycero-3-phosphoethanolamine-N-lactosyl ; (Lactosyl PE);E) Ganglioside GM1

Lipids (Avanti Polar Lipids, Inc. Alabaster, AL) shown in **Fig.**4.2 were mixed and dissolved in chloroform in the desired ratios to obtain membrane surface charges of -10, -5, $0,+5$ and $+10$ mol%. This included 1 mol % of MarinaBlue - DHPE (Life Technologies, Carlsbad, CA) as shown in **Fig.**4.3 that carries a negative charge and was used for imaging the bilayer.

The lipid mixtures were dried on the walls of a glass flask in a rotovap and then left in vacuum for 1 hr. to remove residues of solvent. After hydrating the dry layers of lipids with doubled dionized water, they swell and were shaked to form large multilamellar vesicles. The solution was extruded 12 times through a 100nm polycarbonate membrane. The resulting solution of small unilamellar vesicles were
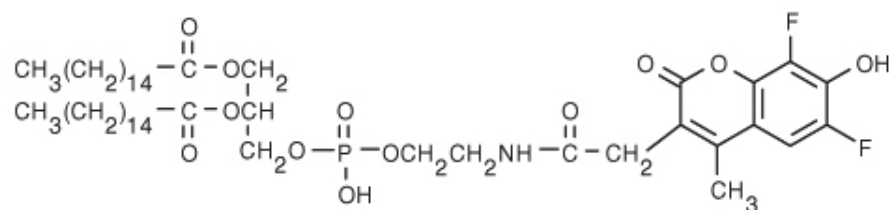
Figure 4.3: Marina Blue labeled lipids (Life Technologies, Carlsbad, CA) were used to confirm fluidity of the lipid bilayer using fluorescence recovery after photobleaching (FRAP) experiments

deposited on glass cover slips of 25 mm diameter via the vesicle fusion technique [2]. No. 1 (170 um thickness) glass cover-slips (Fisher Scientific International Inc., Hampton, NH) were cleaned with piranha as described in section chapter 5 section 9.1. Small unilamellar vesicles (100 nm diameter) of the different lipid/ganglioside compositions were prepared by vesicle extrusion methods [3, 4]. Typically, lipids and ganglioside suspended in chloroform/methanol were mixed in a glass vial. The solvent phase was then evaporated under a stream of nitrogen and subsequently evacuated for at least 1 h under vacuum. The dried lipid film was then resuspend in deionized water and hydrated overnight at 4℃. The total lipid concentration was 2 mg/ml. Vesicles for the experiments were homogenized after hydration by passing them with 1800 kPa, 11 times through polycarbonate filters of 100 nm pore diameter (Whatman Inc., Clifton, NJ) within a high pressure extruder (Northern Lipids Inc., Vancouver, Canada).

4.1.1.1 Vesicle Preparation

4.9, extensively rinsed with DI water and then dried with a stream of nitrogen. The SUV suspension was mixed 3 : 1 (v/v) with TRIS and 35 ul of the resulting solution was pipetted into a plastic Petri dish, after which the cover slip was placed on the droplet. The Petri dish was submerged in TRIS, where the cover slip, now covered with a single lipid membrane, was carefully removed and repeatedly moved through the buffer to wash away excess vesicles. Finally, the cover slip was mounted in an Attofluor cell chamber (Molecular Probes, Eugene, OR)

4.1.1.2 Bilayer Formation on glass cover slides

Supported lipid membranes were formed on glass cover slips of 25 mm diameter via the vesicle fusion technique described in [2]. Briefly, No. 1 (170 nm thickness) glass cover-slips (Fisher Scientific International Inc., Hampton, NH) were cleaned with piranha solution (3:1 concentrated sulfuric acid: hydrogen peroxide), extensively rinsed with DI water and then dried with a stream of nitrogen. The SUV suspension was mixed 3:1 (v/v) with PBS and 35 ul of the resulting solution was pipetted into a plastic Petri dish, after which the cover slip was placed on the droplet. The Petri dish was submerged in PBS, where the cover slip, now covered with a single lipid membrane, was carefully removed and repeatedly moved through the buffer to wash away excess vesicles. Finally, the cover slip was mounted in an Attofluor cell chamber (Life Technologies, Carlsbad, CA) and placed onto the cell culture hood for cell seeding.

4.1.2 Cell seeding, counting and poly-lysination

Prior to cell seeding, the TRIS buffer in the sample chamber was replaced by DMEM. $NIH3T3$ cells were seeded at 5100 cells/cm^2 on the different substrates. After 24hrs at 37℃ the cells were stained with a fluorescence live (green) - dead (red) stain (Life Techonologies, Carlsbad, CA). Cell counting of DAPI stained nucleus was done using images acquired by an inverted epi-fluorescence microscope. Before starting to use Hoechst stain which staines live cell DNA we tested weather DAPI stain can be used for live cell experiments and the result is shown in fig.4.4. The number of cells per image were measured using the cell counting plug-in for ImageJ. To increase adhesion with the glass it was modified with a layer of electrostatically adsorbed α-poly-l-lysine. This coat of the cationic peptide is known to increase cell adhesion [5]. To that end, 0.1 mg/ml solution of α-poly-l-lysine (Sigma Aldrich, St.Louis, Mo) has been prepared in PBS. 500ul of the solution was added to a parafilm tapped on a flat place in the hood for uniform coating. Etched coverslips have been inverted on the solution and incubated for 1hr. The coated coverslips were washed thrice in PBS and mounted in an Attofluor cell chamber (Life Technologies, Carlsbad, CA) for cell seeding.
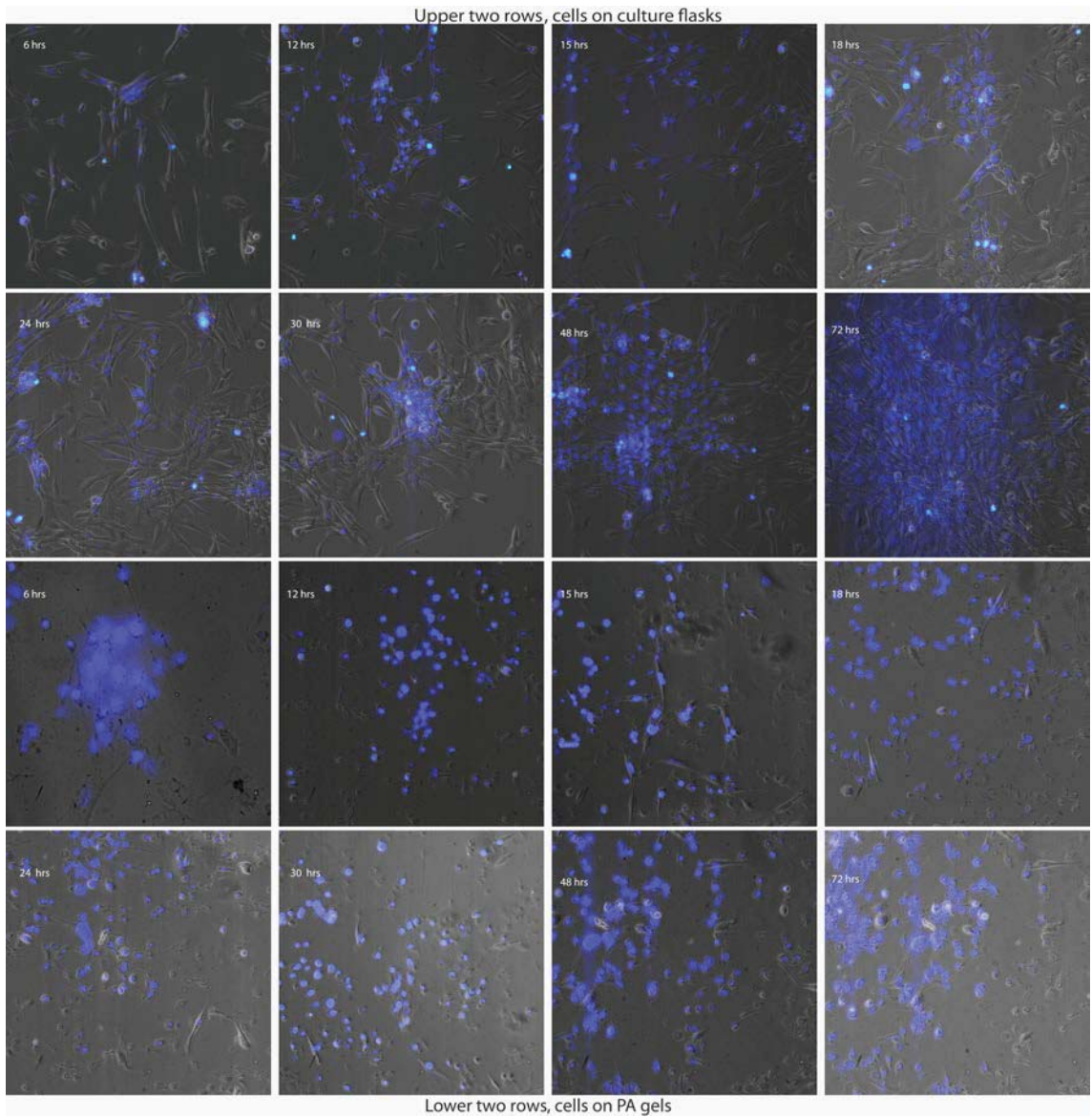
Figure 4.4: Cell viability was checked at different time points after DAPI staining on culture flasks and PA gels to check the effect of the labeling on cell morphology and helath for cell counting
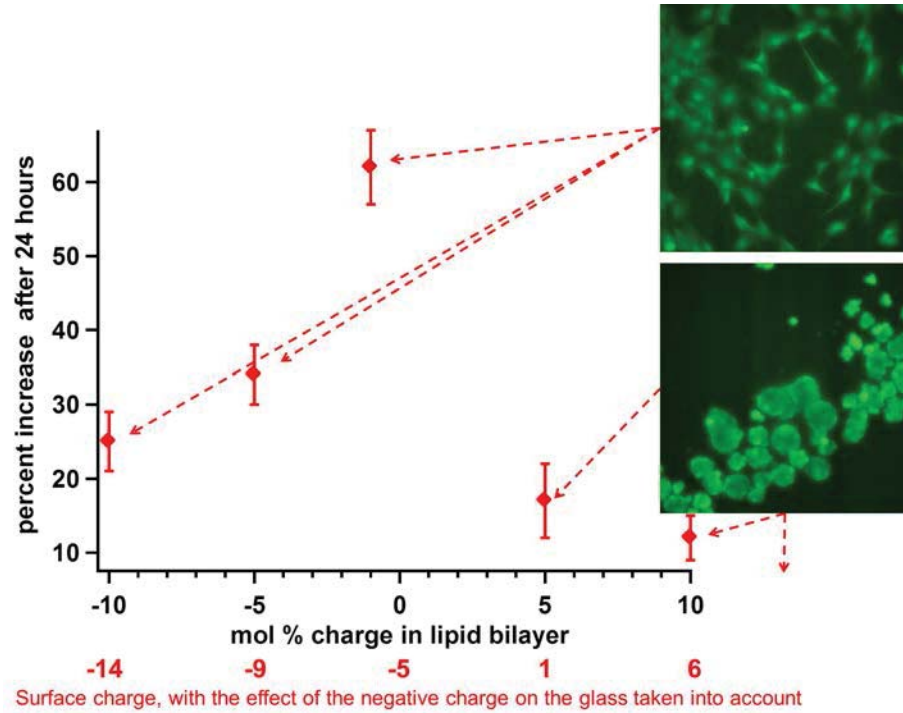
Figure 4.5: Live-dead staining was performed with calcein-AM (live-green), and with ethidium homodimer(dead red) to measure cell ploriferation and morphology (adhesion). On lipids of different surface charge composition The effective surface charge is obtained by including the charge on the etched coverslip (-4) [6,7]

The primary observation is that, on negatively charged substrates cells proliferate much faster than on positively charged bilayers. This observation correlates also with the morphological differences of the two charge scenarios. On negative charged bilayers cell morphology is similar to cell growing on the poly-l-ysinated glass control surface. In contrast, on positively charged bilayers large cell-clusters form that have apparently problems of successfully adhering. Nevertheless, the green stain indicates that they are alive and proliferating. Despite our expectation enriching the bilayers with 5 mol% of lipids with sugar elaborated head groups did not improve proliferation behavior. In fact inclusion of GM1 in the bilayer leads to diminished cell

80
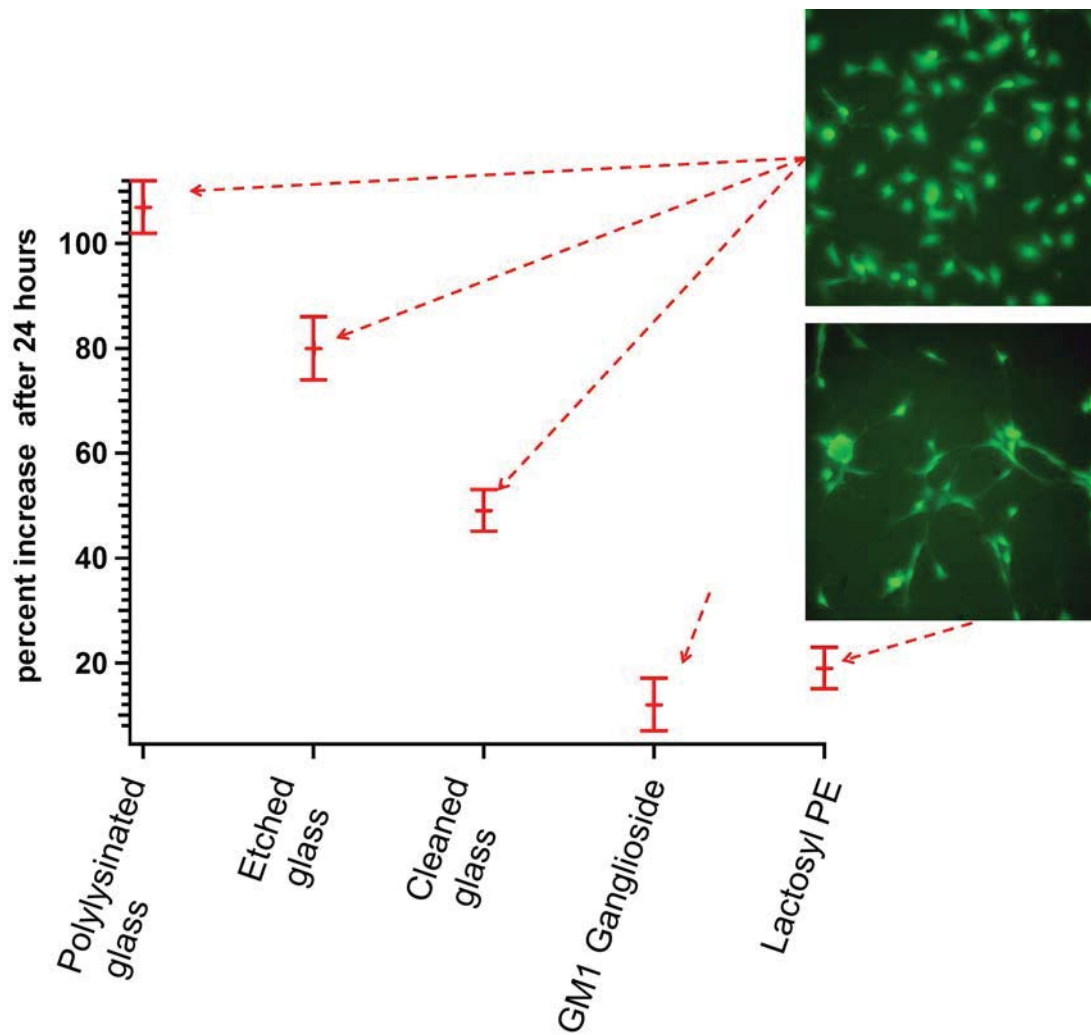
Figure 4.6: Live-dead staining was performed on cells seeds on commonly used substrates to compare with the ploriferation of cells on bilayers coposed of GM1 Ganglioside and Lactosyl PE sugar head groups

growth and morphology similar to the cells on positive bilayers. Surprisingly, cells grown on membranes containing lipids with lactosyl head groups exhibited new cell morphology, but also diminished growth. The presented study is only a first part of a more systematic investigation of cell behavior on supported bilayers. The immediate next experiments involve comparison of these results with different cell types as well as the inclusion of the fusiogenic lipids mixtures with a phosphoethanolamine head group that are natively located at the extracellular membrane leaflet and are thought to be protein and cell repellent [8].

4.2 References

1.   Pautot, S., et al., Neuronal synapse interaction reconstituted between live cells and supported lipid bilayers. Nature Chemical Biology, 2005. 1(5): p. 283-289.

2.   Brian, A.A. and H.M. Mcconnell, Allogeneic Stimulation of Cyto-Toxic T-Cells by Supported Planar Membranes. Proceedings of the National Academy of Sciences of the United States of America-Biological Sciences, 1984. 81(19): p. 6159-6163.

3.   Mayer, L.D., M.J. Hope, and P.R. Cullis, Vesicles of Variable Sizes Produced by a Rapid Extrusion Procedure. Biochimica Et Biophysica Acta, 1986. 858(1): p. 161-168.

4.   Groves, J.T., N. Ulman, and S.G. Boxer, Micropatterning fluid lipid bilayers on solid supports. Science, 1997. 275(5300): p. 651-653.

5.   Ardjomandi, N., et al., Indirect coating of RGD peptides using a poly-L-lysine spacer enhances jaw periosteal cell adhesion, proliferation, and differentiation into osteogenic tissue. J Biomed Mater Res A, 2012. 100(8): p. 2034-44.

6.   Parthasarathy, R., P.A. Cripe, and J.T. Groves, Electrostatically driven spatial patterns in lipid membrane composition. Physical Review Letters, 2005. 95(4).

7.   Behrens, S.H. and D.G. Grier, The charge of glass and silica surfaces. Journal of Chemical Physics, 2001. 115(14): p. 6716-6721.

8.   Afanasenkau, D., Supported lipid bilayer as a biomimetic platform for neuronal cell culture, in Dissertation2012.

9.   Chiou, Y.W., et al., The influence of physical and physiological cues on atomic force microscopy-based cell stiffness assessment. PLoS One, 2013. 8(10): p. e77384.

10.   Li, C., et al., The use of polyacrylamide gels for mechanical calibration of cartilage--a combined nanoindentation and unconfined compression study. J Mech Behav Biomed Mater, 2011. 4(7): p. 1540-7.

Chapter 5

Materials and Methods

In this chapter, the materials and methods that were modified, re-developeD and used in this work to address the research problems are stated in detail, for the purpose of reproducing the experiments whenever such needs arise.

5.1   Cell culture

$3T3$ fibroblasts, $10T\frac{1}{2}$ mesenchymal stems, $H9c2(2-1)$ cardiomyocytes and CHO Chinese hamster ovary cell lines (all from ATCC, Manassas, VA) were cultured at 37℃ under 5% CO_2 enriched atmospheric air. They were routenly subcultured in 25 cm^2 angled neck cell culture flasks (Fisher Scientific, Pittsburgh, PA) in Dulbecco's modified eagle's medium (DMEM)(ATCC, Manassas, VA) for the first three and F-12 media (ATTC) for the CHOs. The media were supplimented with 10% fetal bovine serum (FBS) and 1% Penicillin-streptomycin complex (both from Life Technologies, Carlsbad, CA). The sub-culture was done in a ratio of $1:4-1:10$ on average three

times a week depending on the number of cells needed for a specific experiment and the type of cell used. When ever a large number of cells were needed for an experiment, they were splitted on average in a 1:4 ratio. This ratio varies from one cell type to another because of a difference in the doubling rate of the different cell lines. Standard aseptic techniques were followed to keep the cells healthy and free of contamination, such as sterile filtered phosphate buffered saline (PBS), trypsin-EDTA (Life Technologies, Grand Island, NY) and appropriate media is used for sub culturing procedures by carefully checking and handling the cells to avoid reaching complete confluence during their growth. Whenever they become fully confluent, cells stop growing due to contact inhibition (confinement). In addition, due to high metabolic waste accumulation, the pH of the media changes to acidic which in turn is toxic to cells and causes cell death. During the sub-culturing procedure, the different cell lines were splitted one cell type at a time and were incubated in different sections of the incubator to avoid possible problem of cross contamination. Cells of passage number up to 25 were used by repeatedly freezing and thawing some of the cells at their low passage number.

5.2   Periodic force application to cells

For the actual application of equi-biaxial stretch to adherent cells, a Flex cell $FX-5000$ tension system shown in Fig.5.1 (Flex Cell International Corp., Hillsborough, NC) utilizing six well plates with collagen modified, silicon membranes was used. By applying vacuum from below the flexible membranes are stretched over a cylinder, thus applying strain to the cells adhering to the membrane. Cells were counted with

a Hemacytometer (Fisher Scientific, Pittsburgh, PA) and plated at $160,000$ cells/well on each well of the collagen type-I coated bioflex plates. Typical experimental parameters were a stretching magnitude of 20% at frequencies of 1Hz for a stretching duration of 24hrs. Forces were applied to the cells growing in three of the six wells of each plate, while the remaining three wells were kept unactuated and thus served to grow the cells for the controls.
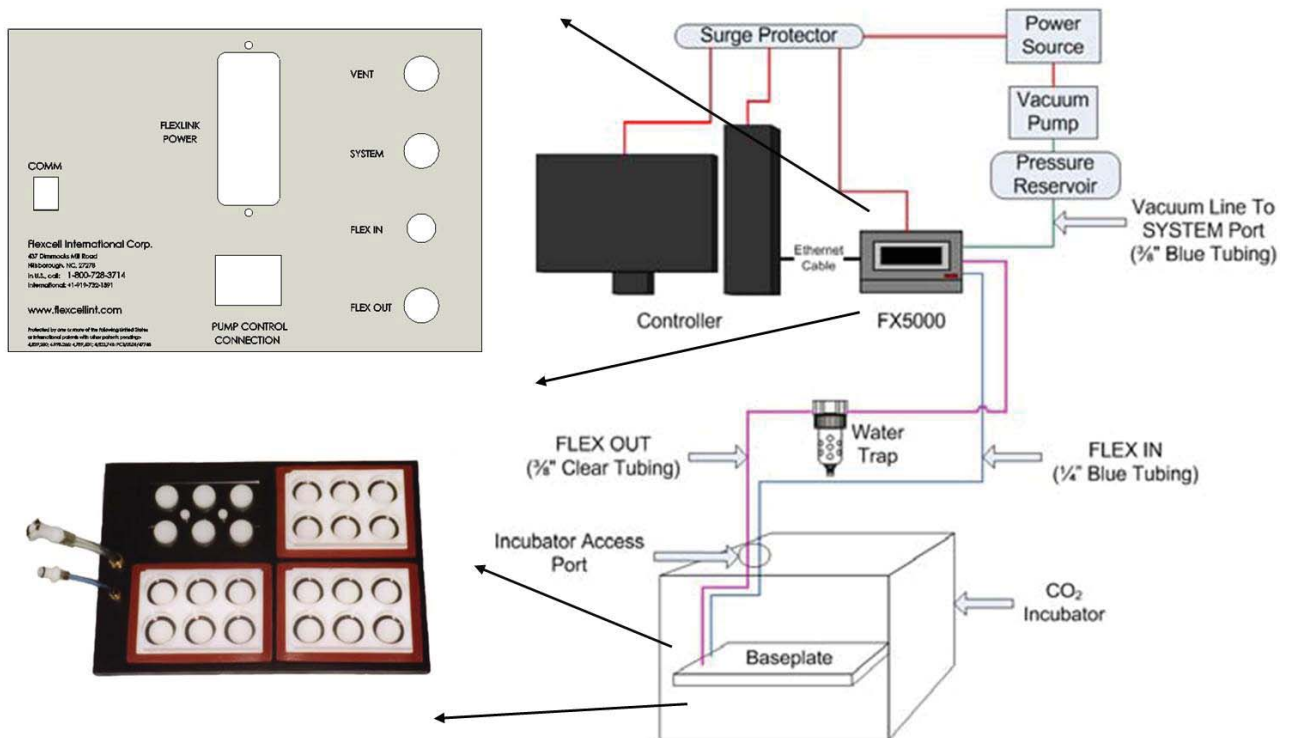
Figure 5.1: Strain application system used for force application (Flexcell International Corp.)

5.3 Spectrin and ankyrin labeling using immuno-staining.

Equal number of control and stimulated cells were equilibrated with poly ethylene glycol (PEG) solution in fresh PEM (100 mM PIPES, 1 mM $MgCl_2$, 1 mM EGTA, pH 6.9) buffer. They were fixed for 2hrs with a 3% formaldehyde solution in PEM buffer, permeabilized with 0.5% Triton X-100 solution in PEM buffer and incubated over the night at 4°C in a 1 : 40 dilution of rabbit anti-spectrin (Abcam, Cambridge, MA) and 1% BSA or a 1 : 300 dilution of mouse anti-ankyrin B (Life Technologies Grand Island, NY) and 1% BSA, respectively. For visualization, optimized amounts of 2 ug/ml AlexaFluor 488 labeled anti-rabbit and 2.5 ug/ml Alexa Fluor 647 labeled anti mouse secondary antibodies (both from Life Technologies, Grand Island, NY) were utilized.
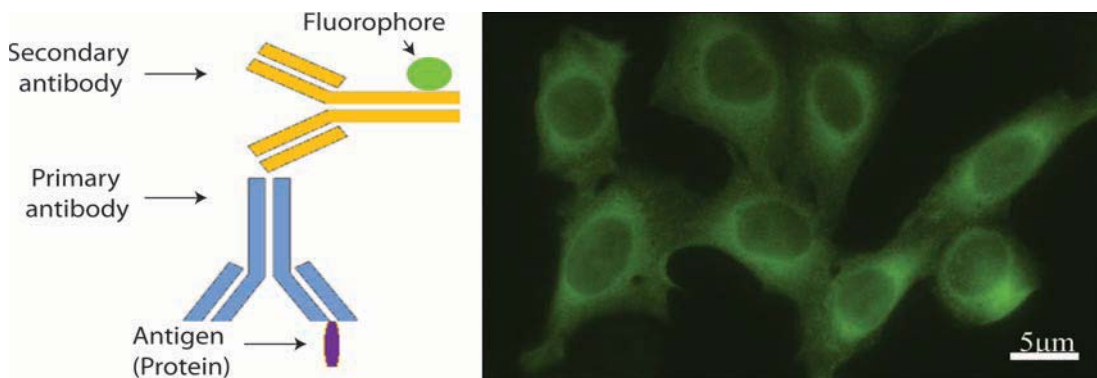
Figure 5.2: Basics of fluorescent Immunostaining: schematic specific fluorescence staining using a primary and fluorescence conjugated secondary antibody, in the right is an example of the resulting fluorescence image (immunostained spectrin in CHO cells).

5.4 Quantitative epi-fluorescent and bright field imaging

Immunostained spectrins and ankyrin B in the fixed cells were imaged under wide field epi-fluorescent illumination. Keeping all image acquisition settings the same allows to use the recorded fluorescence intensity as a direct measure of protein abundance for comparison. Image J (National Institutes of Health Bethesda, MD) image processing software was used to measure and analyze the mean intensity per area of the protein expressions from equal number of cells from 30 different images pairs for each of the four cases. Special care was taken that images from the samples and the control were taken at identical illumination and acquisition conditions and settings. This enables us to use the intensity readout as a direct measure of relative protein content.
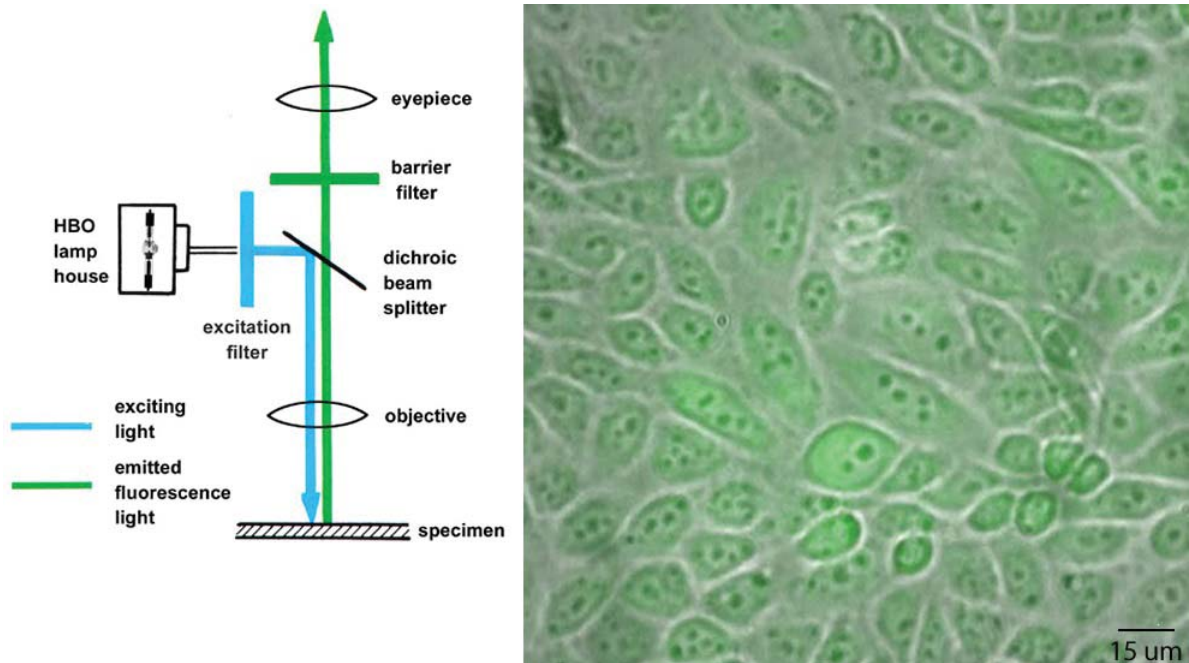
Figure 5.3: Schematics of an epi-fluorescent microscope (on the left) and overlay of fluorescent image of labeled spectrin (green) and a phase contrast bight field image that shows the cell boundaries and viability is shown on the right.

5.5 Immuno- and co-immunoprecipitation

After lysing cell monolayers with lysis/wash buffer for immunoprecipitation (IP), for each sample the lysate was combined with $6 - 10$ ug of the appropriate primary antibody (anti-spectrin or anti-ankyrin) in a micro-centrifuge tube and was incubated over the night to form immune complexes. Protein A/G (a recombinant fusion of Protein A and Protein G) magnetic beads (Pierce, Rockford, IL), prewashed with wash buffer, were then added to the immune complexes and incubated for an hour at room temperature. The beads were collected with a strong magnet and the unbound samples were saved for the analysis and calculation of the capturing efficiency of the method. After washing the complexes three times with wash buffer and one

times with DI water, spectrin and ankyrin B were eluted from the beads. This was performed under reducing conditions in lane marker sample buffer (Pierce, Rockford, IL) for the SDS measurements. And a colorless elution buffer (Thermo Scientific, Pittsburgh, PA) was used for the Bradford measurements to avoid interference with concentration dependent color change to be measured. The elution releases spectrin or ankyrin, respectively, from the insoluble complex.
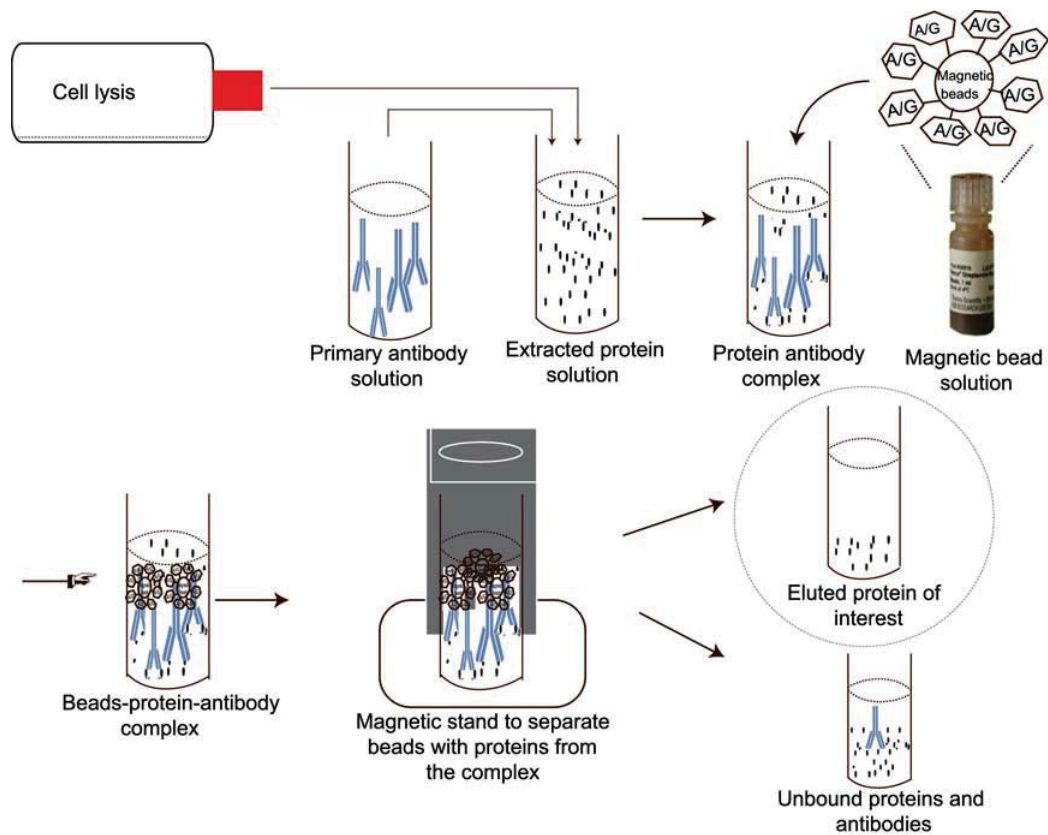
Figure 5.4: An illustration of the different steps in the immunoprecipitation procedure starting at cell lysis step until the target protein is eluted.

5.6 SDS-PAGE (Sodium dodecyl sulfate polyacry-lamide gel electrophoresis)

Protein samples from equal number of control and stimulated cells obtained from the IP were loaded either in 7.5% or any-kD gradient precast gels (Bio-Rad, Hercules, CA). Gels were electrophoresed in Tris-Glycine-SDS buffer for 45min at 60 mA. Gels were stained with 0.3% coommassie blue stain (Sigma-Aldrich, St.Louis, Mo) prepared in 50% methanol and 10% acetic acid in DI water. After imaging the stained gels with a 5sec exposure with a bioimager (ChemiDoc XRS system, Bio-Rad, Hercules, CA), the mean intensity per area of the protein bands were measured and analyzsed with Image Studio Lite (LI-COR Biosciences, Lincoln, NE). Overall it is important to assess from how many cells the protein sample should be prepared to get a good signal in the SDS gel. Thus, the sensitivity of the system was tested for a decreasing amount of bovine serum albumin (BSA). As shown in Fig.5.5, it was determined that protein amounts in the order of nanograms can be measured using this method.

5.7 Western blotting

Co-immunoprecipitated spectrin extracts and whole cell lysates of $20,000$, $10,000$ and 5000 cells were run on a 7.5% Tris glycine gel (Bio-rad) at 45 mA. They were transferred to a PVDF membrane. Unspecific binding sites were blocked by submerging the membrane in superbloack blocking buffer (Thermo scientific, Pittsburgh, PA) for 1 hour at room temperature before immunodetection. Membranes were incubated
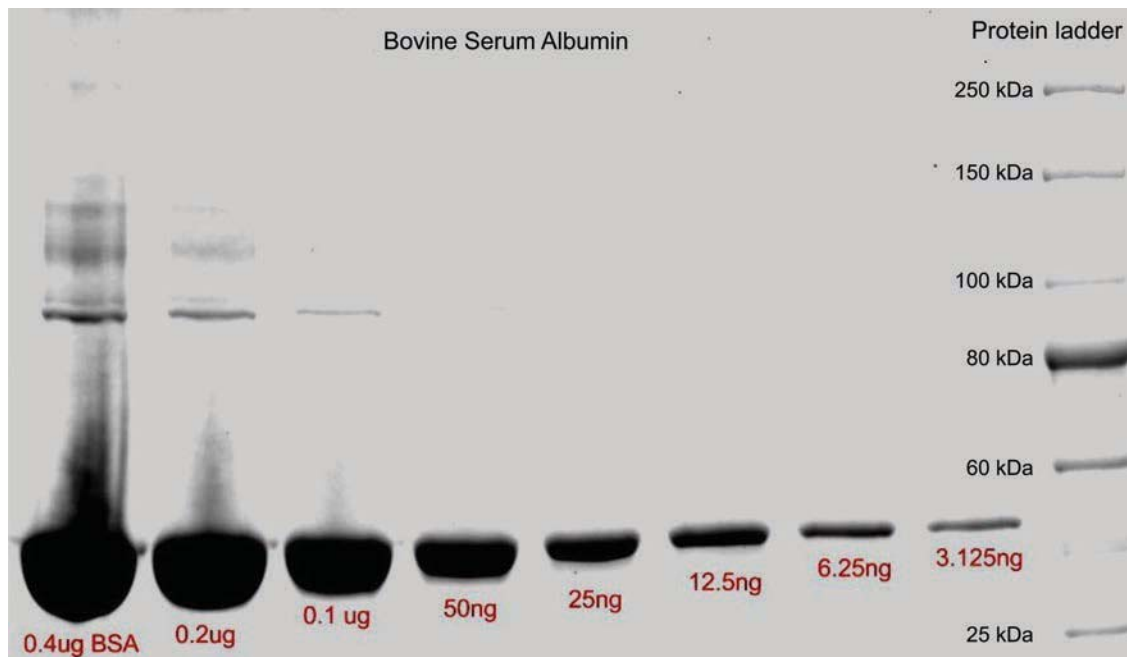
Figure 5.5: Testing the sensitivity of coommassie blue dye reagent used for staining the gel. It is shownn that the system can detect as small as 3 ng of a protein. This was considered before samples were prepared and loaded to the gels.

overnight in a 1 : 1000 dilution of Lys 48-specific rabit anti-polyubiquitin antibody (Milipore, Temecula, CA) diluted in 10% Super block blocking buffer. Membranes were washed 3 times for 5min each in Phospate Buffer Saline and 0.05% Tween 20 (PBST) and then incubated for 1hr with horseradish peroxidase (HRP) conjugated anti-rabit antibody (Cell-Signaling, Technology Inc., Danvers, MA, USA), which was also diluted in 10% Super block blocking buffer. The membrane was again washed three times for 5 minutes each in PBST (0.05% Tween 20) and incubated with and incubated with enhanced chemilumescent (ECL) substrates (Pierce, Rockford, IL) for 3min. Finally, the membrane was exposed to the bio imager (ChemiDoc XRS system, Bio-Rad, Hercules, CA) for the protein signal collection. The protein bands

were analyzed using densitometry. The mean intensity per area for each protein band in the stimulated cells was compared with the control to obtain the fraction of each protein density.

5.8   Bradford assay and spectrophotometry

7 ul of BSA standards of 1 mg/ml,0.5 mg/ml, 0.25 mg/ml, 125 mg/ml, 0.0625 mg/ml, 0.0312 mg/ml and unknown concentration samples of whole cell lysate protein, immunoprecipitated spectrin, ankyrin and blank samples were mixed for 30sec with 250 ul of the coomassie protein assay Reagent (Thermo scientific, Pittsburgh, PA) in labelled 96-well Plates. Samples were prepared in triplicates. The plates were incubated for 10min at room temperature and absorbances were measured at 595 nm with a microplate reader (BioTeK, Winooski, VT). Measurements were corrected for the blank measurement before preparing the standard curve. The curve was then used to determine the protein concentrations of each spectrin, ankyrin and whole cell lysate sample.

5.9   Traction force microscopy

5.9.1   Coverslip preparation

5.9.1.1   Etching coverslips

To ensure maximum coating, eight 25 mm No-1 coverslips (Thermo Scientific, Pittsburgh, PA) were arranged in a rack and submerged in isopropanol (Sima Aldrich, St.

Louis, MO). They were degassed for 5min and sonicated for 15min before rinsing six times in DI water (from a MiliQ-system, Millipore, Billerica, MA). The were etched carefully with a mixture of 75% sulfuric acid and 25% hydrogen peroxide (both from Sigma Aldrich, St. Louis, MO) solutions for 5 minutes before another $10x$ rinsing with DI water.

5.9.1.2   Bottom coverslip activation

Coverslips were dried with N_2 gas, labeled to track the activated side, and placed separately on a hot plate. They were quickly passed through a flame of a Bunsen burner for uniform coating formation. 500 ul of 0.1 M $NaOH$ was added immediately to the flamed side of each coverslip and distributed uniformly on the surface of the glass. They were then heated at 80℃ until all the NaOH evaporated. In cases were the coating was not uniform, the $NaOH$ layering had been repeated one more times.

In a chemical fume hood, 60ul of 3-aminopropyltrimethoxysilane was added to each surface of the coverlips and allowed to react for 6 minutes. Immediately both the top and bottom faces of the coverslips were washed thoroughly three times with DI water by incubating (agitating) them for 5 minutes between each wash. Amino-silane containing solutions were disposed as hazardous waste.

After the final wash, the solutions were decanted and coverslips were inverted on to 1ml, 0.5% glutaraldehyde solution in PBS on a parafilm. Coverslips were incubated in the solution for 30min before rinsing three times with DI water. The glutaraldehyde wastes were disposed as hazardous waste. Coverlsips were tranfered in to a rack in a glass beaker, covered with aluminum foil and were incubated for 24 hours to dry naturally in air.

5.9.1.3   Top coverslip activation

18mm No-2 coverslips (Fisher Scientific, Pittsburgh, PA) were etched and dried using
the procedure in subsection 4.8.1.1. Coverslips were arranged in a fume hood for a
coating with 10% surfasil siliconizing fluid (Pierce Biotechnology, Rockford, IL) in
acetone (v/v). Coverlsips were fully immersed in the diluted surfaSil Solution for
6sec to form a thin film coating on the surface. Quickly, coverslips were rinsed with
acetone and methanol respectively. This was quickly done to prevent reaction of
surfaSil coating with water which reverses siliconization. Coverslips were allowed to
dry by heating at 100℃ for 30 minutes.

5.9.2   Polyacrylamide (PA) hydrogel substrate preparation

Polyacrylamide (PA) gels of stiffnesses of 3 kPa, 16 kPa, 36 kPa and 60 kPa were
prepared in Eppendorf tubes. This stiffness range is going from "soft" to "hard"
in terms of physiological conditions encountered by fibroblasts and cardiomyocytes.
The variation in stiffness was achieved by varying the amounts of acrylamide/bis-
acrylamide (the crosslinker) from 40% acrylamide and 2% bis-acrylamide (both from
Fisher Scientific). The resulting stiffness of the polymerized PA gels can be calcu-
lated from measurements of shear stress and strain. By carefully applying a vertical
known force to a well clamped cylinderical gel and it's extention due to the force
can be measured to calculate the shear modulus (G') of the gels [1]. The result was
shown in **Fig.**4.6 and was used to calculate the elastic modulus $E = 2G(1+\nu)$ where ν
is the posson ratio (mean Poisson's ratio of PA gels was measured to be 0.48) [2].
Fluorescent beads (Bangs Laboratories, Inc. Fishers, IN) (1% by v) were sonicated

for 10 minutes and added to 600 ul of acrylamde mix for each desired stiffness. The solution was degassed in a sonicator for 30minto reduce oxygen within the solution which affects the speed of polymerization. Fresh 10% ammonium persulfate (APS) (Biorad Hercules, CA) solution (10 mg/100 ul) was prepared. 2.5ul of the APS solution and 0.6 ul of TEMED (Biorad, Hercules, CA) were added and mixed througly to initiate gel polymerization. Immediately, 25 ul of the mixture was diposited on the top silconized coverslips and the amino-silaneated bottom coverslips were placed on the top of the dropped PA solution. The uniform distribuition of the PA solution was checked and maintained by smoothing out bubbles that appear in the solution. The PA gel sandwich was kept in the fume hood to allow polymerization at room temperature for $15 - 20$min. The state of polymerization was monitored by the un-used solution in the eppendorf tube and by observing the edges of the coverslips where the PA gels pull away when polymerized. At that point, the top coverslips were separated carfully from the sandwich by submerging the polymerized gel in DI water and using the tip of a pair of tweezers. When ever the next step was perofmed on the next day, the PA gels on the bottom coverlips were stored in 35 mm petridishes under PBS with 1% penicillin-streptomycin complex.
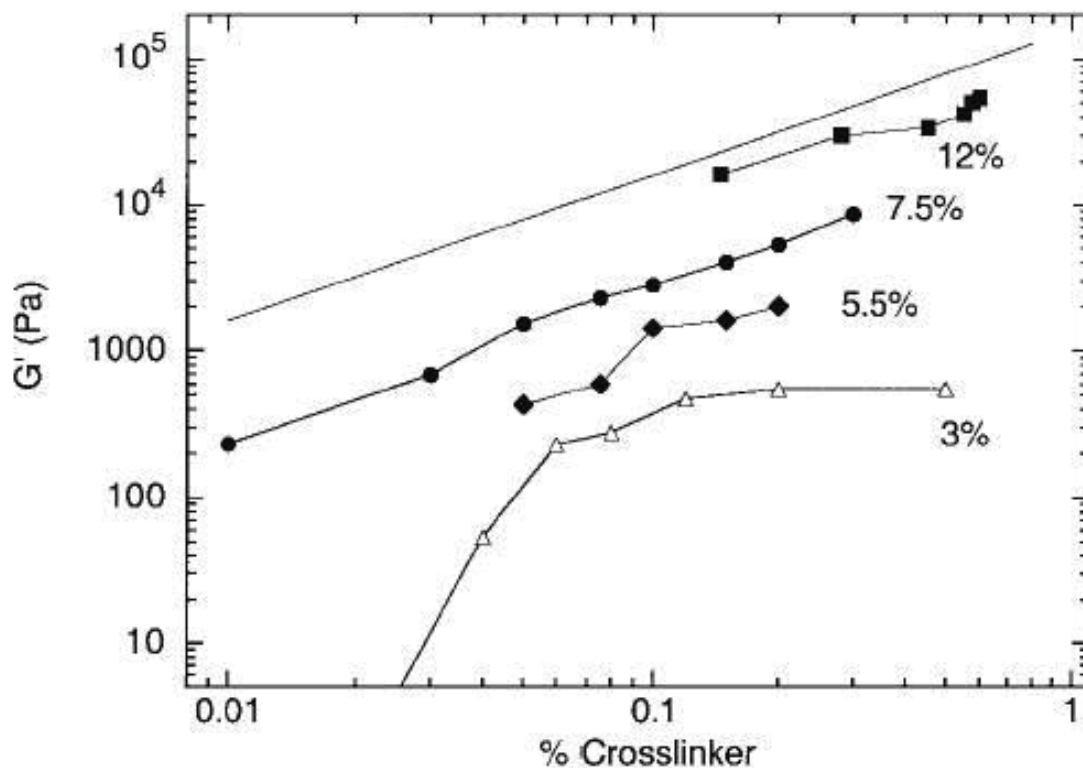
Figure 5.6: Mechanical properties (shear modulus) of PA gels with different acrylamide/bis-acrylamide ratio. Increasing the percentage of the crosslinker (bis-acylamide) in the acrylamide solution for different percentages of acrylamide increases the shear modulus ($G'(Pa)$). The measurement agrees with the theretical prediction of a rubber like material shown as a solid line [1].

5.9.3 Functionalization and characterization of PA gels for cell culture

PA gels do not easily associate with proteins or cell. Thus a covalent binding of extracellular proteins to the gel is needed to create a bio-functionalized top layer that ensures approproate cell attachment [3]. There are four different methods used to attach ECM proteins to the PA gels for creating adhesive surface for cell culture.

The first, the hydrazine hydrate method, utilizes the formation of acyl azide groups on methylated carboxyl groups of collagen using hydrazine and nitrous acid. It provides the largest range in ligand density but the steps are long to execute and can not be used for proteins which lack appropriate carbohydrate groups necessary for oxidation [4].

The second an easier to execute conjugation method is using 6-((acryloyl)amino) hexanoic acid into the gel solution as it polymerizes. The hexanoic acid copolymerizes into the gel and displays an N-hydroxysuccinimide ester for amine-containing proteins to bind[5].

The third and expensive method uses $Cell-Tak$ (BD Biosciences, San Jose, CA) cell and tissue adhesive which is a formulation of polyphenolic proteins extracted from Mytilus edulis (blue mussel) [6]. It is used to attach cells or tissue sections to many types of surfaces, including plastic, glass, metal, polymers, and biological material and is biocompatible [7]. It has been used to conjugate laminin with ply ylamide substrate for the study of nuronal mechanics [8].

The fourth robust mthod and used for my experiments is based on the use of Sulfo-SANPAH, a heterobifunctional protein cross-linker. It covalently binds proteins to the polyacrylamide substrates. Sulfo-SANPAH contains a nitrophenylazide group that is photoreactive toward polyacrylamide [9]. Exposure of the gel in a solution of Sulfo-SANPAH with a UV light source covalently links the sulfo-SANPAH to the polyacrylamide hydrogel [10]. The N-hydroxysuccinimide ester in sulfo-SANPAH can then react with the primary amines of proteins to complete the attachment of proteins to the surface of the gel [11].

2 mg of Sulfo-SANPAH powder (Thermo Scientific, Pittsburgh, PA) was dissolved in dimethyl sulfoxide (DMSO) to form 40 ul aliquots and were covered with aluminium foil and stored at -20℃. The PBS in the stored PA gels was removed and decanted while avoiding gel drying. Sulfo-SANPAH-DMSO aliquots were mixed in ddH2O (2mg/ml) immediately before use and 200ul was used to coat gel surface. The gel was exposed to a UV light (BrainyTrade, New Jersy, USA) (4 9W UV lamps 370nm wavelength at a distance of 2 inches for 1.5min). Sulfo-SANPAH changed its color from orange to brown when activated. Gels were washed twice in DI water, decanted, the Sulfo-SANPAH coating and UV light esposure were repeated one more times. 200ul of 0.3mg/ml collagen type-I in PBS was placed on a parafilm in petri dishes, the PA gels with Sulfo-SANPAH were Inverted on the top of the collagen solution and incubated to react at room temperature for 1.5hrs. Coverslips were placed and washed extensively in new culture dishes containing a filtered PBS under strile conditions in a cell culture hood. PA gels were incubated in cell culture media (DMEM + FBS) for $2hrs$. The only down side of this method could be poor coupling due to loss of reactivity of sulfo-SANPAH due to poor storage or time delays during preparation [12] which can be avoided by stricktly following the experimental procedures.

5.9.4 Protein coating characterization

In order to get an as precise measurement of traction forces as possible, the prepared protein coated PA gel surface needs to be smooth and uniform throughout the area. It had to be checked weather the procedure resulted a uniform coating of the protein

on the gel surface. BSA and texas-red congugated BSA each 500ug were dissolved in 1ml PBS (PH 8). 200ul of the solution is added to a parafilm in the form of four droplets, Sulfo-SANPAH treated and untreated 2.5kPa and 10kPa gels were inverted on to the solution and was incubated for 1.5hrs. PA gels were washed extensively with a filtered PBS (PH 7.4). Fluorescent images were taken using a texas-red filter set were taken to compare the intensity of the fluorescent congugated BSA as a readout of half of the protein density for all the cases. As mentioned in the beginning, BSA and Texas Red conjugate BSA were mixed at a 1:1 ratio to avoid signal saturation during imaging which could affect the data acquisition and interpretation. Using a similar experiment, it was also checked and determined that agitation during BSA coating is very important for the uniformity and distribution of the coating.

5.10 Forster resonance energy transfer (FRET) based cellular mechanosensors

As described in detail in chapter 3, FRET experiments on live cells usually involves proteins of interest with the approproate donor and acceptor fluorophores that are capable of FRET. The plasmid DNA containing both fluorophores were amplified, extracted and purified before starting to have repeatitive bulk experiments. Measurements of FRET signals are in general performed in different ways either by using wide-field or confocal imaging to measure the intensities of absorption and emission of the donor and acceptor molecules. Here I utilized optical microscopy combined with sensitized emission FRET as described in detail in chapter 3 section 3.3 to study
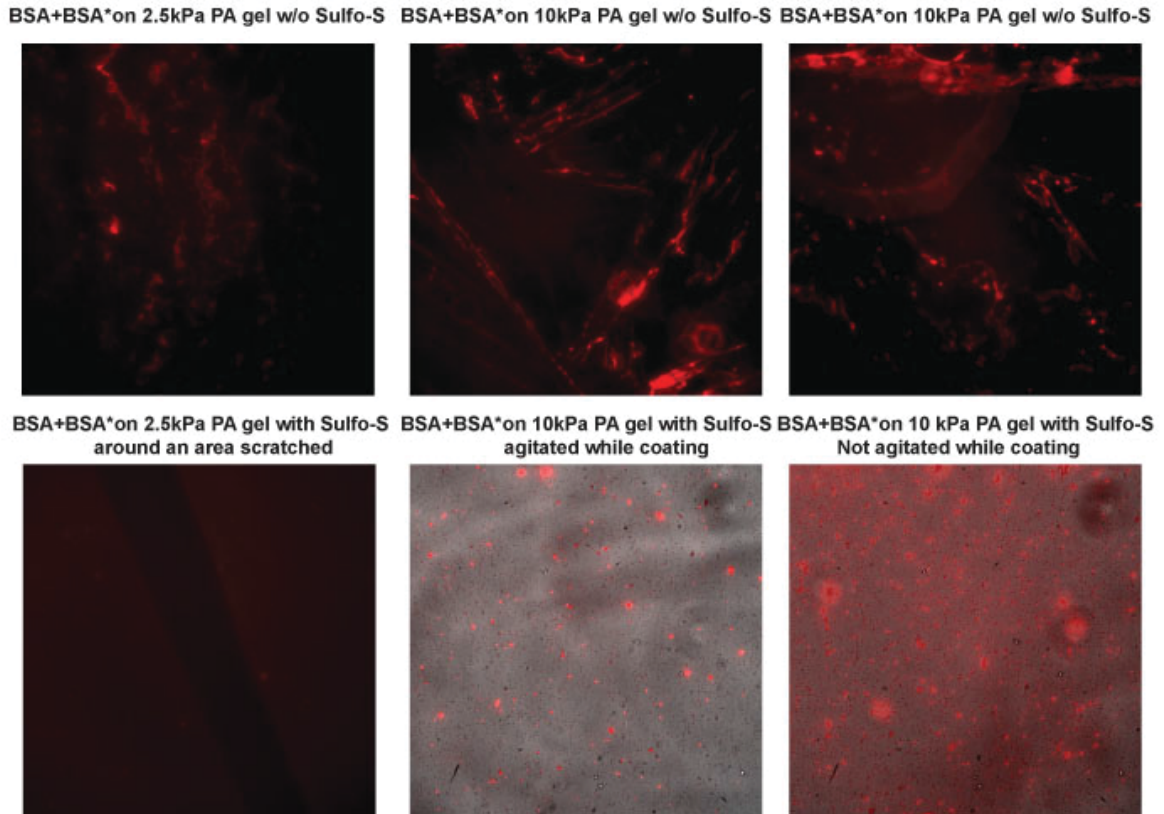
Figure 5.7: Uniform protein coating characterization. BSA and Texas Red conjugate BSA solutions were mixed in equal proportion to coat the polyacrylamide gels of stiffnesses 2.5kPa and 10kPa. The top panels samples were not treated with Sulfo-SANPAH and the bottom ones were treated.

the mechanical response of the non-erythroid membrane skeleton.

5.10.1   DNA amplification

0.7 ul of plasmids shown in **Fig.**5.9 [13] were mixed with 0.1 ml top-10 competent E. coli cells (Life technologies Grand Wasland, NY) in a clean eppendorf tube on ice, was mixed gently and incubated on ice for 15min. It was heat shocked at 42℃ for 1.5min and incubated on ice for 1min. 1 ml of SOC medium was added with a sterile

101
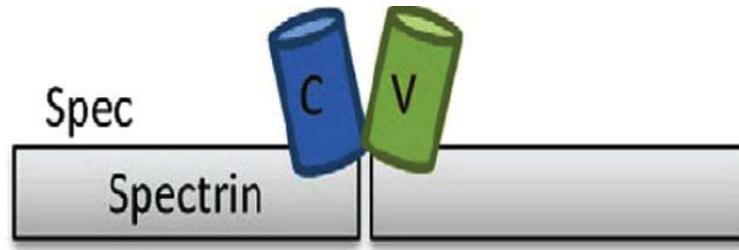
Figure 5.8: Circularly permutated cerulean (donor) and venus (acceptor) inserted at amino acid position 1200, which located in the linker domain between the 10th and 11th spectrin repeat domains (Dr. Fredercik Sachs , SUNY Buffalo, NY).[18]

technique, mixed gently and incubated for 45min at 37℃ by shaking at 216 rpm. $10-300$ ul of the solution was spread onto the pre-prepared agar plate (5g Tryptone, 2.5g Yeast extract, 5g Sodium Chloride and 7.5 g Agar and DI water with total solution volume of 500ml) containing 60 ug/ml kanamycin. The plate was tilted back and forth for uniform coverage with the E. coli was gently distributed uniformly with ethanol soaked and flamed pipets. To avoid condensation, the plate was incubated upside down over the night at 37℃. The next day, 5 ml of LB with kanamycin was added to a 15 ml conical tube. Isolated and smooth edged colony was selected and picked up with a sterile pipet tip from the incubated agar plate. Transferred into the LB medium with kanamycin, placed on a shaker and incubated at 37℃, with 216 rpm for 6hrs. The medium turned cloudy which was a signal of bacterial cell growth. To amplify the DNA, 300 ul of E.coli was added to 125 ml LB with 60 ug/ml kanamycin in a 500 ml sterile flask to leave enough room for airation. The culture was incubated for 16hrs at 37℃. In order to avoid overgrowth the DNA concentration has to be determined starting from the 12th hour. The most commonly used and easiest technique to determine DNA concentration and cell density is absorbance

102

measurement with a spectrophotometer which measures the scattering intensity or commonly termed optical density (OD). Absorbance measurements were taken at 260 nm where DNA absorbs light most strongly. A measurement was also taken at 280 nm for purity calculation of the sample. Another absorbance measurement is also done at 320 nm to subtract the non-nucleic acid absorbance. The cell density was measured optically in a spectrophotometer with a UV lamp and transparent cuvettes. 1ml of the culture is tranffered to a cuvette, a light shined through the cuvette was scattered by the cells depending on their density. The OD is proportional to the cell density $OD \propto \frac{N_{sample}}{V_{sample}}$

$$Concentration(ug/ml) = \frac{A260 - A320}{A280 - A320}(dilution factor)(50ug/ml). \qquad (5.1)$$

Good quality DNA have an absorbance ratio $\frac{A260-A320}{A280-A320}$ of $1.7 - 2.0$, while a lower ratio indicates the presence of contaminations [14]. For those measurements with low ratio, experiments were repeated until acceptable purity with ratios between 1.8-1.96 were obtained.

5.10.2 Protein extraction and purification

QIAprep spin miniprep kit (Qiagen, Valencia, CA) was used for DNA extraction and purification steps described below following the manufacturer's protocol with few modifications.

Six 5 ml of the overnight cultured bacteria with amplified DNA were transferred to six sterile microcentrifuge tubes and pelleted at 8600 rpm for 3min at room temperature. Each bacterial cell pellet was resuspended in 250 ul buffer P1 (resuspention buffer) and transferred to a microcentrifuge tube while checking that cell clumps are

not formed after resuspention.

250 ul of buffer P2 (lysis buffer) was added to each and mixed thoroughly by inverting the tube 7 times until the solution becomes viscous and slightly clear. 350 ul of buffer N3 (neutralization buffer) was added to each and immediately mixed thoroughly by inverting the tube 7 times until the solution became cloudy. They were then centrifuged for 10min at 12, 600 rpm in a microcentriguge.

The supernatants were applied to the QIAprep spin columns by decanting or pipetting, centrifuged for 1min and each flow-through was discarded.

The QIAprep spin columns were washed by adding 0.75 ml buffer PE (wash buffer) to each and centrifuged for 1min. The flow-throghs were discarded and the tubes were centrifuged for an additional 1min to remove residual wash buffer. The QIAprep columns were placed in a clean 1.5ml microcentriguge tube. The DNA was eluted with 30 ul buffer EB (elution buffer) or water that was added to the center of each QIAprep spin column and then incubating it for 1min and centrifuging for another 1min. Eluted DNA was collected, combined and concentrations were determined using a spectrophotometer as described in this chapter section 10.1 The DNA was stored in the dark at -20℃.

5.10.3   Cell transfection with stress-FRET sensor constructs

Transfection is a powerful method of introducing foreign DNA and RNA into mammalian cells [15]. Different chemical, physical and lipid transfection techniques have been used by different groups to deliver the plasmid DNA in to the nucleus. Initially, liposome-mediated transfections using lipofectamine LTX and Lipofectamine

2000 with Plus transfection agent were performed. In this system, positively charged liposomes interact with, encapsulate and coat the negatively charged DNA which neutralizes or gives a net positive charge to the complex. This makes it easier for the DNA-transfection complex to be engulfed by the membrane via endocytosis. Performances of transfection methods and agents depend higly on several factors such as the type of cell lines, experiments being performed or the size and purity of plasmid DNA used. Although the two transfection agents gave a reasonable tranfection efficiency of about 12% for transfecting actin on CHO and $3T3$ fibroblasts, they were not suitable for the transient transfection of spectrin-cspFRET constructs on 3T3 and 10T1/2 cells. Therefore, we used Fugene-HD transfection agent (Promega Corporation, Madison, WI), which is a non-liposomal way of delivering the DNA to the nucleus. It forms complexes with the plasmid DNA which then have the potential to form micelles. $NIH3T3$ and $H9c2(2-1)$ cells were plated the day before transfection at a density of 5 X 10^4 cells on a 25 mm functionalized PA gel layer which is placed on a 60 mm, uncoated, sterile petri dish. It is supplied with 3 ml of complete growth medium (DMEM + 10% Fetal Bovine Serum). The next day when the cells reach about 75% confluence, the transfection mix was prepared. The transfection was optimized with a number of experiments by varying the DNA:Fugene-HD and the volume of the transfection mix to get the highest possible transfection efficiency. Using the measured DNA concentration (460 ug/ml) and follwing the manufacturer protocol, different amounts of DNA were added to 210 ul of OptiMed (GIBECO). 16 ul of FuGENE HD (Promega, Madison, WI) reagent was added to the DNA-Optimed complex and mixed carefully by pipetting 16 times. The mixture was incubated at

105

room temprature for 12min. The transfection was performed on the PA gels than the culture dishes because in a transient transfection as opposed to stable trasfection, cells express the foreign gene but do not integrate it into their genome[16]. Which means the gene is not replicated. The cells express the transfected gene for days after which the gene is lost through cell division or other processes. Subculturing also decreases the number of tranfected cells used for imaging.

5.10.4   FRET microscopy

Measuring fluorescence resonance energy transffer (FRET) by the detection of acceptor-sensitized emission is the most popular and non-destructive live cell FRET imaging technique [17]. It was implemented on the Eclipse Ti inverted microscope (Nikon Instruments, Inc., Melville, NY) in the lab. 48hrs after transfection, cspFRET-transfected containing Cerulean (a variant of CFP), Venus (a variant of YFP) cells were visualized with the microscope and 16 bit iXon Ultra 888 (Andor technology, South Windsor, CT). A 175 W xenon arc lamps (shutter instruments, Novato, CA) was employed for excitation. Phase contrast, fluorescent images of Hoechst stain, Cerulean (donor), Venus (accep- tor) FRET and red fluorescent beads (Bangs Laboratories, Inc. Fishers, IN) for the TFM measurement were obtained with a 60x water-immersion objective (Nikon Instruments, Inc., Melville, NY) with a numerical aperture of 1.2. The appropriate filter sets (Chroma Bellows, Falls, VT) were used for the donor excitation at 433 nm /donor emission at 475 nm, acceptor excitation at 515 nm/acceptor emission at 528 nm and donor excitation at 433 nm/ acceptor emission at 528 nm emission (FRET channel) for sensitized emission measurements. Data

acquisition were automated and facilitated with NIS-elements AR 3.0 and Andor technology 5.509 software. RiFRET intensity based live FRET image analysis image J plugin [17] is used to calculate FRET correction coefficients and analysis introduced in chapter 3.3. Fiji (Image J) image processing packages (National Institutes of Health Bethesda, MD), NIS instruments (Nikon, Melville, NY), Image studio lite (LI-COR Biosciences, Lincoln, NE) , Igor (Wavemetrics, Tigard, OR), Chemdraw (CambridgeSoft Cambridge, MA), Adobe illustrator (Adobe Systems Incorporated, San Jose, California) were used as analysis and plotting tools.

5.11   References

1.   Yeung, T., et al., Effects of substrate stiffness on cell morphology, cytoskeletal structure, and adhesion. Cell Motility and the Cytoskeleton, 2005. 60(1): p. 24-34.

2.   Boudou, T., et al., An extended relationship for the characterization of Young's modulus and Poisson's ratio of tunable polyacrylamide gels. Biorheology, 2006. 43(6): p. 721-8.

3.   Pelham, R.J. and Y.L. Wang, Cell locomotion and focal adhesions are regulated by substrate flexibility. Proceedings of the National Academy of Sciences of the United States of America, 1997. 94(25): p. 13661-13665.

4.   Aratyn-Schaus, Y., et al., Preparation of complaint matrices for quantifying cellular contraction. J Vis Exp, 2010(46).

5.   Kraning-Rush, C.M., et al., Quantifying Traction Stresses in Adherent Cells. Computational Methods in Cell Biology, 2012. 110: p. 139-178.

6.   Chung, T.L., et al., Seroma prevention using Mytilus edulis protein in a rat mastectomy model. Breast Journal, 2006. 12(5): p. 442-445.

7.   Notter, M.F.D., Selective Attachment of Neural Cells to Specific Substrates Including Cell-Tak, a New Cellular Adhesive. Experimental Cell Research, 1988. 177(2): p. 237-246.

8.   Koch, D., et al., Strength in the Periphery: Growth Cone Biomechanics and Substrate Rigidity Response in Peripheral and Central Nervous System Neurons. Biophysical Journal, 2012. 102(3): p. 452-460.

9.   Tse, J.R. and A.J. Engler, Preparation of hydrogel substrates with tunable mechanical properties. Curr Protoc Cell Biol, 2010. Chapter 10: p. Unit 10 16.

10.   Thakar, R.G., et al., Cell-Shape Regulation of Smooth Muscle Cell Proliferation. Biophysical Journal, 2009. 96(8): p. 3423-3432.

11.   Yip, A.K., et al., Cellular Response to Substrate Rigidity Is Governed by Either Stress or Strain. Biophysical Journal, 2013. 104(1): p. 19-29.

12.   Kalkhof, S. and A. Sinz, Chances and pitfalls of chemical cross-linking with amine-reactive N-hydroxysuccinimide esters. Analytical and Bioanalytical Chemistry, 2008. 392(1-2): p. 305-312.

13.   Meng, F.J. and F. Sachs, Orientation-based FRET sensor for real-time imaging of cellular forces. Journal of Cell Science, 2012. 125(3): p. 743-750.

14.   Manchester, K.L., Use of UV methods for measurement of protein and nucleic acid concentrations. Biotechniques, 1996. 20(6): p. 968-70.

15.   Titomirov, A.V. and A.V. Zelenin, New Methods of Transfection of Mammalian-Cells - a Minireview. Molecular Biology, 1988. 22(6): p. 1155-1159.

16.   Kim, T.K. and J.H. Eberwine, Mammalian cell transfection: the present and the future. Analytical and Bioanalytical Chemistry, 2010. 397(8): p. 3173-8.

17.   Elder, A.D., et al., A quantitative protocol for dynamic measurements of protein interactions by Forster resonance energy transfer-sensitized fluorescence emission. Journal of the Royal Society Interface, 2009. 6: p. S59-S81.

18.   Meng, F.J. and F. Sachs, Orientation-based FRET sensor for real-time imaging of cellular forces. Journal of Cell Science, 2012. 125(3): p. 743-750.

Chapter 6

Conclusion, limitations and outlook

6.1   General accomplishments and relevance

The spectrin based membrane skeleton has been the focus of much study in the context of red blood cells, as it determines their mechanical properties due to the lack of an extended actin based cytoskeleton. In stark contrast, the corresponding structure in non-erythroids is much less studied and understood, although it seems to play important roles in organization of membrane associated proteins, cellular mechanics, and possibly mechanotransduction. The amount-down to the average copy number per cell- of the main protein components of the non-erythroid membrane skeleton in model cell lines commonly used in cell-mechanics studies has been provided. The results of the measurements provided by combining a variety of optical microscopic and biochemical techniques, demonstrate that proteins associated with

the membrane skeleton constitute at large (10%) fraction of cellular proteins. These results are then compared with the respective quantities after mechanical stimulation of the cells. It is found out that external forces result in up to 60% of both the overall amounts of proteins as well as the protein composition of the membrane skeleton. In addition, it was established that the fraction of polyubiquitinated spectrin is significantly increasing due to stimulation. This suggests that the ubiquitin the proteasome pathway is one particular mechanism involved in membrane skeleton regulation, possibly through a mechanically dependent self-ubiquitination activity of some spectrin isoforms. Technically speaking, it was established that through direct comparisons with more traditional techniques, that quantitative fluorescence microscopy of immunostained cells is a suitable approach to detect relative changes in protein content and concentration. A variety of spectrin isoforms including traditional erythroid spectrins in non-red blood cells were detected, the work supports a revision of the historical classification of membrane skeleton proteins based on their occurrence in the rather specialized red blood cells. The work helps establishing the fact that the spectrin based membrane skeleton, while often overlooked, is indeed a verily generic and important system in mammalian cells that is also quite sensitive to external forces. Thus, the skeleton should be taken into account when studying cellular mechanics, membrane structure or composition.

Cells also use internally generated forces to probe the mechanical properties of their environment and show a variety of responses. To that end, it has also been shown that in $3T3$ Fibroblast and $H9c2(2-1)$ Cardiomyocytes cell lines (force bearing cells) traction forces cells exert on polyacrylamide hydrogels of varying elastic

modulus is correlated with the amount of force mechanically sensed by the spectrin membrane skeleton. Our data demonstrates that the internal strains in the membrane skeleton are associated with the varying polyacrylamide substrate stiffness which are definitely correlated with the alterations in cellular traction forces. These findings open questions whether the existing scientific descriptions of cytoskeletal and membrane changes and developments of focal adhesion complexes when traction forces are exerted by cells are complete or there are other missing pieces in the descriptions.

What has been observed in separate experiments is that, cell morphology seeded on negatively charged bilayers is similar to cell growing on the poly-l-lysinated glass control surface and on positively charged bilayers large cell-clusters encountered a problem of successfully adhering. Enriching the bilayers with lipids with sugar elaborated head groups also did not improve proliferation behavior but resulted a new cell morphology (adhesion). It has been thought that fusiogenic lipids with a phospho-ethanolamine head group that are located at the extracellular membrane leaflet are protein and cell repellent [1]. But this work suggests that cellular behavior of 3T3 fibroblasts on supported lipid bilayers depend on the detail of lipid charge mixtures and sugar group compositions and extensive cellular behavior characterizations have to be performed before creating a better platform.

6.2 Outlook and limitations

Since I have established that quantitative fluorescence microscopy can be used for comparison of relative protein contents. The flex-cell tension system in figure 4.1

could be integrated with epi-fluorescence microscopy. It would be interesting to look with such an instrument at the change in relative protein contents for different frequency, duration of stimulation and strain magnitudes on live cell lines and primary cells.

The work in chapter three can be extended to time lapse cell migration experiments in order to produce a data set with the required temporal resolution to support our findings. These could not be achieved in part because of the lack of live cell chamber integrated with our optical instruments to keep the cells healthy for several hours of imaging. Also, a fluorescence-activated cell sorting (FACS) machine needed for single cell experiments in order to significantly increase the number of fluorescently labeled cells was not available at the time of the experiments. However, such a machine has been recently acquired by SU and would play a central role in future single cell migration experiments. In the experiments presented in this thesis transfection was done on cells growing on PA gels which were $> 75\%$ confluent. After the time it takes for the transient transfection to take hold (usually the next day) imaging was performed on cultures that were thus usually more than 95% confluent. Under these conditions it is essentially not possible to find a single cell that is sufficiently separated from other cells to enable single cell migration experiments.

The validated local stiffness measurements of PA gels using the steel ball experiment needed further validation with atomic force microscopy (AFM) which is more reliable. Although both use the same theory (Hertz), using different ball sizes and densities gives different results for the ball indentation method. The accuracy depends on how much the two measured bead positions can be resolved clearly. But

113

in the case of the AFM, if appropriate tips are used, very localized stiffness can be measured, the penetration depth of the AFM tip is controlled automatically and measured by a laser deflection and it has high resolution in the order of nm [2] than the steel ball (um). But the AFM machine in the department has been broken and could not be fixed within the time frame of the project. Currently nano-indentation, which a better optical method of measuring stiffness in terms of obtaining a fast quantitative information is being introduced in the field [3].

Finally, the stress-strain work in chapter 3 can be combined with the cell on the bilayer work described in chapter 4 in order to address some of the many open questions raised in the thesis on the roles of the non-erythroid membrane skeleton.

6.3   References

1.   Afanasenkau, D., Supported lipid bilayer as a biomimetic platform for neuronal cell culture, in Dissertation2012.

2.   Chiou, Y.W., et al., The influence of physical and physiological cues on atomic force microscopy-based cell stiffness assessment. PLoS One, 2013. 8(10): p. e77384.

3.   Li, C., et al., The use of polyacrylamide gels for mechanical calibration of cartilage--a combined nanoindentation and unconfined compression study. J Mech Behav Biomed Mater, 2011. 4(7): p. 1540-7.

Chapter 7

Appendix

7.1   List of abbreviations

APS - Ammonium Persulfate

TFM - Traction Force Microscopy

KPa - Kilo Paskal

DAPI - 4',6-diamidino-2-phenylindole

IP - Immunoprecipitation

IF - Immunofluorescence

AFM - Atomic Force Microscopy

DMEM - Dulbecco's Modified Eagle Medium

EDTA - EhtyleneDinitriloTetraaceticAcid

MgCl2 - Magnesium Chloride

mM - Millimolar

NaCl - Sodium Chloride

nm - Nanometers

nM - Nanomolar

FRET - Forster Resonance Energy Trasfer

TEMED - Tetramethylethylenediamine

PIV - Particle Image Velocimetry

pN - Piconewton

FTTC - Fourier Transform Traction Cytometry

SDS-PAGE - Sodium Dodecyl Polyacrylamide Gel Electrophoresis

SLB - Supported Lipid Bilaer

7.2 Biography

Research interests

Soft-condensed matter and cellular biophysics, mechano-transduction, the physics of neuronal,

cancer and cardiovascular diseases.

Expertise and research skills

Six years of research experience focused in the area of cellular mechano-transduction. Has demonstrated expertise in the field of experimental cell biophysics, optical microscopy and imaging sience, mamalian cell handling, protein extraction, detection and purification, DNA amplifica-tion and transfection techniques and creative problem solving skills. Has mentored 10 undergraduate students over the years in parallel with concentrating on the progresses of research projects.

Publications

Eleni K. Degaga and Martin B. Forstner, "Quantification of Compositional Changes in the Non-Erythroid Membrane Skeleton due to External Forces" under review at the PNAS.

Eleni K. Degaga and Martin B. Forstner, "Correlating Traction Strains of Migrating Cells with Their Internal Strains" in Preparation.

Eleni K. Degaga Ian P. McCabe and Martin B. Forstner "Behavior of 3T3 Fibroblast Cultures on Supported Lipid Bilayers" in Preparation.

Selected conference presentations

Eleni K. Degaga, Ian P. McCabe and Martin B. Forstner "Behavior of 3T3 Fibroblast Cultures on Supported Lipid Bilayers" at the centre for the physics of living cells, the University of Illinois at Urban-Champaign, July 28-29 2014.

Eleni K. Degaga and Martin B. Forstner "Quantifcation of force induced Changes in the Non-Erythroid Membrane Skeleton due to External Forces" invited talk at the Physics department, Georgetown University 9th April, 2014.

Eleni K. Degaga and Martin B. Forstner "Quantifcation of force induced Changes in the Non-Erythroid Membrane Skeleton due to External Forces" invited talk at the National Institute of Health 8th April, 2014.

Eleni K. Degaga and Martin B. Forstner "Quantifcation of Compositional Changes in the Non-Erythroid Membrane Skeleton due to External Forces" 58th Annual Meeting of the American Biophysical Society (BPS) San Fransisco, California, 19th February, 2014.

Eleni K. Degaga and Martin B. Forstner "Optical Tools in Cellular Biophysics" African Institute for Mathematical Sciences, Cape Town, South Africa, 27th June 2013.

Eleni K. Degaga, Ian P. McCabe and Martin B. Forstner "Behavior of 3T3 Fibroblast Cultures on Supported Lipid Bilayers 5th Annual Biotechnology Symposium, State University of New York, 16th May 2013.

Eleni K. Degaga and Martin B. Forstner "Force Dependent Modulations In Non-Erythroid Spectrin and Ankyrins" Soft Interfaces IGERT Retreat, Syracuse Biomaterial Institute (SBI), Syracuse, NY 2nd of March 2013.

Eleni K. Degaga and Martin B. Forstner "Force Dependent Modulations In Non-Erythroid Spectrin and Ankyrins" Soft Interfaces IGERT Retreat, Syracuse Biomaterial Institute (SBI), Syracuse, NY 2nd of March 2013.

Eleni K. Degaga and Martin B. Forstner "Force Dependant Changes in Non Erythroid Spectrin and Ankyrin" 57th Annual Meeting of the American Biophysical Society (BPS) Philadelphia, Pennsylvania, 2rd February, 2013.

Eleni K. Degaga and Martin B. Forstner "Force Dependant Changes in Non Erythroid Spectrin and Ankyrin" Annual Meeting of the American Physical Society (APS), Boston Massachusetts, 27th February 2012.

Eleni K. Degaga and Martin B. Forstner "Force Dependent Enzymatic Activity of Non-Erythroid Spectrin and Cell Proliferation" 55th Annual Meeting of the American Biophysical Society (BPS), Baltimore Maryland,7th March 2011.

Eleni K. Degaga and Martin B. Forstner "Optical tools to study mechano-trasduction in cells" International Center for Theoretical Physics, Winter College on Optics in Imaging Science, Trieste Italy, 2nd February 2011.

Undergraduates mentored

Pauline Hua, Now at Downstate Medical School.

ChaoJie Zhen, Now Medical Technologist at University of Chicago Medicine.

Adam Dobson, Now a Senior Researcher at Oregon Health and Sience University.

Adhana Asfaw, Now Admitted to Harvard Medical Scool.

Tiyani Zohu

Jasmine Roddey

Sundus Mian

Zoe Nicole Kazzaz

Tomas Rafael Daviu

Navjyot Singh Parmar

Awards and Honors

Travel Award to the American Biophysical Scoiety Meeting San Fransisco, CA 2014.

Award of Appreciation from the African Institute of Mathematical Sciences, Cape Town, SA 2013.

Faculty for the Future Predoctoral Fellowship from the Schlumberger Foundation 2013-2014.

Fellowship Women in Science and Engineering, Syracuse University 2011-2013.

Full scholarship to Study and Travel to the African Institute for Mathematical Sciences in Cape Town 2007-2008.

Award of Appreciation for Serving as the Vice President of the Student Council of Bahirdar University, 2006.

 Research Achievement Award in the Partnership Project of Cornell University and Bahirdar University 2005.

Full Scholarship to study in the Physics Department at Bahirdar University, Ethiopia, 2003-2006. **3000 ETB and a Certificate of Honor** from Projynist NGO for Scoring 4.0/4.0 in the Ethiopian School leaving Certificate Examination 2003.

7.3   Dedications

I dedicate this dissertation work to my family and many friends. A special feeling of gratitude to my dearest husband rev. Kassahun, whose love, patience and support with all the sleepless days and nights were more than I can discribe. I also dedicate this dissertation to my family in Ethiopia for their continous words of encouragement. To my special mother Shitaye whose strength to riase us up with out a father was very amazing and inspirational. My sisters Woineshet, Asse, Rahel, Tizita, Jerusalem who were always there to support me and to share ideas when ever I need them and my brothers Wonde, Samuel and Muluken have never left my side. I also dedicate this dissertation to my many friends in Ethiopia, South Africa, here in the US and all church family who have supported me throughout the process. I will always appreciate all they have done.

ማስታወሻነቱ

እጅግ በጣም ለምወደው እና ለማከብረው ፤ በዚህ የትምህርት እና የህይወት ቆይታዬ በእያንዳንዱ ሰዓት እና ደቂቃ በፍቅር ፤ በትህግስት ፤ በጸሎት እና በእንክብካቤ ላልተለየኝ ፤ ድጋፉን በቃላት ገልጬ ለማልጨርሰው ውድ ባለቤቴ ለመልዐከ-ገነት ቀሲስ ካሳሁን ይሁንልኝ ።

እንዲሁም በእያንዳንዱ መውጣት እና መግባቴ ላልተለየኝ በኢትዮጵያ ያሉ ቤተሰቦቹ ፤ ለእናቴ ወ/ሮ ሸታዬ መልካ ፤ ያለ አባት አሳድጋ ለቁም ነገር ላበቃችን ፤ በችግር ውስጥ በነበራት ጥንካሬ ጠንክረን አንድንኖር ላደረገችን ውድ እናታችን ፤ ሁሌም ጭንቀቴን እና ሃሳቤን ለመጋራት ለማይሰለቹት እህቶቹ ፤ ወይንእሸት ፤ አሰጉ ፤ ራሄል ፤ ትዝታ እና እየሩሳሌም ፤ በአካል ተራርቀን ብንኖርም በመንፈስ አልተለዩ ኝም። ጥረታቸው እና መልካም ምኞታቸው ላልተለየኝ ውድ ወንድሞቹ ወንድወሰን ፤ ሳሙኤል እና ሙሉቀን ፤

 በኢትዮጵያ ፤ በደቡብ አፍሪካ ፤ በዚህም በሰሜን አሜሪካ ለሚገኙ ጓደኞቹ እና በቅድስት ቤተክርስቲያን ላሉ ቤተሰቦቹ በተለይም በሲራክዩስ ገነተ-ደናግል ቅድስት አርሴማ- ወክርስቶስ ሰምራ ቤ/ክ ለሚገኙ ወንድሞቹ እና እህቶቹ ይሁንልኝ።

121